# WATER-GUEST INTERACTIONS UNDER CLATHRATE HYDRATE FORMATION CONDITIONS: A MATRIX-ISOLATION APPROACH


A dissertation

submitted by

**Tuan Hoang Vu**

In partial fulfillment of the requirements

for the degree of

Doctor of Philosophy

in

Chemistry

**TUFTS UNIVERSITY**

August 2013



**Advisor: Professor Mary Jane Shultz**

Tufts
UNIVERSITY

ARTS, SCIENCES, AND ENGINEERING

# CERTIFICATE OF FITNESS

This certifies that the undersigned, appointed to determine the fitness of

Thuan H. Vu

for the degree of Doctor of Philosophy in Chemistry

have examined the candidate's thesis/dissertation (or papers) on the subject:

Water-Guest Interactions under Clathrate Hydrate Formation Condition

and have found it satisfactory.

May 1st, 2013
Date of Defense

This certifies further that the candidate this day has successfully passed the customary examination.
We recommend, therefore, that the degree be awarded under the usual conditions.

| SIGNATURES | NAMES |
|---|---|
| Mary Jane Shultz<br>*Chairperson, Examining Committee* | Mary Jane Shultz<br>*Chairperson, Examining Committee* |
| E. Rybak-Akimova | Elena Rybak-Akimova |
| | Arthur Utz |
| T. Keyes | Tom Keyes |

Student Services
Dowling Hall
Medford, Massachusetts 02155
617.627.2000

# Abstract

The eventual depletion of fossil fuels, coupled with the effects of greenhouse gas emission on the global climate, has called for exploration of alternative technologies to address increasing energy demand. Clathrate hydrates, crystalline solids composed of gas and water, is a class of materials with enormous potential both as an energy source and as a medium for gas storage. These peculiar compounds occur naturally in the permafrost and the deep oceans, and are estimated to contain more carbon than all the oil found on Earth. There have been numerous investigations on the kinetics and thermodynamics of clathrate formation; however, a molecular-level understanding of this phenomenon is far from complete. A major challenge has been characterization of the water-guest interactions at the beginning stages of nucleation. Infrared spectroscopy is among the most sensitive probes for detecting interactions involving water, but it is rarely chosen for hydrate studies due to the high absorbance of bulk aqueous samples. This work employs a room-temperature matrix isolation technique to circumvent the opacity problem. Carbon tetrachloride is used as the solvent to disperse water into isolated monomers with ambient thermal energies, providing an excellent environment to investigate interactions with hydrate guest molecules at typical clathrate formation conditions (temperatures near 0 $^{o}$C and pressures between 1-55 atm).

Propane is one of the simplest hydrocarbons that form a stable clathrate hydrate under relatively mild conditions. In carbon tetrachloride, the water monomer signature consists of the symmetric stretch, the asymmetric stretch, and rotational wings associated with the asymmetric stretch. Interaction of water with propane causes a dangling OH (*d*-OH) peak to appear between the symmetric and asymmetric stretches, indicating a guest-induced water cluster. A combination of isotopic substitution and density functional theory calculations has established the presence of

an attractive interaction between the methylene groups of propane and the electron lone pairs of water.

Aside from their potential role in energy applications, hydrate plugs formed during transportation and processing of natural gases have been a longstanding nuisance for the petroleum industry. A number of thermodynamic inhibitors, primarily methanol, have been used to prevent hydrate formation in natural gas pipelines for many years, but their interactions with the hydrate constituents are not very well identified. Matrix-isolation experiments are hence performed to elucidate the mutual interactions between methanol, water and propane in $CCl_4$. Experimental data indicate that while methanol forms hydrogen bond to water via donation of the hydroxyl group (binding constant $K = 4.4 \times 10^2$), it does not have any specific interaction with propane. These results are consistent with a picture in which methanol disrupts formation of the water-guest complex by competing with propane for the oxygen lone pairs in water.

Interactions between water and pentacyclic guests such as tetrahydrofuran (THF) and cyclopentane are subsequently examined. Despite the distinct difference in aqueous solubilities (THF is totally miscible with water and cyclopentane is hydrophobic), both compounds form stable clathrates above 0 $^oC$ at ambient pressure. Knowledge of the nature of the water structure surrounding the cyclic guests is thus a critical component for a deeper understanding of the nucleation mechanism. Experimental results show that compared to propane, cyclopentane gathers significantly larger clusters of water in carbon tetrachloride. The presence of a bridging water molecule is also observed for the cyclopentane-water cluster, providing compelling evidence for arrangement of water molecules in a local five-membered ring motif. The rigidity of the cyclic guest in this instance partially immobilizes water molecules in its vicinity, and reduces the entropic cost for forming a complete hydrate lattice.

# Acknowledgements

I am indebted to my advisor, Prof. Mary Jane Shultz, for her earnest support and guidance both professionally and personally during my time in the group. Her enthusiasm for water is unparalleled, and I thank her for teaching me everything I know about this simple, ubiquitous yet very complicated molecule. I especially appreciate her accessibility and willingness to talk whenever I need help or ideas. These experiences have made graduate school a much more rewarding endeavor.

I am also grateful for the many help and advices I received from my committee members, Prof. Elena Rybak-Akimova and Prof. Arthur Utz, throughout the years. I have greatly benefited from their class lectures and from their constructive critiques of my weaknesses after each study topic and research proposal. Those feedbacks have been crucial for my continued improvement. I also wish to thank Prof. Tom Keyes of Boston University for serving on my thesis defense committee.

A special thank to my undergraduate mentor, Prof. Lesley Davenport, for allowing me the opportunity to conduct scientific research very early on, and for her close contact and continued support. Acknowledgement is also extended to my Physical Chemistry professors at CUNY Brooklyn College, Prof. Mark Kobrak and Prof. Ira Levine, for encouraging me to pursue graduate school. Prof. Levine's textbooks have been an indispensible part of my chemistry education.

I would also like to thank the present and past members of the Shultz group whom I have overlapped with: Dr. Irene Li, Dr. Margaret Kuo, soon-to-be Drs. Faith Dukes and Patrick Bisson, Nkeng Asong, Han Xiao, Jing Wang, and Rui Liang. I am grateful for their friendship,

support and guidance both in lab and in life. I especially thank Margaret for her diligent work on the carbon tetrachloride system, which has paved the way for much of my research. I also like to acknowledge the assistance of two very bright Tufts undergraduates, Sarah Kälin and Bryce Meyer, in setting up various experiments at the beginning stages of the project. I am proud of the success they have since enjoyed in their respective careers.

A sincere thank to my close group of friends at Tufts (Trish and Danny Showalter, Dr. Shannon Stroble, Glen O'Neill, and Calvin Kwon) for keeping me company through these strenuous years. I am blessed with friends who constantly catch me off guard with surprised birthday gifts and whose upbeat attitudes always cheer me up. I really enjoyed the tennis matches, bowling games, and discussions of the English Premier League. Most importantly, thanks for sharing my study topic nightmares and all the hysteria typically associated with the life of a graduate student.

My deepest gratitude goes to my family, especially my parents who have been very supportive with everything I choose to do in life. I thank them for all the sacrifice they made by allowing me to come to the United States at a very young age. I must also mention my sister who, by constantly hassling me with her AP Chemistry questions, has given me a chance to review many fundamental concepts. And to my special one, I simply could not have done this without your company. I am thankful for your kindness, patience, understanding, and presence in my life.

Lastly, I would like to acknowledge the financial support from the U.S. National Science Foundation grant no. CHE-0844986, the Petroleum Research Fund grant no. 46671-AC6, and the U.S. Department of Education GAANN Fellowship.

# Table of Contents

**Cover Page** ..... i
**Abstract** ..... ii
**Ackowledgements** ..... iv
**Table of Contents** ..... vi
**List of Figures** ..... viii
**Chapter 1** Introduction ..... 1
*1.1 Structure of Hydrate Cages* ..... 2
*1.2 Nucleation Models* ..... 4
*a) Labile Cluster Hypothesis* ..... 4
*b) Nucleation at Interface* ..... 5
*c) Local Structuring Hypothesis* ..... 5
**Chapter 2** Experimental Apparatus ..... 7
*2.1 High-Pressure Cell* ..... 7
*2.2 Cold Finger* ..... 8
*2.3 Silanized Glass Cell* ..... 9
*2.4 Vacuum Line* ..... 10
*2.5 Preparing Dried Carbon Tetrachloride* ..... 11
*2.6 Recycling Silica Gel* ..... 12
*2.7 Spectra Acquisition* ..... 13
*2.8 Theoretical Calculations* ..... 13
**Chapter 3** Propane Clathrate - A Macroscopic Perspective ..... 15
*3.1 Making Propane Clathrate Sample* ..... 15
*3.2 Observation and Preservation* ..... 16
**Chapter 4** Propane-Water Interaction ..... 17
*4.1 Sample Preperation* ..... 18
*4.2 Water in $CCl_4$ at at -5 $^oC$* ..... 19
*4.3 Propane/Water System in $CCl_4$* ..... 20
*4.4 Pinpointing Propane-Water Interaction* ..... 22

**Chapter 5** Inhibition of Propane-Water Interaction by Methanol ..... 29
*5.1 Sample Preperation* ..... 30
*5.2 Methanol in $CCl_4$ at -5 $^oC$* ..... 31
*5.3 Methanol-Water Interaction* ..... 32
*5.4 Methanol-Propane Interaction* ..... 34
*5.5 Ternary System* ..... 36
**Chapter 6** Tetrahydrofuran Clathrate ..... 40
*6.1 THF Hydrate Thin Film* ..... 40
*a) Sample Preparation* ..... 40
*b) Results* ..... 41
*6.2 Water and THF in $CCl_4$* ..... 46
**Chapter 7** Cyclopentane Clathrate ..... 49
*7.1 Cyclopentane Hydrate Thin Film* ..... 49
*7.2 Matrix-Isolation Experiments* ..... 51
*a) Sample Preparation* ..... 51
*b) Results* ..... 52
**Chapter 8** Summary and Future Work ..... 57
**Chapter 9** Spectral Signature of Hydroxide Ion in $CCl_4$ ..... 59
*9.1 Sample Preparation* ..... 60
*9.2 Results* ..... 61
**Chapter 10** Appendix ..... 64
*10.1 Supercritical Argon* ..... 64
*10.2 Surfactants* ..... 67
*10.3 Silica Gel* ..... 72
*10.4 Interaction between Benzene/Hexafluorobenzene and Water* ..... 73
*10.5 Free Rotation of $CO_2$ in Freon Clathrate at Ambient Conditions* ..... 76
**Bibliography** ..... 80

## List of Figures


Figure 1.1 Types of clathrate cavities and their corresponding shapes. Hydrogen atoms in the host frameworks are omitted for clarity. ..... 3

Figure 1.2 Comparison of the cluster nucleation theory (a-b-c-e) and the local structuring hypothesis (a-d-e). (a) Water without dissolved guest molecules. (b) Cluster form immediately after dissolution of guest molecules. (c) Cluster prestages agglomerate by sharing faces (equilibrium with step b). (d) No cluster fomration after dissolution of guest molecules. (e) Hydrate nucleation. Reprinted with permission from Lehmkühler et al. *J. Am. Chem. Soc.* 2009, *131*, 585-589. Copyright 2009 America Chemical Society. ..... 6

Figure 2.1 High-pressure stainless steel cell (left) and its internal design (right). The cell cut-out is reprinted with permission from Vu, Kälin, Shultz, *J. Phys. Chem. A* 2010, *114*, 6356-6360. Copyright 2010 American Chemical Society. ..... 7

Figure 2.2 Front view of the cold finger (left) and its schematic design (right) ..... 8

Figure 2.3 Picture of silanized glass cell (1 in. path length) with cold finger attached. ..... 9

Figure 2.4 Stainless steel vacuum line used for sample preparation. ..... 11

Figure 2.5 Typical absorption spectrum of dried carbon tetrachloride at room temperature using recycled silica gel. The inset is an expanded view of the O-H region showing the absence of detectable water absorption. ..... 12

Figure 2.6 Vibrational frequencies, dipole moment, bond length, and partial charges of a single water molecule in the gas phase calculated at the B3LYP 6-31G* level with Spartan ’08 software. The potential surface plot is displayed on an absolute scale showing negative potential as red, positive as blue, and green as neutral. The bounding surface is 92.6%. ..... 14

Figure 3.1 A laboratory sample of propane clathrate after being extracted from the cold finger (left) and set on fire (right) ..... 15

Figure 4.1 Rotational axes of water and the associated rotational constants in the gas phase. In carbon tetrachloride, $R_x$ and $R_y$ are quenched while the rotational lifetime of $R_z$ is shortened (0.83 ps). The value of $B_z$ in $CCl_4$ is 14.8 $cm^{-1}$. ..... 18

Figure 4.2 Absorption spectrum of a saturated solution of water in $CCl_4$ at -5 $^oC$ and 1 atm. The inset shows a magnified view of the H-bonded region. Reprinted with permission from Vu, Kälin, Shultz, *J. Phys. Chem. A* 2010, 114, 6356-6360. Copyright 2010 American Chemical Society. ..... 20

Figure 4.3 Difference spectrum of water/propane minus water in $CCl_4$ at -5 $^oC$ and 1 atm. Note the negative water peaks around 3700 $cm^{-1}$ and the appearance of H-bonded resonances at 3162 and 3338 $cm^{-1}$ (inset). Reprinted with permission from Vu, Kälin, Shultz, *J. Phys. Chem. A.* 2010, 114, 6356-6360. Copyright 2010 American Chemical Society. ..... 21

Figure 4.4 The O-H stretch region of water at -5 $^oC$ from 1 to 55 atm in the presence (a) and absence (b) of propane. The total pressure is adjusted by addition of dry argon gas. The spectra are vertically offset for clarity. Reprinted with permission from Vu, Shultz, *Physics and Chemistry of Ice 2010,* Hokkaido University Press: pp 147-152 (2011). Copyright 2011 Hokkaido University Press. ..... 22

Figure 4.5 Absorption spectra of propane (blue) and propane/water (red) at -5 $^oC$ and 1 atm. Note the altered peaks at 2930 and 2960 $cm^{-1}$. Reprinted with permission from Vu, Kälin, Shultz, *J. Phys. Chem. A.* 2010, 114, 6356-6360. Copyright 2010 American Chemical Society. ..... 23

Figure 4.6 Simulated IR spectrum of propane interacting with a water dimer at the methylene hydrogens. Calculation is performed at the B3LYP 6-31G* level of theory. Reprinted with permission from Vu, Kälin, Shultz, *J. Phys. Chem. A.* 2010, 114, 6356-6360. Copyright 2010 American Chemical Society. ..... 24

Figure 4.7 Deuterated propane $CD_3CH_2CD_3$ in $CCl_4$ at -5 $^oC$ from 1 to 55 atm. The C-H region shows a blue-shifting peak at 2960 $cm^{-1}$ indicating interaction between water and the methylene group. The inset shows the C-D region, which does not change in the presence of water. Reprinted with permission from Vu, Kälin, Shultz, *J. Phys. Chem. A.* 2010, 114, 6356-6360. Copyright 2010 American Chemical Society. ..... 25

Figure 4.8 Spectral deconvolution of propane in anhydrous $CCl_4$ at -5 $^oC$..... 27

Figure 4.9 Spectral deconvolution of propane in the presence of water in $CCl_4$ at -5 $^oC$. ..... 28

Figure 5.1 IR spectrum of 2.5 mM methanol in $CCl_4$ at -5 $^oC$ and 1 atm. The inset shows a magnified view of the H-bonded region. The peak at 3528 $cm^{-1}$ is due to H-bonded methanol polymers (about 2.3%). Reprinted with permission from Vu, Shultz, *J. Phys. Chem. A* 2011, 115, 998-1002. Copyright 2011 American Chemical Society. ..... 31

Figure 5.2 Spectra of water (blue dash), water with methanol (magenta dash-dot) and the difference (crimson solid) in $CCl_4$ at -5 $^oC$ and 1 atm. The H-bonded region (inset) shows a water-methanol H-bond resonance at 3440 $cm^{-1}$. Reprinted with permission from Vu, Shultz, *J. Phys. Chem. A* 2011, 115, 998-1002. Copyright 2011 American Chemical Society. ..... 32

Figure 5.3 Infrared spectra of 2.5 mM propane (green dot) and 1:1 propane-methanol mixture (orange dash dot) in $CCl_4$ at -5 $^oC$ and 1 atm. The spectra are vertically offset for clarity. Reprinted with permission from Vu, Shultz, *J. Phys. Chem. A* 2011, 115, 998-1002. Copyright 2011 American Chemical Society. ..... 34

Figure 5.4 $d_6$-Propane (2.5 mM) in $CCl_4$ at -5 $^oC$ and 1 atm. Main spectrum: methylene C-H modes in 1:1 mixture with water (purple solid) or methanol (orange dash-dot). The inset shows no spectral changes with the presence of either compounds. Reprinted with permission from Vu, Shultz, *J. Phys. Chem. A* 2011, 115, 998-1002. Copyright 2011 American Chemical Society. ..... 35

Figure 5.5 Methanol and water with (black dot) and without (magenta dash-dot) $d_6$-propane in $CCl_4$ at -5 $^oC$ and 1 atm (water concentration is 2.5 mM). Inset shows H-bonded resonances, evidence of propane-induced water clusters. Reprinted with permission from Vu, Shultz, *J. Phys. Chem. A* 2011, 115, 998-1002. Copyright 2011 American Chemical Society. ..... 36

Figure 5.6 C-H stretching modes of $d_6$-propane in $CCl_4$ at -5 $^oC$ and 1 atm showing interaction in the presence (black dot) and absence (purple solid) of methanol. Note the decrease in intensity of the 2960 $cm^{-1}$ peak as methanol is added. Reprinted with permission from Vu, Shultz, *J. Phys. Chem. A* 2011, 115, 998-1002. Copyright 2011 American Chemical Society. ..... 37

Figure 5.7 Proposed mechanism for inhibition of propane hydrate nucleation by methanol. Reprinted with permission from Vu, Shultz, *J. Phys. Chem. A* 2011, 115, 998-1002. Copyright 2011 American Chemical Society. ..... 39

Figure 6.1 Infrared spectra of 85 μm films of (a) water and (b) THF hydrate slurry (19 wt%) going through a temperature cyclce (red to blue to green). Water spectrum at 3 $^{o}$C remains unchanged while THF hydrate spectrum exhibits a red shift in the H-bonded region..... 42

Figure 6.2 Difference spectra of water/THF – water before (red) and after (green) the T cycle illustrating the shift from weak to stronger H-bonds in THF hydrate. ..... 43

Figure 6.3 Difference spectra of water/THF – water d) and after (green) the T cycle showing changes in the COC asymmetric stretch (1000-1200 cm$^{-1}$) and the $CH_2$ vibrations (2700-3100 cm$^{-1}$) of THF upon T cycling. The gas phase spectrum of THF (black curve) is included for comparison..... 44

Figure 6.4 Calculated gas-phase vibrational frequencies of the $\upsilon_{COC,asym}$ mode in THF in the presence (left) and absence of water at the B3LYP 6-31G* level of theory. Note the red shift of this mode in the H-bonded complex..... 45

Figure 6.5 Infrared spectra of THF and water in $CCl_4$ at -5 $^{o}$C at different THF concentrations from 5 mM to 25 mM. The spectrum of neat water (black) is included as a control. ..... 46

Figure 6.6 Magnification of the water region in Figure 6.5. Note the presence of the d-OH peak at higher THF concentrations. ..... 47

Figure 6.7 Spectra of 15 mM THF and water in $CCl_4$ at -5 $^{o}$C with (red) and without (blue) the presence of 1M NaI. ..... 48

Figure 7.1 Macroscopic sample of cyclopentane hydrate (left) formed by temperature cycling a 19 wt% solution and a phase-separated mixture of *n*-pentane and water at 3 $^{o}$C. Note that pentane is 5 times more soluble in water than cyclopentane. ..... 50

Figure 7.2 Infrared spectra of 85 μm films of (a) CP clathrate hydrate and (b) *n*-pentane/water mixture at 3 $^{o}$C before (red solid) and after (green dot) T cycling to -27 $^{o}$C. Presence of C-H resonances in (a) confirms incorporation of CP into the hydrate lattice. ..... 51

Figure 7.3 Absorption spectra of (a) saturated water, (b) 0.9 mM pentane + water, (c) 0.9 mM cyclopentane + water in $CCl_4$ at -5 $^{o}$C before and after T cycle. Note the H-bonded resonance at 3100-3500 cm$^{-1}$ and the *d*-OH feature at 3636 cm$^{-1}$ (inset) in (c). ..... 53

Figure 7.4 Infrared spectrum of a 1:1 v/v mixture of $H_2O$ and $D_2O$ in $CCl_4$ at room temperature. The free O-H stretch is observed at 3663 $cm^{-1}$ while the free O-D stretch is seen at 2692 $cm^{-1}$. ..... 54

Figure 7.5 Calculated infrared spectrum of a cyclopentane-water trimet complex (frequency is corrected by a factor of 0.967). The blue dashes represent van der Waals intercations between the oxygen atoms of water and the methylene hydrogen atoms of cyclopentane..... 56

Figure 9.1 Infrared spectrum of tetramethylammonium hydroxide in $CCl_4$ at room temperature (red) compared to that of neat water (blue). The presence of C-H resonances at 2800-3100 $cm^{-1}$ (inset) indicates the presence of the $(CH_3)_4N^+$ cation in solution. The difference spectrum (red minus blue) reveals a sharp peak, assigned to $OH^-$, at 3634 $cm^{-1}$. Reprinted with permission from Vu, Shultz, *Chem. Phys. Lett.* 2013, doi: 10.1016/j.cplett.2013.04.038 ..... 62

Figure 9.2 Infrared spectrum of 1:1 v/v mixture of $(CH_3)_4NOH$ and $D_2O$ in $CCl_4$ at room temperature showing the $OD^-$ stretch at 2682 $cm^{-1}$ (purple curve). Both the $OH^-$ and $OD^-$ resonances are distinguishable from the free OH and the free OD bonds in HOD. Reprinted with permission from Vu, Shultz, *Chem. Phys. Lett.* 2013, doi: 10.1016/j.cplett.2013.04.038. ..... 63

Figure 10.1 Infrared spectrum of 13.3 torr of water in the gas phase (red) and in supercritical argon (blue, $P_{Ar}$ = 54.26 atm) at room temperature. Note the broadened rotational lines and the vertical scale in the blue spectrum. ..... 64

Figure 10.2 Infrared spectrum of 13.3 torr of water in supercritical argon at 0 $^oC$ ($P_{Ar}$ = 54.26 atm). Note the presence of the H-bonded peak centered at 3300 $cm^{-1}$. ..... 65

Figure 10.3 Infrared spectrum of water and propane in 60.03 atm of argon at room temperature (left) and 0 $^oC$ (right). ..... 66

Figure 10.4 Water clusters created by dipropylamine and $d_6$-propane in $CCl_4$ at -5 $^oC$ and 1 atm. Inset shows the C-H region of $d_6$-propane in the presence of water and amine, contrasted with neat $d_6$-propane and $d_6$-propane-water. ..... 68

Figure 10.5 AOT reverse micelle (~12 nm) in $CCl_4$ as a function of temperature. The concentration of AOT is 1 mM and that of water is 20 mM..... 70

Figure 10.6 AOT reverse micelle (W = 20) in $CCl_4$ at -5 $^oC$ in the presence (black) and absence (blue) of propane. The difference spectrum (where the blue spectrum is scaled down by 25%) shows emergence of H-bonded resonances at 3100-3400 $cm^{-1}$ ..... 71

Figure 10.7 Infrared spectrum of water/silica powder in $CCl_4$ at -5 $^oC$ with (blue) and without (red) 15 mM THF..... 72

Figure 10.8 Infrared spectrum of a 1:1 mixture of water and benzene in $CCl_4$ at room temperature and 1 atm. The concentration of each species is 7.5 mM. Note the presence of the *d*-OH resonance between the symmetric and asymmetric stretches of water. ..... 74

Figure 10.9 Infrared spectrum of a 1:1 mixture of water and hexafluorobenzene at room temperature and 1 atm. The concentration of each species is 7.5 mM. ..... 75

Figure 10.10 Infrared spectrum of adventitious $CO_2$ in trichlorofluoromethane at room temperature showing the rotational lines of $CO_2$ at 3500-3800 $cm^{-1}$ (red). Addition of water (blue) enhances the rotational line intensity while the presence of 1M NaI quenches it (green). ..... 76

Figure 10.11 Infrared spectrum of 680 torr $CO_2$ (g) dissolved in another batch of $CCl_3F$ (yellow) compared to one that contains adventitious $CO_2$ in Figure 10.10 (red). The spectrum of gaseous $CO_2$ (black) is included for comparison. All spectra are obtained at room temperature. ..... 77

Figure 10.12 Unknown peak associated with free rotation of $CO_2$ in $CCl_3F$ compared to the spectrum of $C_6F_6$ in $CCl_4$ in the 2625-2725 $cm^{-1}$ region. ..... 78

# Chapter 1 Introduction

The major goal of this project is to unravel the molecular-level interactions at the beginning stages of clathrate hydrate nucleation. Clathrate hydrates are ice-like crystalline solids where small guest molecules are enclosed in cages form by tetrahedrally hydrogen-bonded water molecules under appropriate pressure and temperature conditions (*clathratus* in Latin means "protected by crossbars"). The existence of clathrate has been known for two centuries: the first discovery of $Cl_2$ hydrate was made in 1810 by Sir Humphry Davy, who at the time was studying the behavior of water and chlorine (then called oxymuriatic gas) at temperatures around 0 $^{o}$C.[1] Michael Faraday later prepared some crystals of this hydrate and proposed a stoichiometry of $Cl_2 \cdot 10H_2O$.[2] Throughout the years, clathrate hydrates have evolved from being just a laboratory curiosity to being recognized as a potential key player in numerous global environmental issues. Today, more than 100 clathrate hydrate systems have been identified.[3]

One of the most intriguing characteristics of clathrate hydrates is their high capacity for gas uptake. For example, the saturated aqueous solubility of methane at 25 $^{o}$C and 1 atm is $2.55 \times 10^{-5}$ while the methane mole fraction in the clathrate hydrate phase can be up to 0.142.[4] Naturally occurring methane hydrates, typically located in the Earth's permafrost and under the deep oceans, contain an estimated 10 Gtons of carbon, more than twice the amount found in all available sources of fossil fuels.[5-9] Knowledge of clathrates, however, is currently too limited to effectively harvest these materials. Besides, an economical procedure for extracting natural gases from clathrate deposits has yet to be developed. Even though the gas density in clathrates is still

smaller than that in the liquid phase, the energy required for hydrate formation is usually smaller than that for gas liquefaction.[10] For this reason, gas hydrates are not only an important source of energy but can also be an effective medium for gas storage and transportation. Greenhouse gas sequestration strategies involving hydrate systems, particular those of $CO_2$, have been actively explored as well.[11-13] On the other hand, clathrates hold the potential for a global warming catastrophe. An accidental release of methane gas due to destabilization of the permafrost could lead to a rapid rise in global temperature, which in turn causes the ocean to warm up and more methane to be released.[14]

*1.1 Structure of Hydrate Cages*

Natural gas hydrates generally crystallize into a cubic structure I (sI), a cubic structure II (sII), or a hexagonal structure H (sH) depending on the size of the guest molecules. In order to form a close-packed clathrate lattice, there needs to be a combination of small and large (and medium for structure H) cages for each structure. The tetrahedral coordinaton of water molecules tends to favor formation of pentagonal and hexagonal faces, the building blocks for convex polyhedra.[15] For example, the small cage of sI is a dodecahedron with 12 pentagonal faces (notated $5^{12}$) while the large cage of sI is a tetrakaidecahedron with 12 pentangonal and 2 hexagonal faces (notated $5^{12}6^2$). Figure 1.1 shows all the cage type necessary to form the sI, sII, and sH clathrates. A unit cell of sI consists of two $5^{12}$ and six $5^{12}6^2$ cages. A unit cell of sII is comprised of sixteen $5^{12}$ and eight $5^{12}6^4$ cages. A unit cell of sH contains three $5^{12}$, two $4^35^66^3$ and one $5^{12}6^8$ cages.[16] The cubic sII lattice is the most frequently encountered hydrate structure in nature.[17] In order to occupy and stabilize the structure, the guest molecules must neither be too big nor too small with respect to the cavity size. A molecular diameter to cavity diameter ratio of approximately 0.75 appears to be optimal.[18]

| | Structure I ($CH_4$, $C_2H_6$, $CO_2$) | | Structure II ($C_3H_8$, Ar, $H_2$) | | Structure H (Xe, cycloheptane) | | |
|---|---|---|---|---|---|---|---|
| | **Small** | **Large** | **Small** | **Large** | **Small** | **Medium** | **Large** |
| Description | $5^{12}$ | $5^{12}6^2$ | $5^{12}$ | $5^{12}6^4$ | $5^{12}$ | $4^3 5^6 6^3$ | $5^{12}6^8$ |
| Average Cavity Radius (Å) | 3.95 | 4.33 | 3.91 | 4.73 | 3.94 | 4.04 | 5.79 |
| Water Molecules per Cavity | 20 | 24 | 20 | 28 | 20 | 20 | 36 |

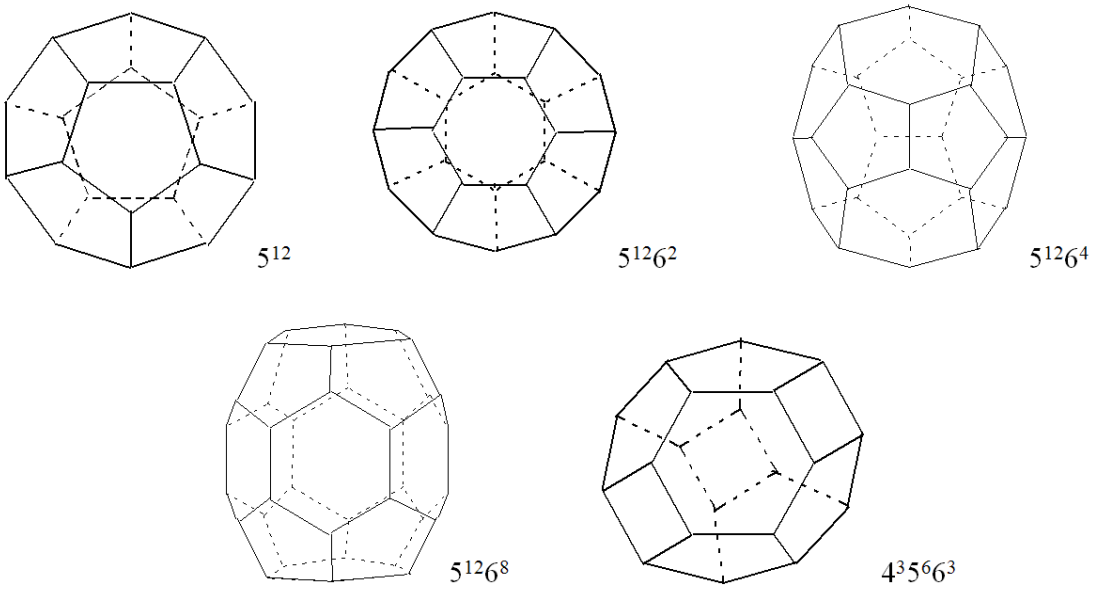


**Figure 1.1** Types of clathrate cavities and their corresponding shapes. Hydrogen atoms in the host frameworks are omitted for clarity.

The high hydrocarbon concentration in the clathrate suggests the existence of a stabilizing interaction between these water cages and the guest molecules. Theoretical modeling has found such an attractive force between water and methane, where the latter acts as an H-bond acceptor resulting in pentacoordinate carbon.[19] However, other calculations have shown that these water cavities are inherent unstable in the absence of a guest molecule.[20,21]

*1.2 Nucleation models*

Previous investigations of clathrate formation fall broadly under three categories: analyzing the crystal structure and composition of the products,[22-24] determining T, P conditions for formation,[25-29] and measuring growth kinetics.[30-35] From a macroscopic thermodynamic perspective, these studies have successfully characterized and yielded ample information about the hydrate formation process. However, microscopic phenomena such as nucleation are not well-understood to date.[36,37] In principle, the onset of hydrate crystallization requires formation of water clusters around the guest and the joining of these clusters to create a critical clathrate nucleus.[38,39] The fact that different guests form clathrates at different conditions and with different cage structures indicates that the molecular-level mechanism by which clathrates nucleate is rather complex and might be guest-dependent. A number of theories have been proposed in the literature to explain how hydrate nucleation is achieved.

*a) Labile Cluster Hypothesis*

Developed by Sloan, this theory is based on the notion that water tends to form small clusters around dissolved gas molecules.[40] When a gas molecule is dissolved in water, the amount of water molecules that cluster around the guest depends on the coordination number. For example, propane has a coordination number of 28. An sII clathrate that is made up of $5^{12}$ and $5^{12}6^4$ cages requires 20 and 28 water molecules respectively to form the water cage. This means that if the dissolved molecules have coordination numbers 20 and 28, then clusters of the right size would be formed and the nucleation of a clathrate would be more likely. Thus, by having only one type of guest molecule nucleation is inhibited, since the clusters would all be a certain size, and in order to form a clathrate structure some of the clusters would have to make or break new hydrogen bonds with other water molecules to make clusters of a different size. Once

clusters of the right size form, they may link together with other clusters to form larger networks, preferentially next to the water surface which eventually would become the clathrate structure.

*b) Nucleation at Interface*

Based on the idea that clathrate nucleation occurs on the vapor side of a liquid/vapor interface,[41] this theory suggests that gas molecules adsorbs onto the aqueous surface and are trapped in the center of partially completed water cavities. Once these clusters are formed, dangling hydrogen atoms extend out to attract other water molecules. Then either by additional water molecules binding to the existing cavities or new gas molecules entering cavities that begin to form, the lattice begins to extend along the liquid/vapor interface. This process is dynamic, so as new cages are added onto the existing lattice, other cages may be disintegrating simultaneously.[18]

*c) Local Structuring Hypothesis*

This theory comes out of molecular dynamics (MD) modeling of a liquid $CO_2$-water interface[42] and is later reinforced by simulations of methane-water system.[43] These calculations point out that the labile clusters discussed in the first theory are more likely to disintegrate than to grow as more clusters link together. Here the water and guest molecules are arranged by thermal fluctuations until their respective orientations reach those in the clathrate lattice by chance. These nascent configurations are stabilized after exceeding a certain size and hydrate crystals start growing. This is hence a stochastic event triggered by random motions of water molecules around the dissolved guest species.

A pictorial representation of these models can be seen in Figure 1.2. The first two models are grouped together due to their similarity in predicting the appearance of hydrate prestages.

The guest is expected to play an active role in these models as they involve formation and diffusion of partial cages. In contrast, the local structuring hypothesis indicates a spontaneous formation with any precursor clusters, implying a less prominent role for the dissolved guests in promoting nucleation.

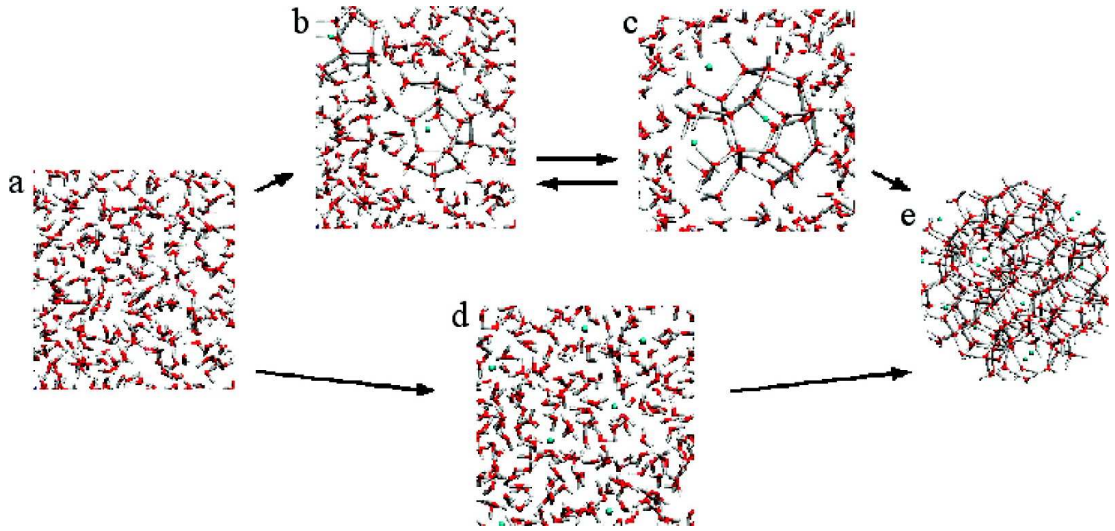


**Figure 1.2** Comparison of the cluster nucleation theory (a-b-c-e) and the local structuring hypothesis (a-d-e). (a) Water without dissolved guest molecules. (b) Cluster form immediately after dissolution of guest molecules. (c) Cluster prestages agglomerate by sharing faces (equilibrium with step b). (d) No cluster fomration after dissolution of guest molecules. (e) Hydrate nucleation. Reprinted with permission from Lehmkühler et al. *J. Am. Chem. Soc.* **2009,** *131*, 585-589. Copyright 2009 America Chemical Society.

While these theoretical models have been useful in providing visualization of the hydrate nucleation process, direct experimental evidence remains scant and controversial. X-ray reflectivity measurements of the $CO_2$-water interface[36] together with several MD simulations[38,42,43] have supported the local structuring hypothesis. Yet, Raman microscopy of an ice-hexane/THF interface[44] and a number of MD simulations[15,45,46] have, on the other hand, hinted at the presence of a hydrate precursor. The purpose of this project is to help bridge this experimental gap by attempting to unravel the molecular interactions between the guest species and small water clusters at the initial stages of nucleation.

# Chapter 2 Experimental Apparatus

## *2.1 High-Pressure Cell*

A grade 316 stainless steel optical cell is custom-built for use in high pressure experiments (Figure 2.1). The cell is usually assembled with 12-mm thick $CaF_2$ windows, resulting in an optical path length of 2.7 cm (when 8-mm thick quartz windows are used, the cell path length is 3.6 cm). The cell has a 5.5 in. diameter, a 0.75 in. clear aperture, a total volume of 120 mL and is designed to hold up to 90 atm of pressure (the safety diaphragm typically ruptures when pressure exceeds 75 atm). The cell-body seal consists of low-density polyethylene gaskets sandwiched between the stainless steel parts. A key design feature is that the internal pressure presses the windows against the O-ring flanges to seal the optical ports. The cell is easily disassembled enabling window replacement or substitution of materials as needed.

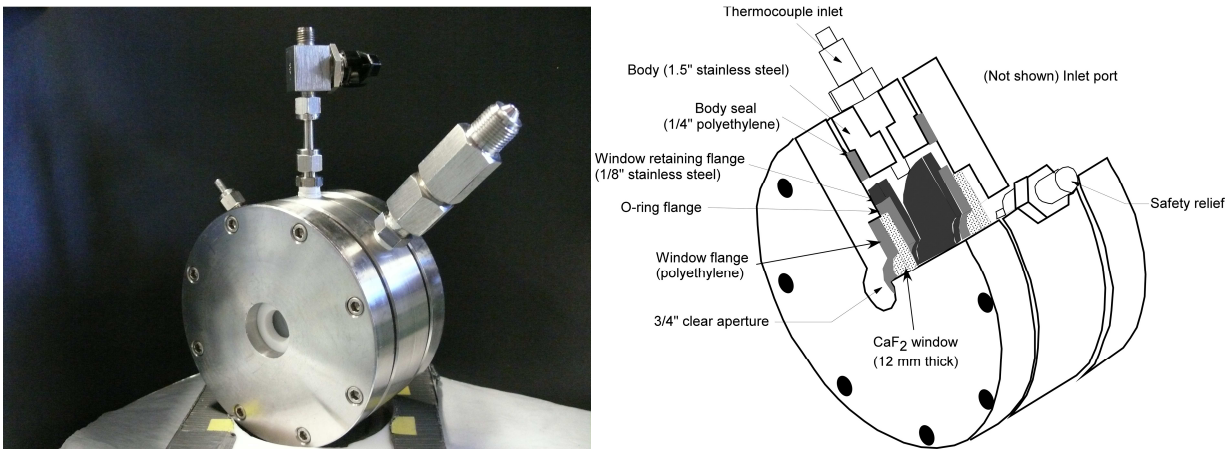


**Figure 2.1** High-pressure stainless steel cell (left) and its internal design (right). The cell cut-out is reprinted with permission from Vu, Kälin, Shultz *J. Phys. Chem. A* **2010,** *114,* 6356-6360. Copyright 2010 American Chemical Society.

*2.2 Cold Finger*

The primary function of the cold finger is to condense large quantities of gases at liquid nitrogen temperature that are later expanded to pressurize the high pressure cell. It can also be used as pressure chambers to make laboratory samples of propane clathrate from ice-gas mixture, as presented in Chapter 3. The cold finger (Figure 2.2) is made out of corrosion-resistive grade 316 stainless steel with a total height of 5.54 in. Its walls are 0.25 in. thick and can withstand pressures up to 120 atm safely. The cold finger has a lid with five screws at the top. The two pieces are held together by a chemical grade Teflon o-ring flange which is secured by knife-edges from both top and bottom. The total internal volume is 106 mL.

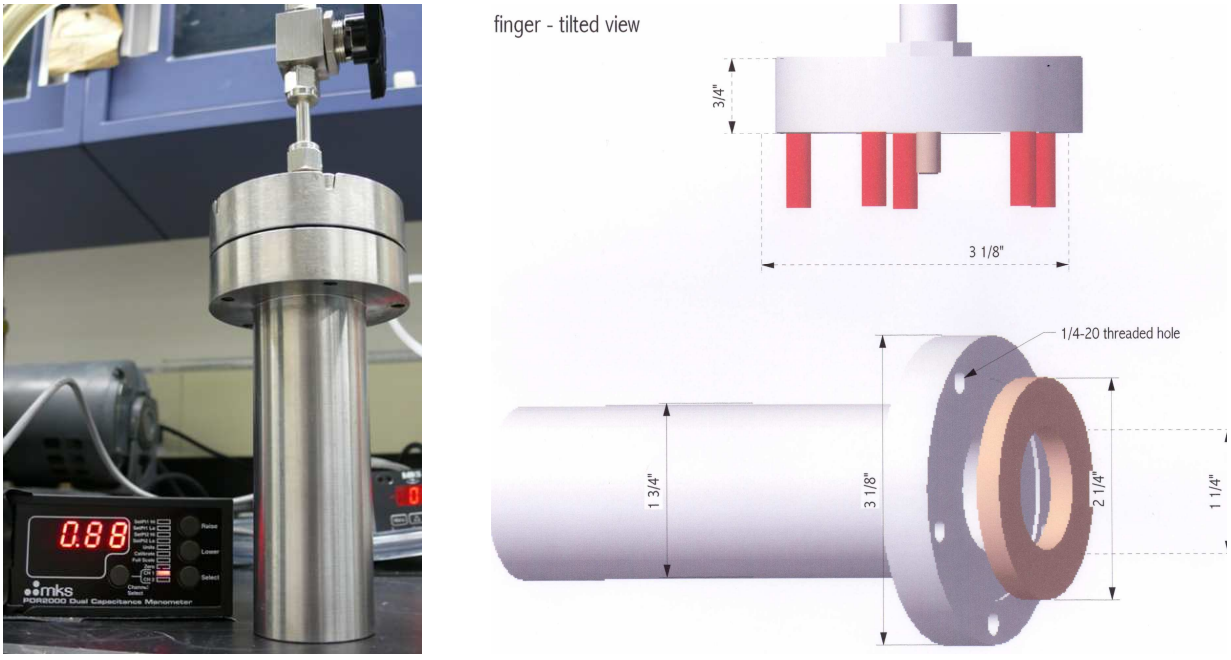


**Figure 2.2** Front view of the cold finger (left) and its schematic design (right)

*2.3 Silanized Glass Cell*

For experiments at ambient pressure, a glass cell with epoxy-glued quartz windows (2.5 cm path length) is used. The cell has a cold finger for gas condensation when needed (Figure 2.3). Both the cell and the quartz windows are silanized before use to prevent water adhesion to internal surfaces.

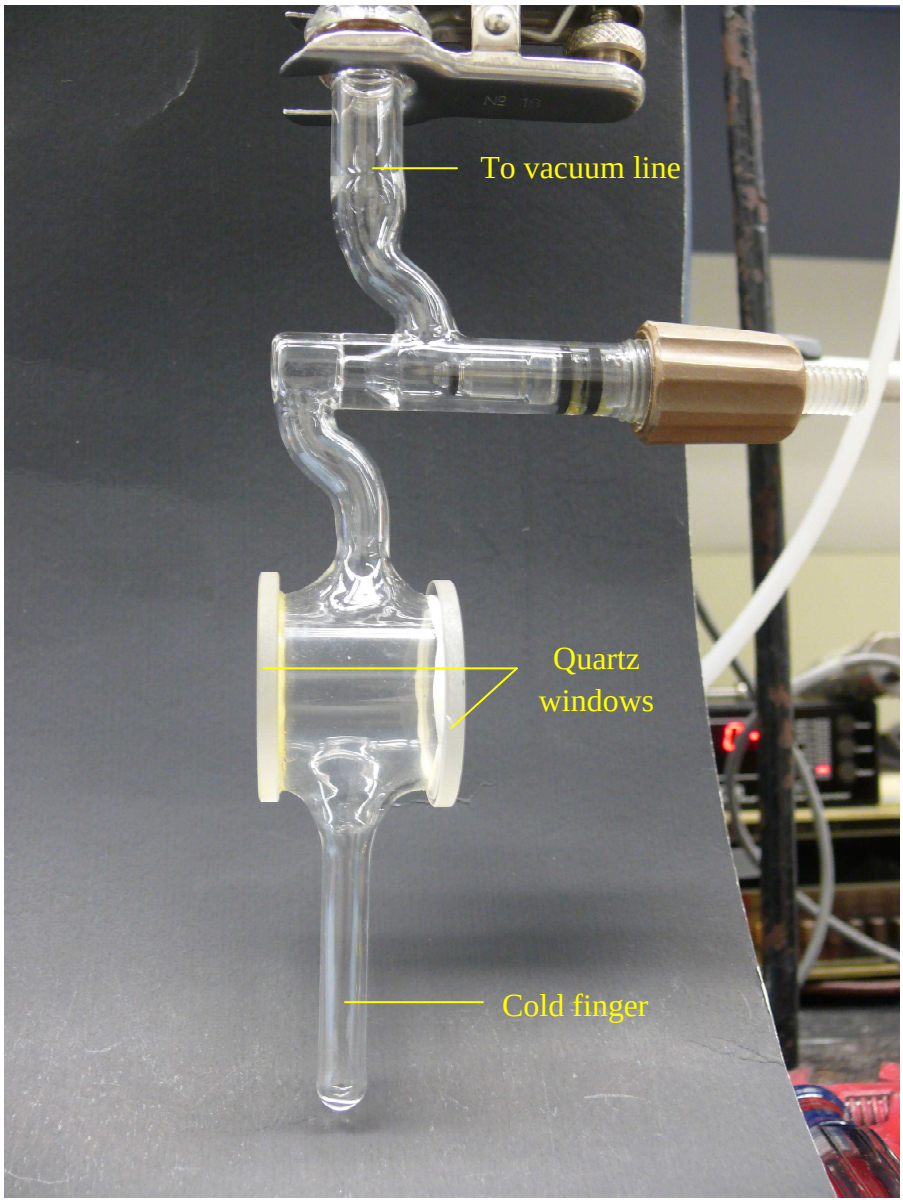


**Figure 2.3** Picture of silanized glass cell (1 in. path length) with cold finger attached.

The silanization procedure is as follows: the glass cell and quartz windows are first cleaned by soaking in NOCHROMIX concentrated sulfuric acid overnight. These items are then submerged in nanopure water (18 MΩ.cm, Barnstead UV radiated) for 3 days to leach out the residual acid (water bath is changed daily to maintain a fresh supply). Meanwhile, the silanization solution is made by mixing 10% v/v diethoxydimethylsilane (Sigma-Aldrich, 97%) with ethanol (Sigma-Aldrich, HPLC grade) on a stirrer plate. The pH of a newly prepared solution is around 6.5 and is adjusted to 4.5 – 5.5 by adding a few drops of glacial acetic acid (Sigma-Aldrich, 99.99+%). The glassware are then transferred into the silanization solution and allowed to soak overnight. The silanol is decanted the next day and the glassware rinsed with ethanol to remove excess material. Finally, the cell and windows are heated for 15 minutes in an 80 $^{o}$C oven to cure the silane layer.

*2.4 Vacuum Line*

The vacuum line used to prepare samples was initially a glass manifold attached to a mechanical pump. To facilitate working with high pressures, it was later switched to ¼" stainless steel tubing (Figure 2.4). In this vacuum line, there are 4 ports with valves leading to other attachments, one of which is permanently attached to U-tubes containing Drierite® and KOH pellets to remove moisture and $CO_2$ from compressed gases and another port is permanently attached to a pressure transducer (MKS Baratron model 722A, range: 0 – 1.3 atm) for pressure monitoring. The remaining 2 ports are switched among the cold finger, the stainless steel cell, and the glass cell when they are in use. Higher pressures are measured with an MKS Baratron model 890B (range: 0 – 207 atm) transducer.

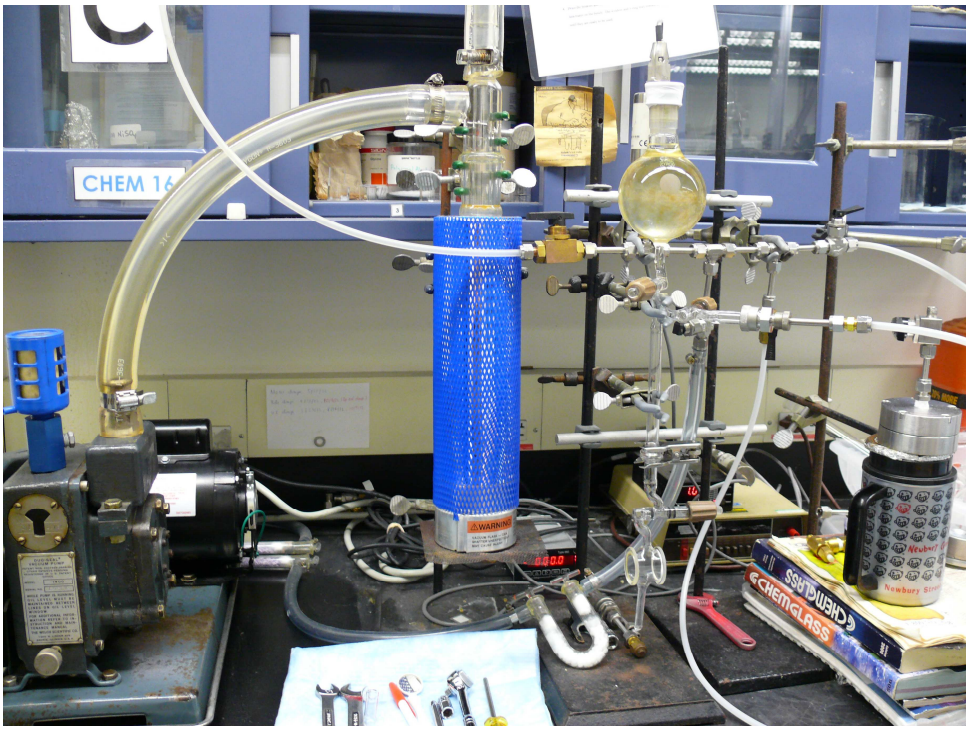


**Figure 2.4** Stainless steel vacuum line used for sample preparation.

*2.5 Preparing Dried Carbon Tetrachloride*

"Anhydrous" carbon tetrachloride (Sigma-Aldrich, > 99.5 % anhydrous) contains some adventitious water and needs to be further dried before use. For this procedure, silica gel (Sigma-Aldrich, grade 03, mesh 8) is added first to the bottom of a flask sealed with a greased rubber septum. The silica gel must be evacuated for at least 24 hrs before injection of carbon tetrachloride in order to be effective in removing water. Carbon tetrachloride comes in a bottle with a septum cap, and disposable syringes are used to extract it. Upon introduction of carbon tetrachloride into the silica reservoir, the flask warms up due to an exothermic reaction. Thus, lowering the temperature could in principle be advantageous to the drying process and may be attempted in the future. A layer of Teflon tape is usually wrapped around the rubber septum to help seal the silica reservoir after injection of carbon tetrachloride. When not in use, the syringe

needle is stored in a desiccator to prevent absorption of moisture from the atmosphere. Carbon tetrachloride is typically usable after 1-2 days of drying; best results are often achieved after 1 week (no detectable water signal in the infrared spectrum).

*2.6 Recycling the Silica Gel*

After being used to dry carbon tetrachloride, the wet silica gel can be recycled by heating in an oven at 105 $^{o}$C for 4 h with occasional stirring and evacuated in a sealed flask for at least 48 h before the next batch of $CCl_4$ is introduced. The beads may turn brownish following the heat treatment but are still effective in removing water. A representative spectrum of $CCl_4$ dried with recycled silica gel is shown in Figure 2.5. The absorption features below 3200 cm$^{-1}$ is due to hydrocarbon impurities in carbon tetrachloride. The intensity of these C-H resonances varies from batch to batch, and can readily be taken out after background subtraction.

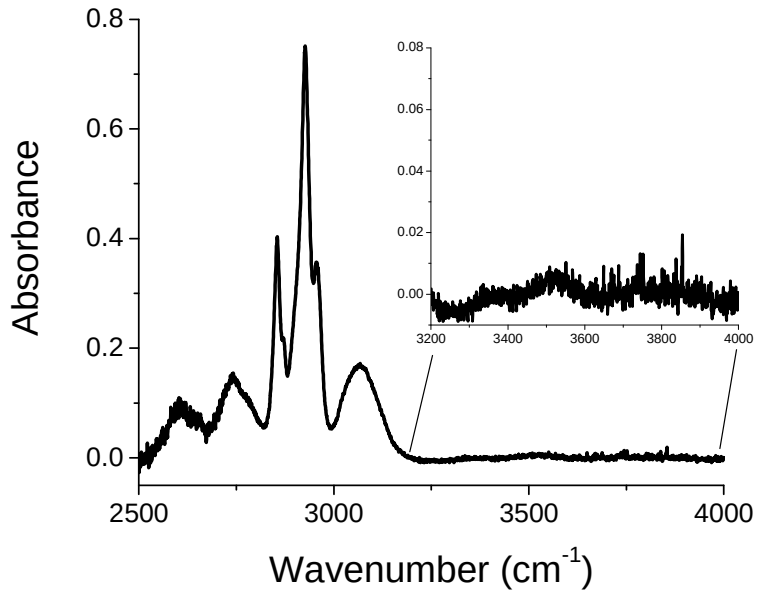


**Figure 2.5** Typical absorption spectrum of dried carbon tetrachloride at room temperature using recycled silica gel. The inset is an expanded view of the O-H region showing the absence of detectable water absorption.

*2.7 Spectra Acquisition*

FTIR absorption spectra are obtained at 64 scans and 1 $cm^{-1}$ resolution using a Nicolet Magna-IR 760 spectrometer equipped with a DTGS KBr detector. Typical collection time for a spectrum at these settings from 1000-4000 $cm^{-1}$ is 2.5 min. The software program used to run the spectrometer is Omnic E.S.P version 4.1a. The sample compartment is always purged with dry nitrogen gas for at least 4 h before use to completely remove spectral interference from atmospheric moisture and $CO_2$.

Before taking a sample spectrum, a background spectrum of the nitrogen-purged chamber is obtained. The spectrum of the evacuated cell with the purged chamber as the background is often obtained before a background spectrum of the evacuated cell is taken. After the cell is filled with dried carbon tetrachloride, its spectrum is taken with the evacuated cell as the background to check for residual water. Finally, a background spectrum of the dried carbon tetrachloride is taken. The spectra of both the evacuated cell and the dried carbon tetrachloride are used as background for all the samples. This protocol is repeated for every new batch of carbon tetrachloride and whenever the cell is reassembled.

*2.8 Theoretical Calculations*

All *ab initio* density functional theory calculations are performed at the B3LYP 6-31G* level of theory using Spartan ’08 suite of programs.[47] Sample calculated results for various parameters of a single water molecule are shown in Figure 2.6. The computational approach always yields an overestimate of the absolute vibrational frequencies and these are usually corrected by a factor of 0.96. A system is determined to have reached a true local energy minimum when imaginary vibrational frequencies are absent at the end of the calculation.

| Normal mode | Gas-phase frequency ($cm^{-1}$) | Calculated frequency ($cm^{-1}$) | Calculated relative intensity |
|---|---|---|---|
| Bend ($\nu_2$) | 1595 | 1711 | 75.71 |
| Symmetric stretch ($\nu_1$) | 3657 | 3730 | 1.71 |
| Asymmetric stretch ($\nu_3$) | 3756 | 3851 | 19.30 |

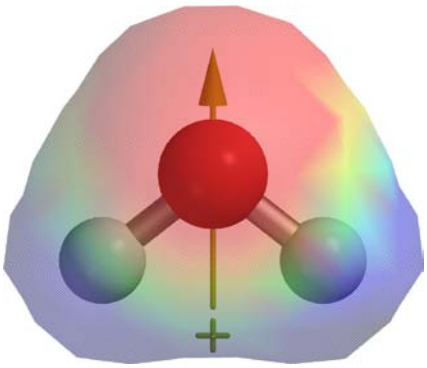

Dipole moment: 2.10 Debye

O-H bond length: 0.969 Å

Partial charges: – 0.934 (O)

+ 0.467 (H)

**Figure 2.6** Vibrational frequencies, dipole moment, bond length, and partial charges of a single water molecule in the gas phase calculated at the B3LYP 6-31G* level with Spartan '08 software. The potential surface plot is displayed on an absolute scale showing negative potential as red, positive as blue, and green as neutral. The bounding surface is 92.6%.

# Chapter 3 Propane Clathrate - A Macroscopic Perspective

*3.1 Making Propane Clathrate Sample*

One of the initial survey experiments is to synthesize macroscopic samples of propane clathrate in a reproducible manner. A procedure for making clathrates, adapted from the Janda group,[48] using the cold finger and the available materials in the lab is described below.

The cold finger is prechilled in a bucket of ice to ensure that its temperature is around 0 $^{o}$C; the interior of the cold finger has to be clean and maintained dry at all times. A shallow dewar is filled with liquid nitrogen, into which droplets of nanopure water are added with a glass pipette to make small pellets of ice. The ice particles are then transferred to a prechilled coffee grinder that turn the ice pellets into a fine snowy powder (snow is used as the starting material to maximize the surface area exposed to the gas). Next, the powdered ice is transferred into the cold finger where it is tightly packed with a copper plunger that had also been cooled. The

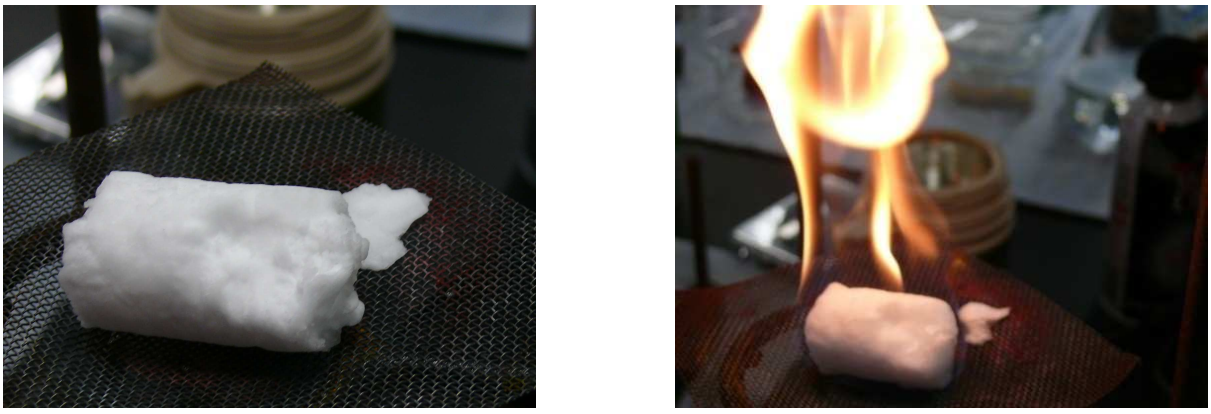

**Figure 3.1** A laboratory sample of propane clathrate after being extracted from the cold finger (left) and set on fire (right)

critical part of this entire process is to prevent melting of the snow powder. The cold finger is subsequently sealed, pressurized with approximately 4 atm of propane and kept in an ice-filled cooler for at least 24 hrs. Clathrates begin to form after a few hours as the pressure inside the cold finger drops to around 1.5 atm. After the incubation period, the excess propane gas is released while the cold finger is kept around 0 $^{o}$C. A solid piece of propane clathrate can readily be extracted and burned to confirm incorporation of the guest gas into the hydrate lattice (Figure 3.1).

*3.2 Observation and Preservation*

The texture of the clathrate sample mostly depended upon how fine the ice powder and how dry the cold finger are initially. Once pressure is relieved, the clathrate sample is metastable for several minutes at ambient conditions but eventually disintegrates upon the release of propane gas.

Since propane clathrate samples could be easily prepared on a daily basis, a method of storing them is also explored. It is found that a sample of propane clathrate quenched in liquid nitrogen and stored at 1 atm and -20 $^{o}$C could be preserved for days or even weeks, and would still burn when exposed to a flame. However, it is unclear whether the structure of the clathrate cages themselves is retained or how much propane is still present after the long period of storage.

# Chapter 4 Propane-Water Interaction

* Materials presented in this chapter are published in *J. Phys. Chem. A* **2010,** 114, 6356-6360 and in *Physics and Chemistry of Ice*, Hokkaido University Press: pp 147-152 (2011)

This project aims to elucidate the early stages of clathrate nucleation by experimentally probing the attractive interaction between clathrate guests and a small number of water molecules. The focus of this chapter is on propane, which forms a metastable sII hydrate under moderate pressures (1.5 – 5.5 atm) near the freezing point of water. In the hydrate lattice, propane only occupies the large $5^{12}6^4$ cages while leaving the smaller $5^{12}$ cavities vacant (the size ratio of a propane molecule to the radius of the $5^{12}6^4$ cage is 0.943, whereas that ratio is 1.25 for the $5^{12}$ cage).[49] In principle, a small secondary guest such as methane can be introduced to occupy the empty $5^{12}$ cages and form a binary hydrate. Inclusion of the smaller guests typically enhances the stability of the entire hydrate lattice and lowers the pressure required for formation. This approach has been successfully explored as a means for storage and transportation of methane at low pressure.[50] Another study has found that incorporation of xenon gas into the propane/water mixture accelerates the rate of propane enclathration from 3 days to 20 min.[51]

The experiments reported herein make use of infrared spectroscopy to investigate the water-propane interactions by means of matrix-isolation in carbon tetrachloride. Since water is sparingly soluble in this hydrophobic solvent, it exists as isolated monomers with ambient thermal energies in the $CCl_4$ matrix (in contrast with classic isolation techniques, which require cryogenic temperatures). The saturated concentration of water in $CCl_4$ is found to be 7.5 mM at room temperature.[52,53] The infrared spectrum of water consists of the symmetric stretch ($A_1$ symmetry), the asymmetric stretch ($B_1$ symmetry) and the rotational wings underlying the two

fundamental vibrations. Compared to gas-phase water, the relative intensity of the symmetric stretch is significantly enhanced, indicating an interaction between water and carbon tetrachloride via the oxygen lone pair. From symmetry consideration of the $C_{2v}$ point group, the broadened rotational structure is determined to be the P, R branches associated with the asymmetric stretch (Figure 4.1). This is due to a nearly free $C_2$ rotation ($R_z$) of water in the carbon tetrachloride matrix while the other two rotations are hindered, a consequence of the direct interaction between oxygen lone pair and the somewhat electropositive carbon atom in $CCl_4$.

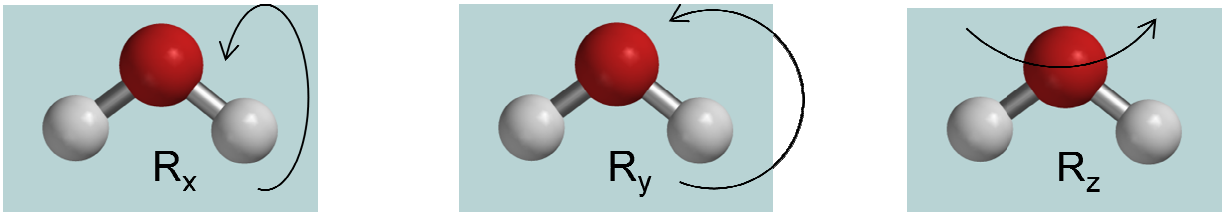


$B_x = 27.8761\ cm^{-1}$ $B_y = 9.2877\ cm^{-1}$ $B_z = 14.5074\ cm^{-1}$

**Figure 4.1** Rotational axes of water and the associated rotational constants in the gas phase. In carbon tetrachloride, $R_x$ and $R_y$ are quenched while the rotational lifetime of $R_z$ is shortened (0.83 ps). The value of $B_z$ in $CCl_4$ is 14.8 $cm^{-1}$.[53]

A limited water environment greatly assists investigation of interactions between water and other small molecules, as cluster formation can be readily detected via the well-established O-H frequency shift and oscillator strength enhancement of H-bonded water. Propane is also soluble in $CCl_4$ making this solvent an excellent medium to probe water-propane interaction.

*4.1 Sample Preparation*

A saturated solution of water in $CCl_4$ is made by loading 90 μL of nanopure water and 90 mL of dried $CCl_4$ into the high pressure cell. The mixture is then sonicated for 1 hr at room

temperature and left to equilibrate overnight at -5 $^{o}$C. The resulting sample is found to be stable for weeks, giving a reproducible IR spectrum. Addition of propane into the water-$CCl_4$ solution is done as follows: the solution is first frozen at -80 $^{o}$C and the head space is evacuated. 25 torr of propane is then introduced into the 30-mL head space via stainless steel tubing and the cell is warmed up to -5 $^{o}$C over a period of 24 hrs to reach equilibrium. This freeze-thaw procedure allows for accurate pressure reading of propane, as the desired amount of propane is much less than the vapor pressure of carbon tetrachloride in the head space. Samples at higher pressures (23 – 55 atm) are prepared by pressurizing the cell with dry argon gas. Propane (Airgas, instrument grade), $d_6$-propane $CD_3CH_2CD_3$ (C/D/N Isotopes, 99.8% atom D) and argon (Airgas, ultrahigh purity) are all treated with Drierite® and KOH prior to use to remove residual water and $CO_2$. Temperature is measured with an RTD thermistor (Digi-Key, MA100 series) and controlled to within ±0.1 $^{o}$C during data acquisition using a cold nitrogen gas stream at 235 psi.

*4.2 Water in $CCl_4$ at -5 $^{o}$C*

The absorption spectrum of water at -5 $^{o}$C, the target temperature for propane hydrate formation, is shown in Figure 4.2. The peaks at 3615 and 3705 $cm^{-1}$ are the well-known symmetric and asymmetric stretches of water. The inset is a magnified view of the 3100-3400 $cm^{-1}$ region, showing the absence of any hydrogen-bonded resonance. These features together with the distinct rotational structure similar to that at room temperature demonstrate that water still exists primarily as monomers in $CCl_4$ at -5 $^{o}$C. The simplicity of the spectrum, relative to gas-phase water, is again the result of a free rotation about the symmetry axis ($R_z$) and highly quenched rotational motions about the two axes perpendicular to the symmetry axis ($R_x$, $R_y$). The $R_z$ rotation is diagnostic of water monomers interacting via the lone pair, hence free of donor

interactions.[54] On the basis of the known saturated concentration of water in $CCl_4$ at room temperature, the concentration of water monomers at -5 $^oC$ is determined to be 3 mM.

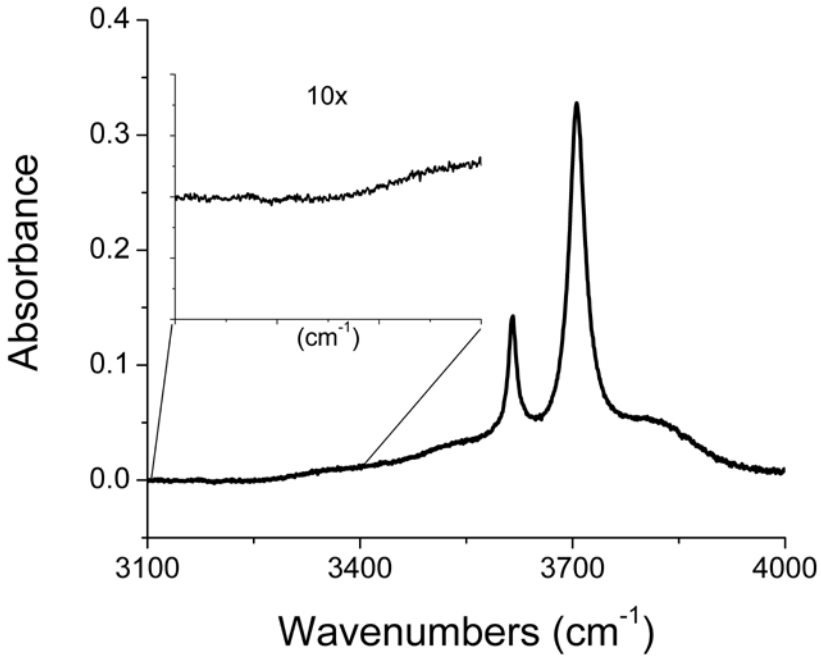


**Figure 4.2** Absorption spectrum of a saturated solution of water in $CCl_4$ at -5 $^oC$ and 1 atm. The inset shows a magnified view of the H-bonded region. Reprinted with permission from Vu, Kälin, Shultz, *J. Phys. Chem. A* **2010,** 114, 6356-6360. Copyright 2010 American Chemical Society.

*4.3 Propane/Water System in $CCl_4$*

In contrast to neat water, the spectrum of the propane/water mixture in $CCl_4$ exhibits a number of important features (these are more clearly seen in the difference spectrum of water/propane – water in Figure 4.3). The first feature is the negative water peaks at around 3700 $cm^{-1}$, indicating an overall decrease in the water monomer concentration. In addition, two hydrogen-bonded resonances appear at 3162 and 3338 $cm^{-1}$ upon addition of propane into the system (inset). These spectral changes suggest the incorporation of water monomers into H-

bonded clusters in the presence of propane. The frequency and the narrowness of the H-bonded peaks imply the presence of strong and highly directional H-bonds. Since the interaction between water and propane is expected to be weak, the emergent resonances are attributed to water-water H-bonds. The intensity of these resonances also suggests that the number of propane-induced water clusters is relatively small.

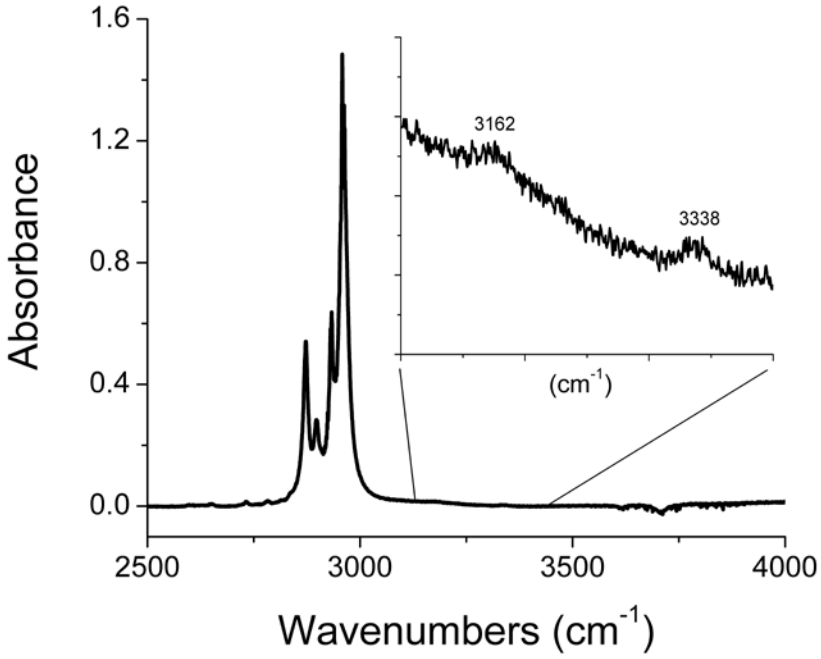


**Figure 4.3** Difference spectrum of water/propane minus water in $CCl_4$ at -5 $^{o}$C and 1 atm. Note the negative water peaks around 3700 $cm^{-1}$ and the appearance of H-bonded resonances at 3162 and 3338 $cm^{-1}$ (inset). Reprinted with permission from Vu, Kälin, Shultz, *J. Phys. Chem. A.* **2010,** 114, 6356-6360. Copyright 2010 American Chemical Society.

Figure 4.4 juxtaposes the O-H stretch region of water with and without propane (the spectra have been vertically offset for clarity). In the presence of propane (panel a), a new peak emerges at 3643 $cm^{-1}$ right in between the symmetric and asymmetric stretches of water. This feature is characteristic of a dangling OH (*d*-OH) bond that results from decoupling of the two

O-H oscillators when water acts as a proton donor. Consistent with the H-bonded resonances in Figure 4.3, this *d*-OH peak provides additional evidence for water cluster formation. The intensity of the *d*-OH feature is further enhanced by addition of argon pressure, in tandem with the decrease in intensity of both the symmetric and asymmetric stretches of free water monomers. In contrast, pressurization of the water/$CCl_4$ system in the absence of propane shows neither a reduction of water monomer intensity nor any evidence for a *d*-OH. The constancy of the neat water spectrum affirms that water does not self-associate at -5 $^{o}$C even under pressure, but only does so in the presence of the propane guest gas.

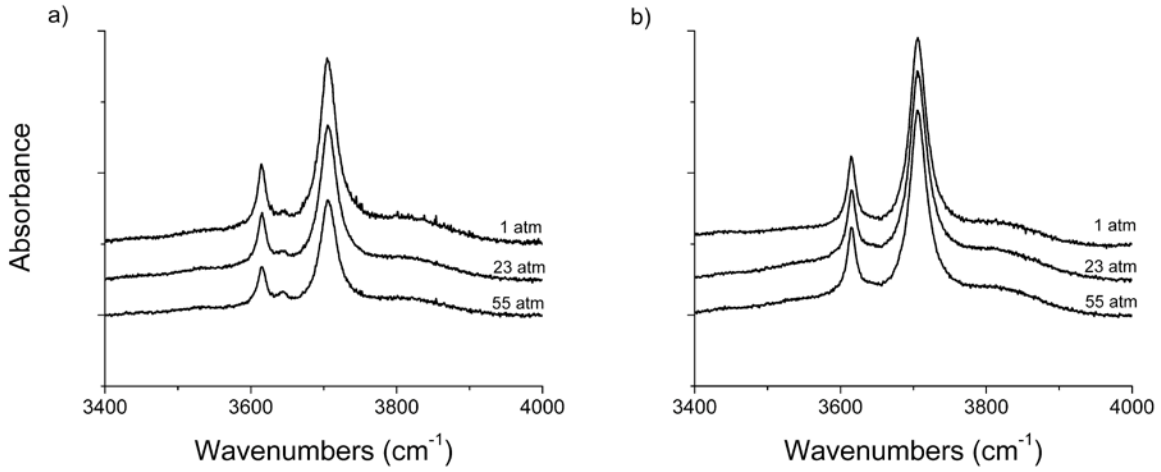


**Figure 4.4** The O-H stretch region of water at -5 $^{o}$C from 1 to 55 atm in the presence (a) and absence (b) of propane. The total pressure is adjusted by addition of dry argon gas. The spectra are vertically offset for clarity. Reprinted with permission from Vu, Shultz, *Physics and Chemistry of Ice 2010*, Hokkaido University Press: pp 147-152 (2011). Copyright 2011 Hokkaido University Press.

*4.4 Pinpointing Propane-Water Interaction*

Since propane induces clustering of water molecules, an attractive interaction is expected between the two species. In order to determine the nature of this interaction, it is instructive to examine the vibrational resonances of propane in $CCl_4$ and compare those to propane in the

presence of water. These spectra are shown in Figure 4.5. Note that addition of water induces splitting of the propane resonances, especially at around 2930 $cm^{-1}$ and 2960 $cm^{-1}$. However, the infrared spectrum of propane in this region is rather complicated due to coupling among the eight C-H bonds, leading to C-H collective modes. A density functional theory calculation is hence performed to simulate the IR spectrum for a propane-water dimer complex at various configurations. Interaction between the oxygen atom of water and the C(2) methylene hydrogens yield a good agreement between the simulated spectrum (Figure 4.6) and the experimental spectrum (Figure 4.5, red). The global energy at this configuration is found to be more stable than one in which the water dimer interacts with propane via the methyl groups by about 460 J/mol.[54]

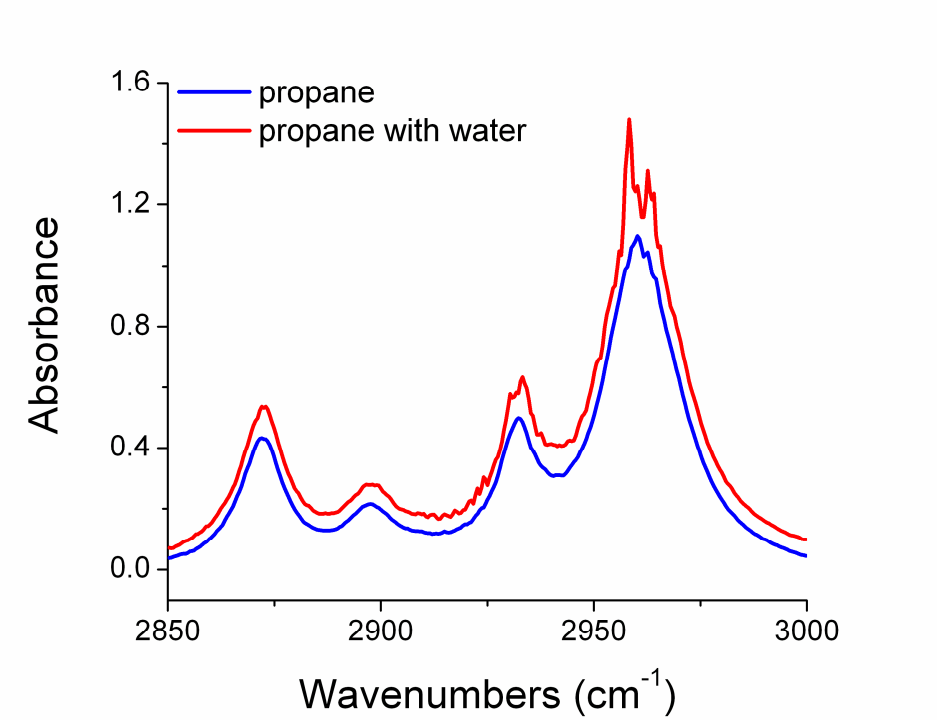


**Figure 4.5** Absorption spectra of propane (blue) and propane/water (red) at -5 $^{o}$C and 1 atm. Note the altered peaks at 2930 and 2960 $cm^{-1}$. Reprinted with permission from Vu, Kälin, Shultz, *J. Phys. Chem. A.* **2010,** 114, 6356-6360. Copyright 2010 American Chemical Society.

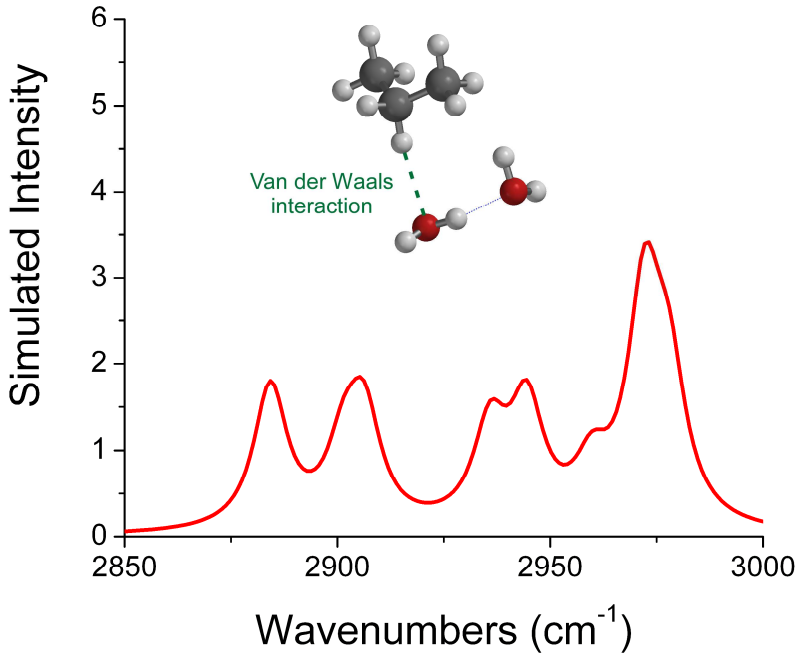


**Figure 4.6** Simulated IR spectrum of propane interacting with a water dimer at the methylene hydrogens. Calculation is performed at the B3LYP 6-31G* level of theory. Reproduced with permission from Vu, Kälin, Shultz, *J. Phys. Chem. A.* **2010,** 114, 6356-6360. Copyright 2010 American Chemical Society.

To assess the validity of the DFT model, isotopically substituted $CD_3CH_2CD_3$ ($d_6$-propane) is used to prepare propane/water samples in $CCl_4$. Due to the significant mass difference between deuterium and hydrogen, the methyl C-H modes are decoupled from those of the methylene. Accordingly, the spectrum of $d_6$-propane in $CCl_4$ (Figure 4.7) is separated into two sets of bands: the $CH_2$ symmetric and asymmetric stretches are observed at 2870 $cm^{-1}$ and 2930 $cm^{-1}$, respectively, while the $CD_3$ methyl vibrations are grouped together at 2000 - 2250 $cm^{-1}$. The latter region is virtually unaffected by the addition of water (inset), in contrast to the C-H region where the presence of water causes a third peak resonance to appear at around 2960 $cm^{-1}$. This feature establishes the existence of an interaction between water and $d_6$-propane, and is assigned to a C-H···O interaction at the methylene group.

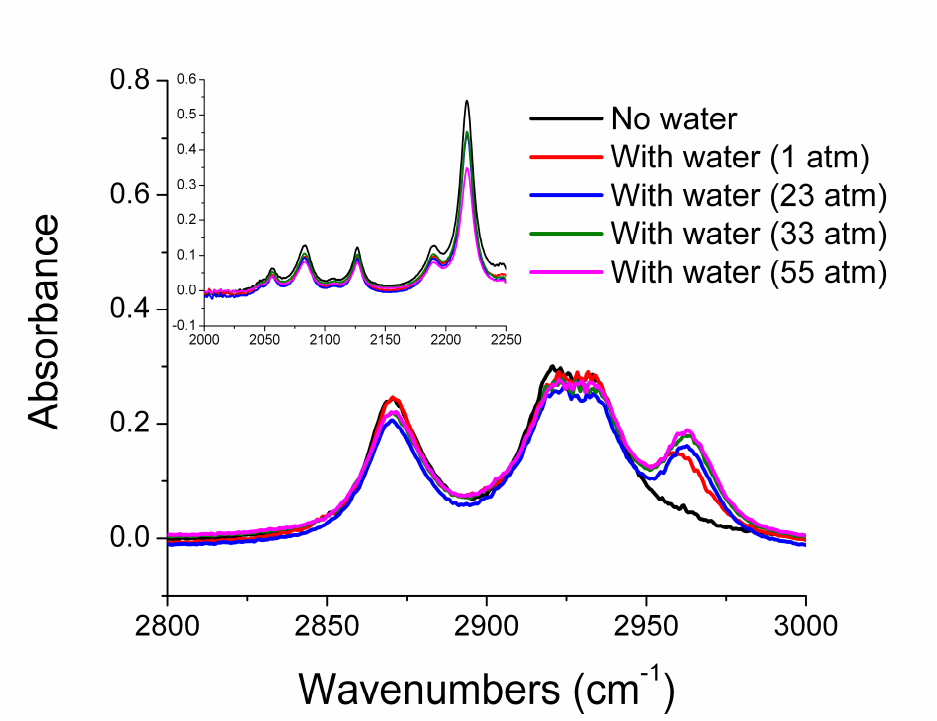


**Figure 4.7** Deuterated propane $CD_3CH_2CD_3$ in $CCl_4$ at -5 $^oC$ from 1 to 55 atm. The C-H region shows a blue-shifting peak at 2960 $cm^{-1}$ indicating interaction between water and the methylene group. The inset shows the C-D region, which does not change in the presence of water. Reproduced with permission from Vu, Kälin, Shultz, *J. Phys. Chem. A.* **2010,** 114, 6356-6360. Copyright 2010 American Chemical Society.

Note that the new 2960 $cm^{-1}$ peak appears on the high frequency side of the two fundamental $CH_2$ symmetric and asymmetric vibrations, and an increase in pressure causes it to further blue shift. This observation is not unique: other instances of a blue shifting interaction between hydrocarbons and water have been documented in the literature.[55-57] Usually there is a red shift upon interaction due to the increase in effective mass and weakening of the donor bond. How then does the C-H oscillator shift to the blue? The answer lies in the distinctive characteristic of carbon to adapt various hybridization states, ranging from *sp* to $sp^3$. When water interacts with propane, electron density from the oxygen lone pairs is transferred into the LUMO

of the hydrocarbon, which is centered on the C(2) atom. Some of that electron density goes into its antibonding orbital, resulting in the weakening of one of the tetrahedral bonds around the central $sp^3$ carbon and modification of the hybridization state towards $sp^2$. The higher *s* character consequently strengthens the remaining C-H bonds and gives rise to the blue shift, relative to the unperturbed propane. Shifting electron density along with proton transfer is also involved in water-catalyzed reactions.[58] Since methyl groups generally lack the requisite antibonding LUMO to accept electron density, the blue shift of the C-H resonance by water in $d_6$-propane strongly supports the methylene C(2)-H as the site of interaction.

It could be argued that deuterium substitution at the C(1) and C(3) methyl groups biases the water interaction due to difference in the zero-point energy between H and D. However, deuterium bonding is often favored over hydrogen bonding. At the ice surface, for instance, dangling O-H bonds are much more preferred over dangling O-D bonds.[59] In the case of water dimers in krypton matrices,[60] D-donation is favored over H-donation by 60 $cm^{-1}$. Thus, deuterating the methyl groups, if anything, would bias interaction toward those sites. The observation in the $d_6$-propane/water system is that water interacts solely with the methylene hydrogens. Thus, deuterium substitution does not bias the interaction, thereby supporting the conclusion that the C(2)-H group is also the site of interaction in nondeuterated propane. Interaction at the methylene group is further supported by a recent computer modeling of solvation free energies for nonpolar solutes in water.[61] Modeling results find that the center regions of alkanes tend to form interaction "hot spots" for first-shell water molecules. Interactions at the methyl end-groups, on the other hand, are found to be less favorable. The interaction between the water oxygen and the propane methylene hydrogens is thus responsible for the clustering of water in $CCl_4$ and could account for the initial stage of clahrate nucleation.

From the deuterated propane study and Spartan simulation, the vibrational modes of propane in $CCl_4$ can be resolved with least-square fittings. Figure 4.8 and Figure 4.9 show spectral deconvolutions and the tentative peak assignments for neat propane and propane with water, respectively. The anhydrous spectrum (Figure 4.8) has contributions from five resonances in the 2800-3000 $cm^{-1}$ region: two methylene modes (symmetric/asymmetric), two methyl modes (symmetric/asymmetric), and one coupled vibration ($CH_2$+$CH_3$). By comparison, the propane spectrum in the presence of water (Figure 4.9) is resolved into seven IR-active modes. It is easily identifiable that some of the spectral features of propane have noticeably changed under the influence of water. In particular, water's interaction with C(2)-H blue shifts its resonance to 2964 $cm^{-1}$, in agreement with the deuterated propane results. The presence of water also slightly splits the C(2)-H asymmetric stretch into two components, evidenced by a new band at 2933 $cm^{-1}$. This feature is assigned to the dangling C(2)-H coupled to the adjacent methyl group, which causes it

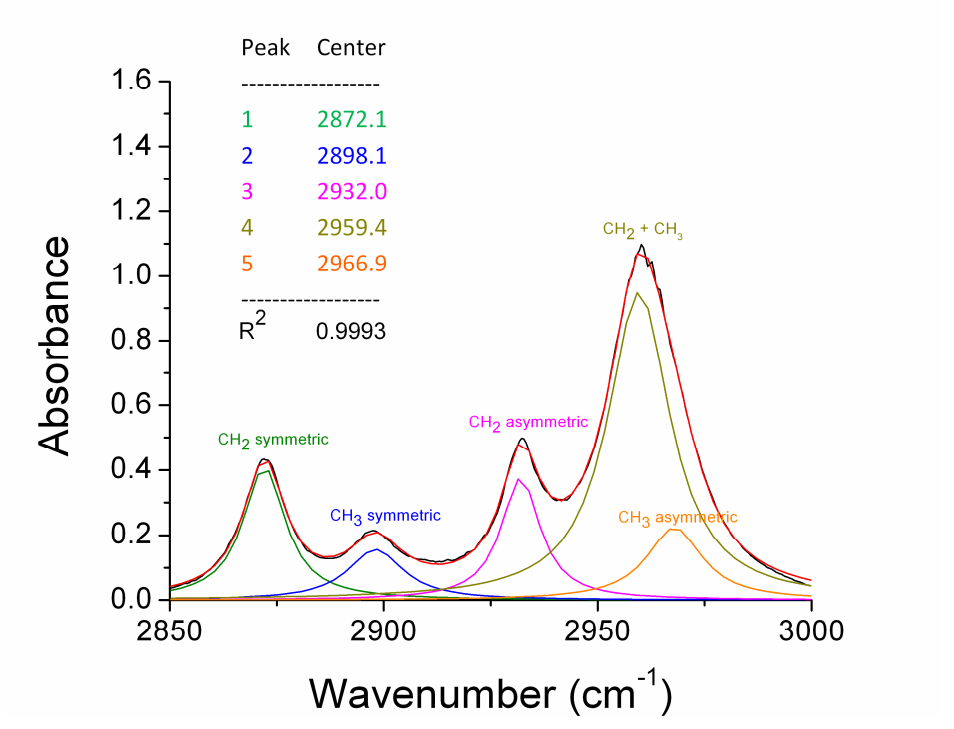


**Figure 4.8** Spectral deconvolution of propane in anhydrous $CCl_4$ at -5 $^oC$.

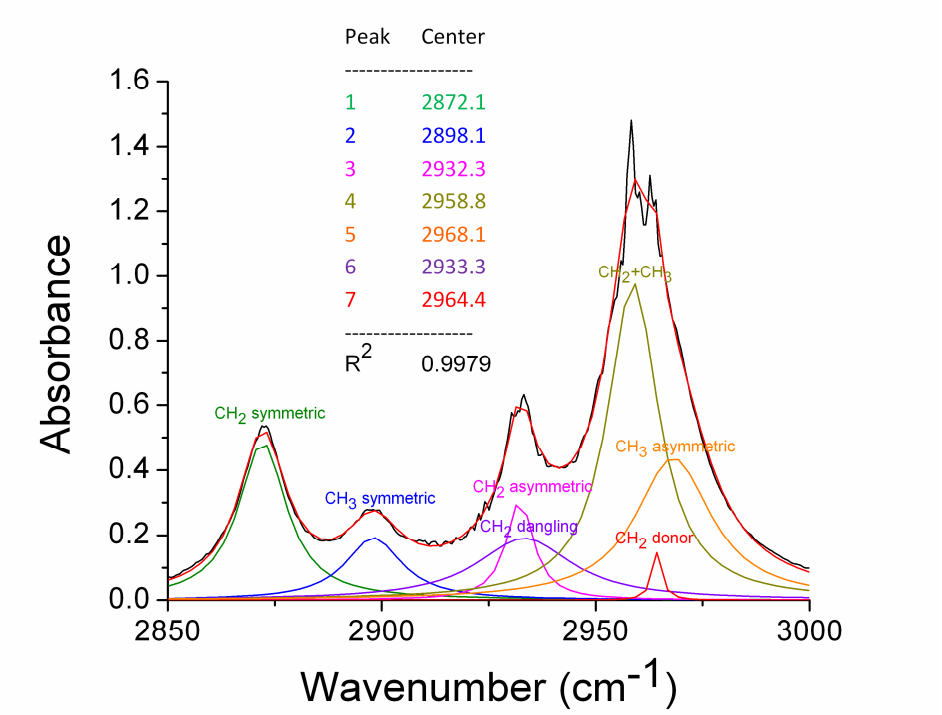


**Figure 4.9** Spectral deconvolution of propane in the presence of water in $CCl_4$ at -5 $^{o}$C.

to blue shift instead of being in between the $CH_2$ symmetric and the asymmetric stretch. These assignments are also consistent with the $CH_3$ symmetric stretches (blue peak) being intact and the $CH_3$ asymmetric stretches (which coupled to the dangling C(2)-H) being slightly enhanced (orange peak) upon addition of water. Changes to the propane vibrational signatures together with the $d_6$-propane results provide compelling evidence for an attractive interaction between the oxygen lone pair of water and the electropositive methylene hydrogens of propane. This van der Waals-type interaction is likely responsible for the propane-induced formation of water cluster in $CCl_4$.

# Chapter 5 Inhibition of Propane-Water Interaction by Methanol

* Materials presented in this chapter are published in Vu, T. H.; Shultz, M. J. *J. Phys. Chem. A* **2011,** *115 (6),* 998-1002

In addition to their potential as a viable solution to growing energy demands, clathrate hydrates formed during processing and transportation of natural gases have been a long standing nuisance for the petroleum industry – most recently demonstrated in the 2010 Gulf of Mexico oil spill. The conditions in the pipelines – high gas pressures and subzero temperatures - are particularly favorable to clathrate formation. Once formed, hydrate growth is accelerated by high-velocity movement of the gas stream, which collects small crystals of nascent hydrate seeds until the line becomes entirely plugged.[62] This clogging phenomenon builds up hydrostatic pressure that can be as high as several hundred atmospheres, causing serious safety hazards and substantial economic risk.[63] Thus, there exists a need for the development of effective clathrate inhibitors. Compounds such as alcohols, glycols, and antifreeze proteins are well-known thermodynamic inhibitors as they typically shift the hydrate formation conditions to higher pressures and/or lower temperatures. However, this strategy requires significant inhibitor concentrations, which means that, as the T, P conditions in the field become more severe, the cost for preventing hydrate formation also increases dramatically.[63]

Methanol is a popular commercial choice for hydrate inhibition in natural gas pipelines and has been widely used for many years. Nevertheless, little is known about the mechanism by which the inhibitory action occurs on the molecular level aside from the general consensus that methanol interferes with the growth of extended hydrogen-bonded networks of water. Several contradictory reports, both experimental and theoretical, on the effects of methanol on various

clathrate systems have also added another layer of complexity. For example, at 50% v/v methanol is an inhibitor[64] but at below 20% v/v, it has been shown to tremendously accelerate clathrate formation from deuterated ice.[65] At cryogenic temperatures, methanol also forms mixed clathrates with small ethers[66] and facilitates the crystallization of these hydrates from solution nanodroplets.[67] Theoretically, molecular dynamics simulations suggest that conventional hydrate structures containing methanol as a guest species are inherently unstable at any temperature.[68] This model is supported by dielectric relaxation and differential scanning calorimetry experiments that show no evidence for existence of any type of methanol hydrate.[3]

This chapter deals with the molecular-level interactions among water, propane, and methanol with an intention to provide insights into the role of methanol as an inhibitor in the nucleation step of propane hydrate. The experimental approach is based upon earlier results of the water/propane system in $CCl_4$ presented in Chapter 4. Since methanol is completely miscible with carbon tetrachloride,[69,70] a desired methanol-water-propane concentration ratio can be readily obtained and their mutual interactions investigated. The next section details the sample preparation procedure while the rest of the chapter will be focused on discussing the experimental findings.

*5.1 Sample Preparation*

A subsaturated solution of water in $CCl_4$ are made by sonicating 10 μL of nanopure water with 90 mL of dried $CCl_4$ in the high pressure cell for 1 h and leaving it to equilibrate at -5 $^oC$ overnight. This results in a reproducible infrared absorption spectrum with $[H_2O]$ = 2.5 mM. Methanol (Fisher Scientific, ACS certified) is added volumetrically at the desired concentration of 2.5 mM and is prechilled at -5 $^oC$ before injection to avoid temperature variation. Propane

(both $C_3H_8$ and $CD_3CH_2CD_3$) is introduced by means of condensing 2.5 atm of gas into a 2-mL stainless steel vessel and expanding into the head space of the optical cell.

*5.2 Methanol in $CCl_4$ at -5 $^oC$*

The infrared spectrum of methanol in $CCl_4$ has been well-characterized at room temperature for several concentrations.[69-73] The initial phase of the experiment is thus to examine the methanol spectrum at -5 $^oC$, the temperature at which water-propane interaction is investigated in Chapter 4. Figure 5.1 shows the absorption spectrum of 2.5 mM methanol in $CCl_4$, which is dominated by a sharp free O-H peak at 3643 $cm^{-1}$ (FWHM = 17 $cm^{-1}$). The inset is a magnified view of the H-bonded region showing a small, broad shoulder at 3528 $cm^{-1}$. The

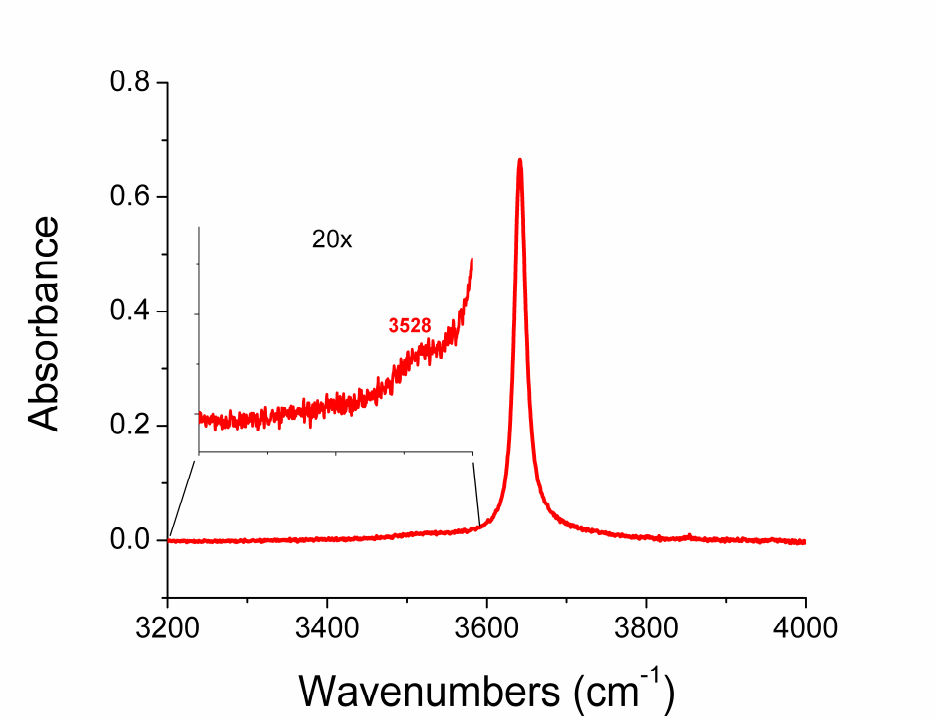


**Figure 5.1** IR spectrum of 2.5 mM methanol in $CCl_4$ at -5 $^oC$ and 1 atm. The inset shows a magnified view of the H-bonded region. The peak at 3528 $cm^{-1}$ is due to H-bonded methanol polymers (about 2.3%). Reprinted with permission from Vu, Shultz, *J. Phys. Chem. A* **2011,** 115, 998-1002. Copyright 2011 American Chemical Society.

latter peak is red-shifted by 115 $cm^{-1}$ from the free O-H, and is thus assigned to the donor O-H of hydrogen-bonded methanol dimers. These attributes are similar to other reports for room-temperature solutions of $CH_3OH$ and $CD_3OH$ in $CCl_4$.[69-73] The integrated area of the 3528 $cm^{-1}$ peak is ~ 8% of the total area. Since there is a factor of 3.5 gain in oscillator strength upon H-bonding,[69] the dimer concentration is less than 2.3%. Figure 5.1 thus indicates that at 2.5 mM concentration, almost 98% of methanol molecules exist as monomers in $CCl_4$ at -5 $^oC$.

*5.3 Methanol-Water Interaction*

In order to examine the effect of methanol on the water-propane interaction, it is useful to first examine the direct interaction between methanol and water. Figure 5.2 displays the

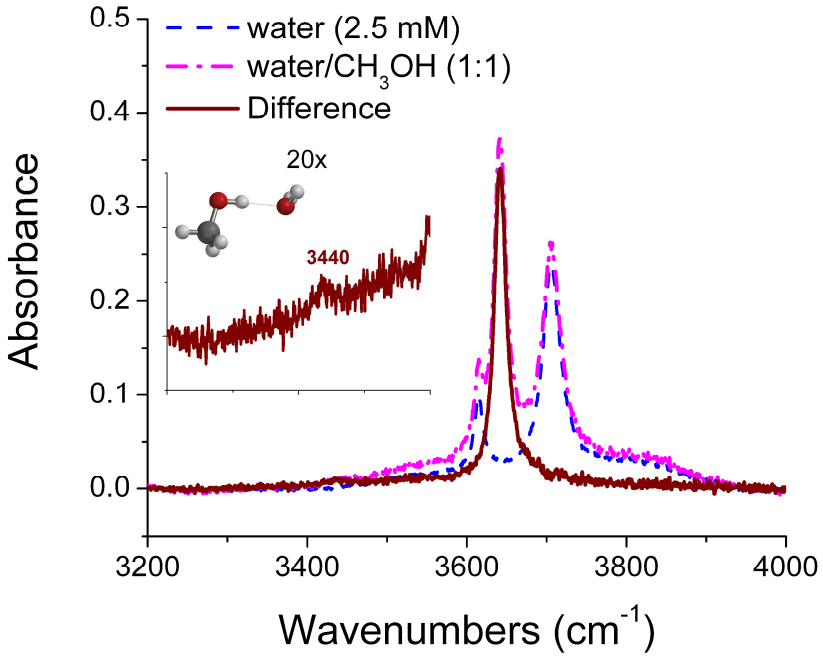


**Figure 5.2** Spectra of water (blue dash), water with methanol (magenta dash-dot) and the difference (crimson solid) in $CCl_4$ at -5 $^oC$ and 1 atm. The H-bonded region (inset) shows a water-methanol H-bond resonance at 3440 $cm^{-1}$. Reprinted with permission from Vu, Shultz, *J. Phys. Chem. A* **2011,** 115, 998-1002. Copyright 2011 American Chemical Society.

spectrum of a 1:1 mixture of methanol and water at 2.5 mM for each species. The selection of this particular concentration is mainly dictated by the saturation limit of water, which is 3 mM at -5 $^{o}$C (Section 4.2). A subsaturated water concentration is chosen so that a pure methanol-water monomeric interaction can be identified in the absence of excess water. In Figure 5.2, the water spectrum (blue dash) is comprised of the familiar symmetric stretch at 3615 $cm^{-1}$, the asymmetric stretch at 3705 $cm^{-1}$, and the underlying rotational bands. Upon the addition of 2.5 mM methanol (magenta dash-dot), the difference spectrum (water/methanol minus water) exhibits two features of interest. Compared to that of neat methanol in $CCl_4$ (Figure 5.1), the intensity of both the free and H-bonded methanol clusters decreases. In addition, a new H-bonded resonance centered at 3440 $cm^{-1}$ is observed (inset). This emergent feature is not due to methanol clusters because that resonance occurs at 3528 $cm^{-1}$. It is also not due to H-bonded water clusters because water does not self-associate at -5 $^{o}$C. Therefore, the H-bonded resonance is assigned to direct methanol-water H-bonds. Comparison of the integrated area of the free methanol peak in Figure 5.1 and Figure 5.2 indicates that ~ 40% of methanol monomers form H-bonds with water. The intensity loss of the methanol free O-H peak suggests that methanol donates a proton to water in making the H-bonded complex. This is consistent with the difference spectrum (Figure 5.2) showing only the methanol peak in the 3600 – 3800 $cm^{-1}$ region; the spectral features of water have not changed. It is known that water interacting through the oxygen lone pairs has an unaltered spectral profile, aside from a slightly enhanced oscillator strength (illustrated by the small blip at 3705 $cm^{-1}$ in the difference spectrum). Thus the H-bonded feature at 3440 $cm^{-1}$ is assigned to the O-H stretch of methanol acting as a proton donor to water. A similar interaction has been observed on the surface of $D_2O$ ice, where methanol is found to adsorb with the hydroxyl group pointing towards the dangling lone pairs.[74] Previous dielectric relaxation measurements[3] have

also indicated that methanol prefers formation of a 1:1 complex with water. Such a 1:1 complex is consistent with the present experimental observation of only one narrow hydrogen-bonded resonance. Based on this assumption, the association constant K can be calculated as follows.

$$K \equiv \frac{[CH_3OH \cdot H_2O]}{[CH_3OH][H_2O]}$$

The initial concentration of methanol is 2.5 mM, 40% of which is bound in the 1:1 complex with water. Hence, the equilibrium concentration of free methanol is 1.5 mM and that of the complex is 1 mM. This results in K = 4.4 x $10^2$, a rather modest binding constant.

*5.4 Methanol-Propane Interaction*

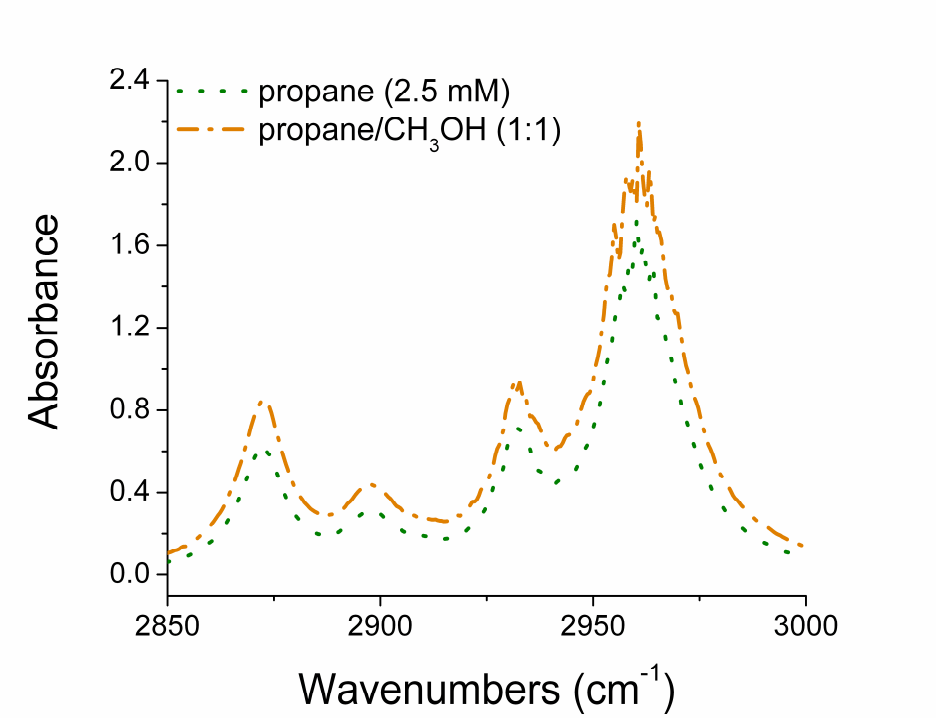


**Figure 5.3** Infrared spectra of 2.5 mM propane (green dot) and 1:1 propane-methanol mixture (orange dash dot) in $CCl_4$ at -5 $^oC$ and 1 atm. The spectra are vertically offset for clarity. Reprinted with permission from Vu, Shultz, *J. Phys. Chem. A* **2011,** 115, 998-1002. Copyright 2011 American Chemical Society.

The next objective is to inspect the methanol-propane interaction. Figure 5.3 shows the spectrum of 2.5 mM propane in the presence (orange dash-dot) and absence of methanol (green dot). This concentration is chosen because methanol primarily exists as monomers at 2.5 mM. Notice that the addition of methanol virtually does not affect the C-H stretching modes of propane, in contrast with the water-propane system (Figure 4.5). This suggests that there is not a strong or specific interaction between the two species.

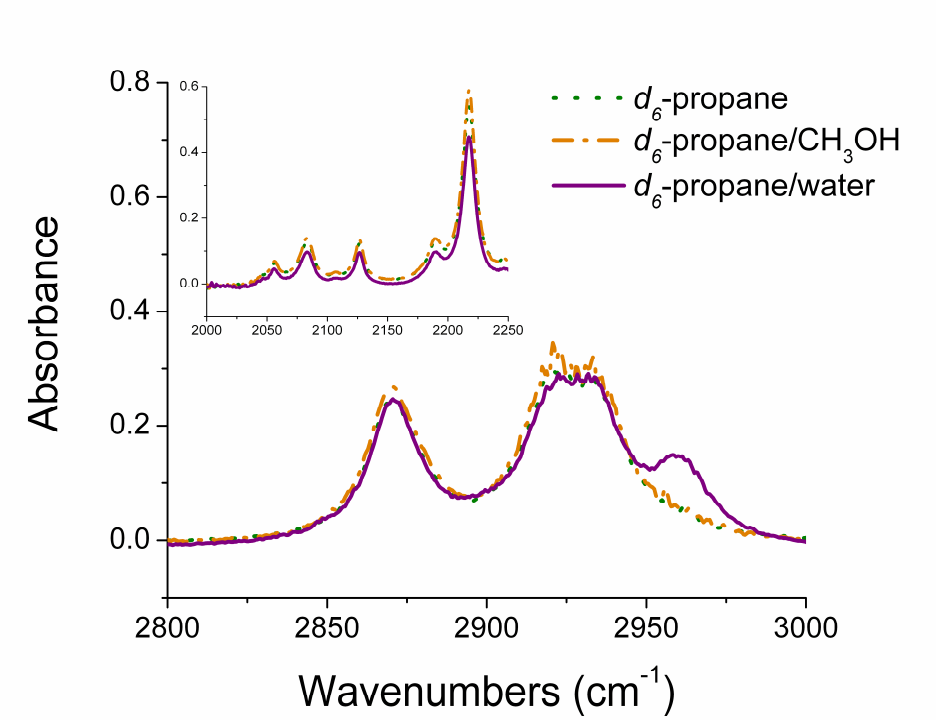


**Figure 5.4** $d_6$-Propane (2.5 mM) in $CCl_4$ at -5 $^oC$ and 1 atm. Main spectrum: methylene C-H modes in 1:1 mixture with water (purple solid) or methanol (orange dash-dot). The inset shows no spectral changes with the presence of either compounds. Reprinted with permission from Vu, Shultz, *J. Phys. Chem. A* **2011,** 115, 998-1002. Copyright 2011 American Chemical Society.

As in the case of the water-propane system in which isotopic substitution of propane proves valuable in determining the site of interaction (Section 4.5), $CD_3CH_2CD_3$ ($d_6$-propane) is similarly combined with methanol here. These data are presented in Figure 5.4, where the

spectrum of the $d_6$-propane-water mixture has also been included to facilitate comparison. For neat $d_6$-propane (green dot), the peaks at 2870 and 2930 $cm^{-1}$ are due to the $CH_2$ symmetric and asymmetric stretches, respectively. Addition of methanol does not alter the spectrum while a blue-shifting feature appears at 2960 $cm^{-1}$ for the case of water. The methyl C-D region at 2000-2250 $cm^{-1}$ (inset) is unaffected by the presence of either water or methanol. Thus with the isotopic substitution, it is clear that water interacts with propane via the methylene groups while methanol does not.

*5.5 Ternary System*

Examination of the pairwise interactions among water, propane, and methanol establishes

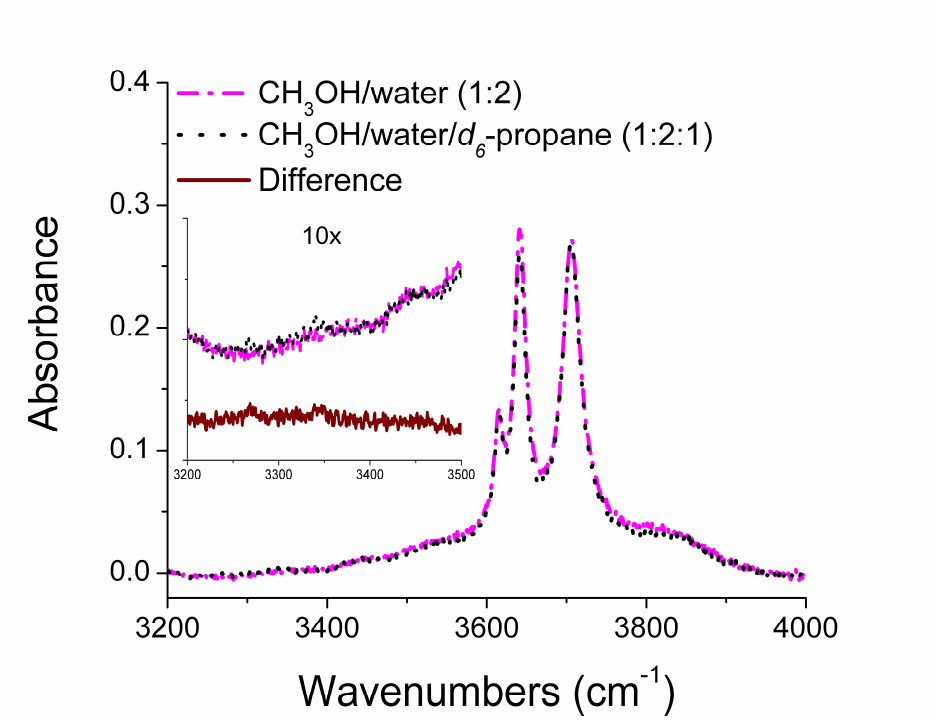


**Figure 5.5** Methanol and water with (black dot) and without (magenta dash-dot) $d_6$-propane in $CCl_4$ at -5 $^oC$ and 1 atm (water concentration is 2.5 mM). Inset shows H-bonded resonances, evidence of propane-induced water clusters. Reprinted with permission from Vu, Shultz, *J. Phys. Chem. A* **2011,** 115, 998-1002. Copyright 2011 American Chemical Society.

that both propane and methanol interact with water at the oxygen lone pairs. Methanol likely dominates this competitive binding due to its ability to form H-bonds with water. This model is examined in the ternary system of water, propane, and methanol in $CCl_4$ (Figure 5.5). Since the spectrum of a 1:1:1 mixture of methanol-water-$d_6$-propane is expected to be similar to that of a 1:1 mixture of water and methanol, a 1:2:1 molar ratio is chosen for this particular set of experiments (water concentration is maintained at 2.5 mM). Here the difference spectrum between the ternary system and the binary water-methanol system (inset) consists of H-bonded resonances at 3269 and 3344 $cm^{-1}$. Since water does not self-associate and the water-methanol H-bond occurs at 3440 $cm^{-1}$ (Figure 5.2), these features are assigned to propane-induced water clusters. Previous observation of the propane-water binary system reveals similar H-bonded

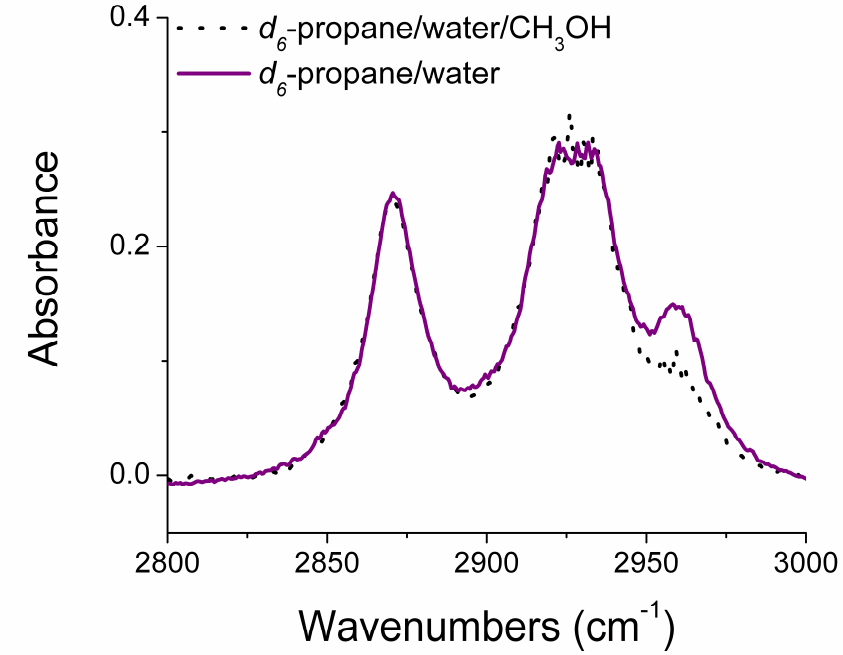


**Figure 5.6** C-H stretching modes of $d_6$-propane in $CCl_4$ at -5 $^oC$ and 1 atm showing interaction in the presence (black dot) and absence (purple solid) of methanol. Note the decrease in intensity of the 2960 $cm^{-1}$ peak as methanol is added. Reprinted with permission from Vu, Shultz, *J. Phys. Chem. A* **2011,** 115, 998-1002. Copyright 2011 American Chemical Society.

features, but at considerably lower frequencies (Figure 4.3). This indicates that the water H-bonds in the propane-induced cluster are weakened due to interference from methanol.

The ability of methanol to hinder formation of a water-propane cluster is further illustrated in Figure 5.6, where the introduction of methanol clearly affected the propane-water interaction. The intensity drop of the diagnostic blue-shifting peak at 2960 $cm^{-1}$ indicates that methanol reduces the concentration of propane-induced water clusters. Note that some propane-water complexes remains (2960 $cm^{-1}$ peak is not completely suppressed), consistent with the presence of the observed H-bonded resonances in Figure 5.5. Thus, the conclusion is that although its H-bonding interaction with water is strong enough to inhibit some hydrate cluster formation, methanol is only a modest inhibitor. This is evidenced both by the moderate binding constant with water ($K = 4.4 \times 10^2$) and the fact at some propane-induced water cluster remain even at 1:1 ratio of guest to inhibitor. The moderate inhibitory activity could explain the reason why large volumes of methanol (~ $2.4 \times 10^4$ L, which costs about $16,000)[63] are required daily to suppress clathrate formation in an average oil field. These astonishing statistics have since fueled the search for new and improved hydrate inhibitors. More recently, surfactants have been used to stabilize small hydrate particles and prevent them from becoming large enough to block the gas pipelines.[75]

In summary, this chapter presents data that supports a mechanism in which methanol disrupts the propane-water interaction via direct competition for the oxygen lone pairs of water (Figure 5.7). This conclusion is supported by the observed proton donation of methanol to water, the lack of direct methanol-propane interaction, and the reduction of propane-induced water clusters in the presence of the alcohol. These competitive interaction mechanisms are of

fundamental interest towards the design of new and more effective thermodynamic clathrate inhibitors.

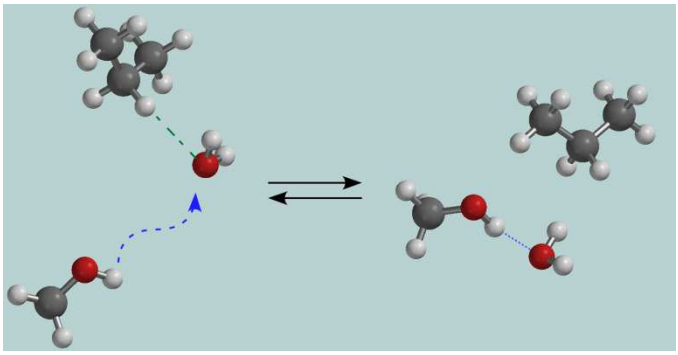

**Figure 5.7** Proposed mechanism for inhibition of propane hydrate nucleation by methanol. Reprinted with permission from Vu, Shultz, *J. Phys. Chem. A* **2011,** 115, 998-1002. Copyright 2011 American Chemical Society.

# Chapter 6 Tetrahydrofuran Clathrate

* Materials presented in this chapter have not yet been published as of May 1st, 2013.

The subsequent two chapters focus on clathrate hydrates of two well-known organic compounds that form clathrates at ambient conditions (4 – 7 $^{o}$C and 1 atm). In particular, this chapter deals with tetrahydrofuran (THF) hydrate while the next one involves that of cyclopentane (CP). Both of these compounds have been extensively used as laboratory proxies for natural gas hydrates, as they adopt the cubic sII structure frequently encountered in the field.[17,44,76] The experiments presented herein seek to examine the vibrational signatures of water-THF and water-CP interactions upon formation of partially completed hydrate clusters. Due to their ease of hydrate formation at atmospheric pressure, the need for high-pressure equipments is eliminated. Instead, the silanized glass cell (Section 2.3) is now used for matrix-isolation experiments. In addition, an approach using thin films of hydrate slurries formed from freezing aqueous solutions of THF or CP is employed. The next section details the preparation procedure for the thin films together with a presentation of the THF hydrate spectra.

## *6.1 THF Hydrate Thin Film*

### a) Sample Preparation

The process of making the hydrate slurries is as follows: 19 wt% aqueous solutions of THF or cyclopentane (corresponding to a stoichiometric ratio of 17 water : 1 guest) are prepared gravimetrically in 30-mL glass vials on an A-250 analytical balance (Denver Instrument Company, ± 0.1 mg precision). THF (anhydrous, 99.9%) and cyclopentane (ReagentPlus® 99%) are purchased from Sigma-Aldrich and used without further purification. The solutions are

sonicated for 1 h at room temperature: THF is completely miscible with water while the cyclopentane-water mixture forms phase-separated layers. Afterwards, the vials are put in a freezer at -20 $^{o}$C for 6 h to completely freeze. The icy solids are then allowed to warm up on the bench with vigorous agitation until most of the ice has melted. The mixtures are subsequently stored at 3 $^{o}$C for at least 24 h with occasional shaking to accelerate hydrate formation. This process melts the ice while allowing the existing hydrate crystals to act as nucleation sites for further growth. Following the incubation period, small aliquots (~0.3 μL) of the slurry mix are extracted using a micropipette and pressed between a pair of KCl windows housed in an optical dust tube to make the thin films. The path length is determined inteferometrically to be approximately 85 μm. The film samples then undergoes a temperature cycle (3 $^{o}$C to -27 $^{o}$C and back to 3 $^{o}$C) inside the FTIR chamber using cold $N_2$ purge gas while their spectra are recorded. To ensure equilibrium, the samples are held at each temperature for 1 h and the absorption spectrum is monitored over time until it is stable over 3 successive scans separated by 20 min. Temperature is measured with a Cu-CuNi type-T thermocouple (Omega Engineering, Inc.) embedded between the KCl windows. For comparison, a thin film of pure water is also prepared and its spectrum similarly acquired. A spectrum of THF in the vapor phase is also obtained using a 1-mm path length cylindrical infrasil quartz cell (Starna Scientific, Inc.).

b) Results

Figure 6.1 shows the absorption spectra of a thin film of water (a) and that of THF hydrate (b) as a function of temperature. The interference pattern from the front and back windows of the thin film is visible especially on the low frequency end of the spectrum. From the interference fringe method and Bragg's law, the thickness of the thin film can be determined in a straightforward manner to be 85 μm. The prominent water features in panel (a) include the H-

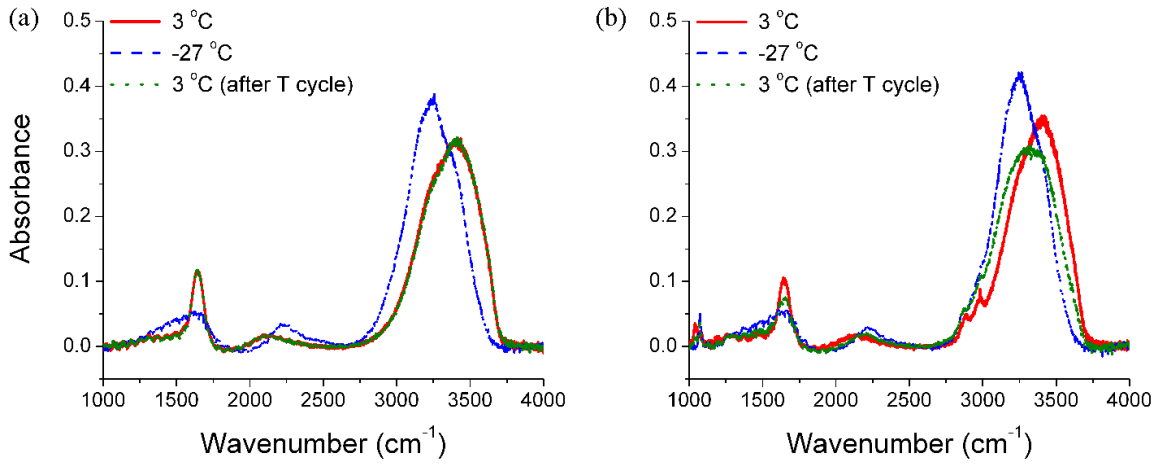


**Figure 6.1** Infrared spectra of 85 μm films of (a) water and (b) THF hydrate slurry (19 wt%) going through a temperature cyclce (red to blue to green). Water spectrum at 3 °C remains unchanged while THF hydrate spectrum exhibits a red shift in the H-bonded region.

bonded peaks at 3000-3700 $cm^{-1}$, the bending mode at 1650 $cm^{-1}$, and a broad resonance around 2000-2300 $cm^{-1}$ that has previously been ascribed to the $\nu_2 + \nu_L$ combination of the water bend and librational modes.[77,78] The spectrum of liquid water at 3 °C (red line) is dominated by the broad H-bonded peak centered at 3400 $cm^{-1}$ while the -27 °C ice spectrum (blue dash) shows a relatively sharper H-bonded resonance at 3200 $cm^{-1}$. This red shift is characteristic of the water-to-ice transition as the H-bonds angles in ice are straighter and the bonds are stronger. Upon warming the ice film to 3 °C (Figure 6.1a, green dot), the ice sample melts and the spectral features revert to those in liquid water. In contrast, the THF hydrate thin film behaves quite differently. After the temperature cycle, the 3 °C spectrum exhibits a significant red shift in the H-bonded region (Figure 6.1b, green dot). This observation is illustrated more vividly in Figure 6.2, which shows the difference spectrum of water/THF minus water before and after the T cycle. The negative peak at 3550 $cm^{-1}$ and the positive peak around 3150 $cm^{-1}$ offers clear evidence for a transition from a relatively weak H-bonded network towards a stronger and more

structured one due to the presence of THF along with temperature variation. Since no ice is present at 3 $^{o}$C, this stronger H-bonded water structure is an indication of at least a partially completed, cage-like structure.

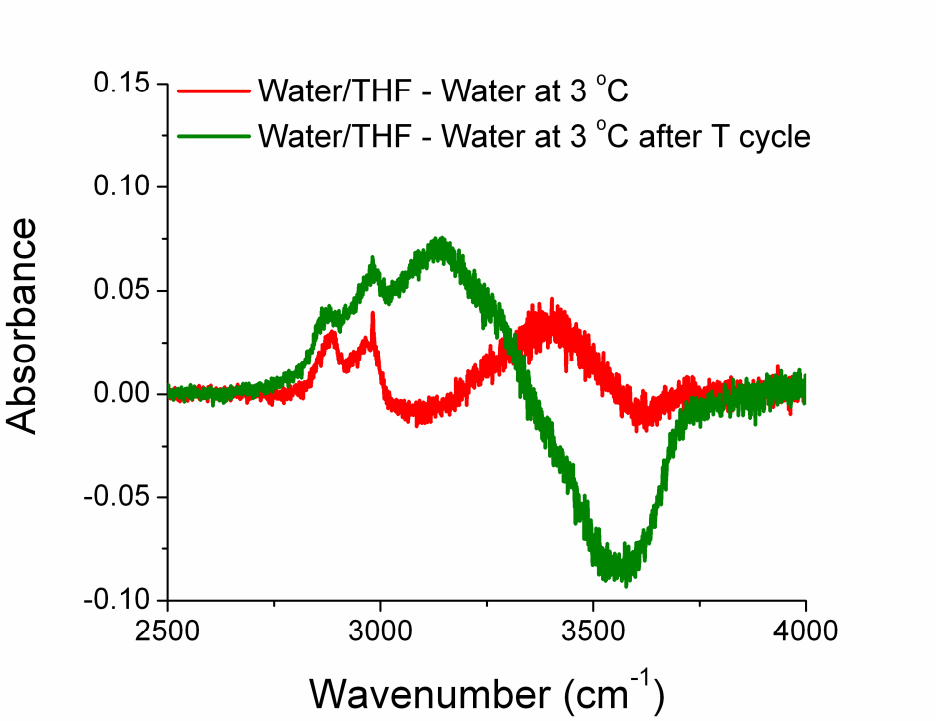


**Figure 6.2** Difference spectra of water/THF – water before (red) and after (green) the T cycle illustrating the shift from weak to stronger H-bonds in THF hydrate.

To elucidate the effect that THF has on the structural transformation of the water network, the water-THF interaction during the T-cycling process is examined. Much information can be deduced from the ether stretch, which is a particularly efficient probe for a change in the molecular environment of THF. Figure 6.3 shows both the COC asymmetric stretch and the collective $CH_2$ stretch region of aqueous THF before (red) and after the T cycle (green). The gas-phase spectrum of THF (black curve) is also included to facilitate comparison. The COC asymmetric stretch is observed at 1084 cm$^{-1}$ in the gas phase while its value is shifted to 1040

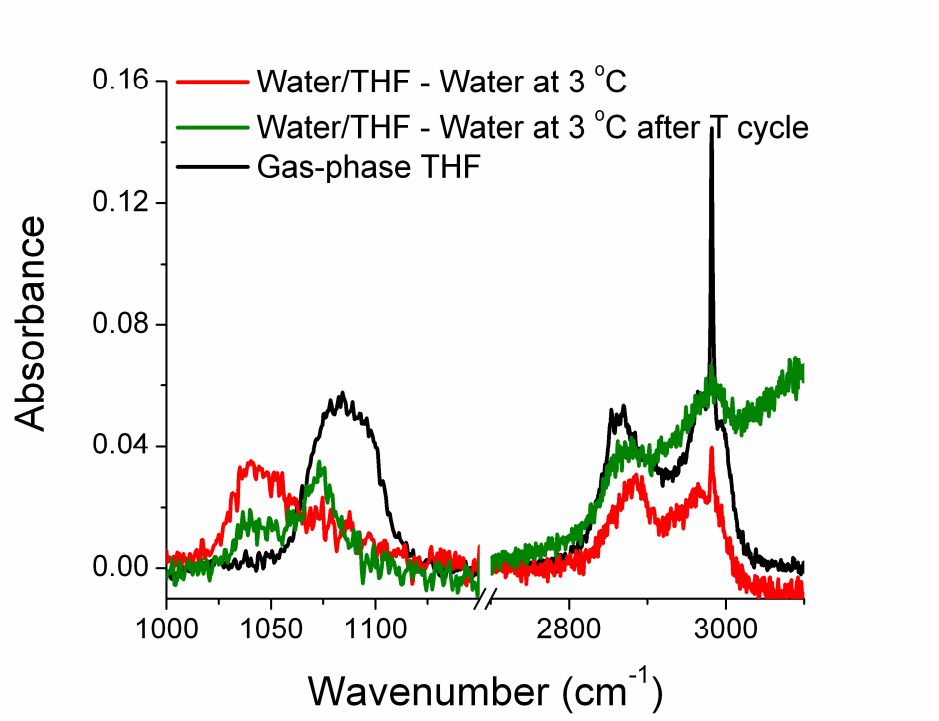


**Figure 6.3** Difference spectra of water/THF – water d) and after (green) the T cycle showing changes in the COC asymmetric stretch (1000-1200 $cm^{-1}$) and the $CH_2$ vibrations (2700-3100 $cm^{-1}$) of THF upon T cycling. The gas phase spectrum of THF (black curve) is included for comparison.

$cm^{-1}$ in the aqueous solution at 3 °C before the T cycle. Due to the significant red shift, the latter peak is assigned to THF molecules that are directly H-bonded to water. This assignment is supported by DFT calculation of a 1:1 THF-water complex in which water acts as the H-bond donor (Figure 6.4). Compared to an isolated THF molecules, the $\upsilon_{COC,asym}$ mode shows a 21 $cm^{-1}$ red shift when it is H-bonded to a water molecule. Aside from a smaller magnitude for the red shift, the result agrees qualitatively with the experimental spectra (the presence of direct THF-water H-bonds is also supported by the 3403 $cm^{-1}$ resonance in the difference spectrum of water/THF – water at 3 °C in Figure 6.2). Temperature cycling causes a decrease in intensity of the 1040 $cm^{-1}$ H-bonded peak, in tandem with enhancement of a peak at 1073 $cm^{-1}$ that

approaches the $\upsilon_{COC,asym}$ frequency in the gas phase (Figure 6.3, green). Together with the observed changes in the water H-bonded network, the decreased intensity of the 1040 $cm^{-1}$ resonance and the shift toward higher frequencies upon temperature cycling unambiguously indicate weakening of the direct THF···water bonds as water···water bonds get stronger, compelling evidence for THF enclathration.

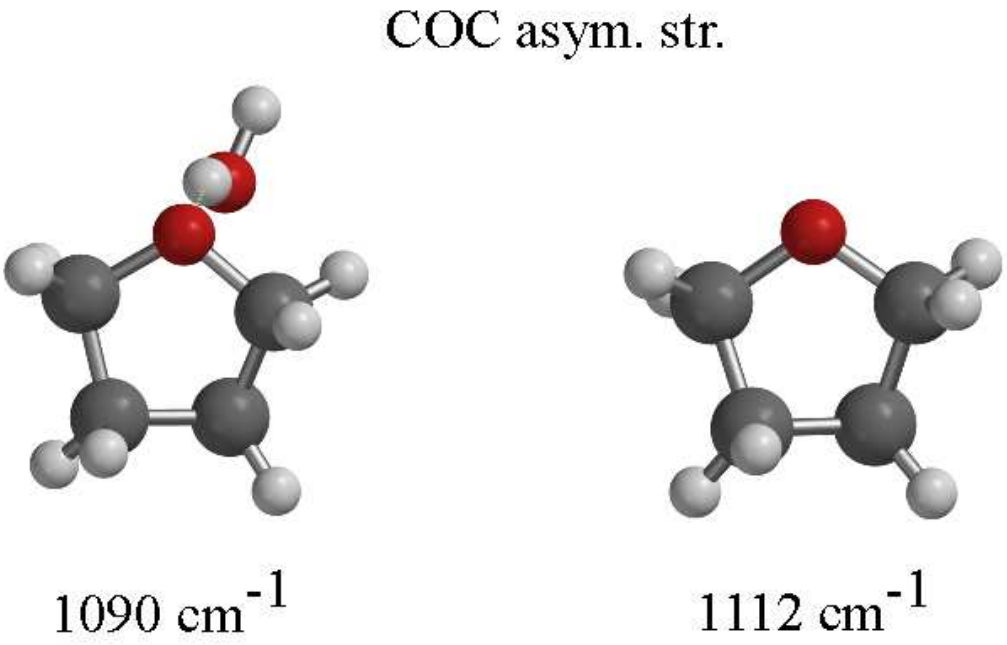


**Figure 6.4** Calculated gas-phase vibrational frequencies of the $\upsilon_{COC,asym}$ mode in THF in the presence (left) and absence of water at the B3LYP 6-31G* level of theory. Note the red shift of this mode in the H-bonded complex.

A similar trend is also reflected in the $CH_2$ stretch region. Due to coupling among the eight C-H bonds, this spectral region is unfortunately too complex to separate specific modes that can identify enclathration. However, methylene groups of hydrocarbons are known for their propensity to interact with water through the oxygen atom, which often result in a blue shift of

the C-H vibrations (section 4.5). In the prehydrate system (Figure 6.3, red), the methylene stretches are visibly blue-shifted from their gas-phase frequencies (black curve). As the hydrate cage grows larger, the trapped THF molecules interact less strongly with the surrounding water molecules, resulting in a relative red shift of the C-H resonances back toward their gas phase values. This result reinforces the importance of the guest-host interaction in the local structuring of the hydrate cluster.

*6.2 Water and THF in $CCl_4$*

Matrix-isolation studies of the THF/water system in $CCl_4$ are carried out to help identify the nature of the THF-water hydrogen bond and provide further support for interpretation of the thin film spectra. Figure 6.5 shows the spectrum of saturated water at -5 $^{o}$C as a function of THF

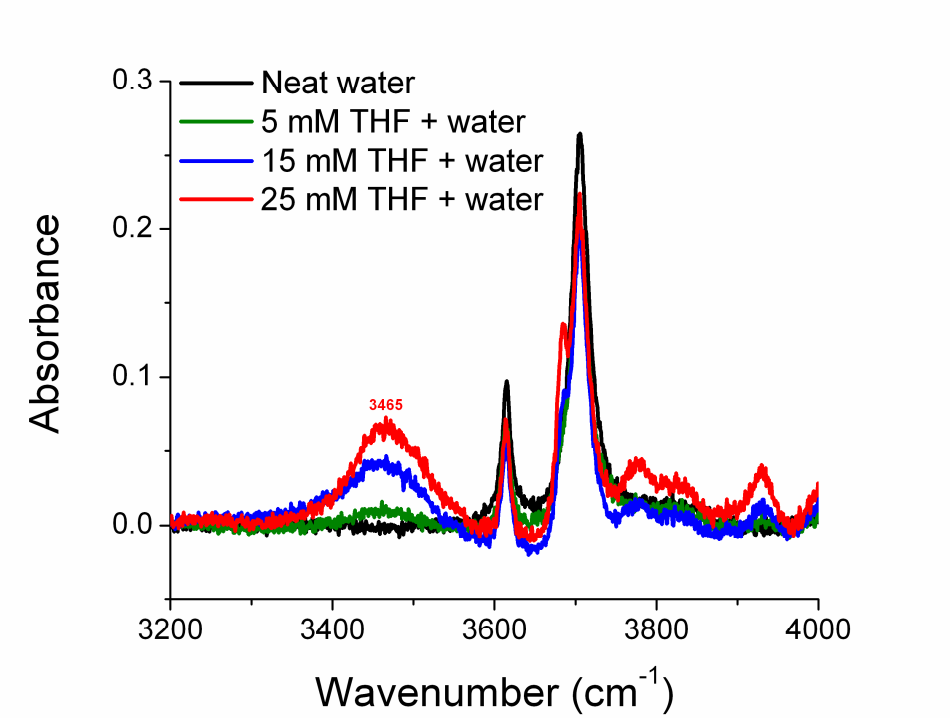


**Figure 6.5** Infrared spectra of THF and water in $CCl_4$ at -5 $^{o}$C at different THF concentrations from 5 mM to 25 mM. The spectrum of neat water (black) is included as a control.

concentration. Compared to neat water (black plot), the presence of THF causes an intensity drop of the free water peaks in tandem with the appearance of a broad H-bonded resonance at 3465 $cm^{-1}$. At THF concentrations of 15 mM and 25 mM, a *d*-OH peak is also visible at 3684 $cm^{-1}$ (magnified in Figure 6.6). Since the frequency of the *d*-OH that is due to a water-water H-bond is at 3643 $cm^{-1}$ (Figure 4.4), the observed *d*-OH resonance is assigned to the decoupled OH of water molecules directly bonded to THF. This assignment is consistent with a weaker THF···water relative to a water···water H-bond, hence a *d*-OH closer to the asymmetric stretch. The companion 3465 $cm^{-1}$ resonance thus indicates the donor water···THF H-bond. However, this broad peak can also contain contribution from a THF-induced water cluster in a slightly strained configuration, similar to the case of salt-induced clusters where the H-bond is observed at 3443 $cm^{-1}$.[58] Note that the resonances at 3850-4000 $cm^{-1}$ are primarily due to THF combination bands and overtones and are unrelated to the water-THF interaction.

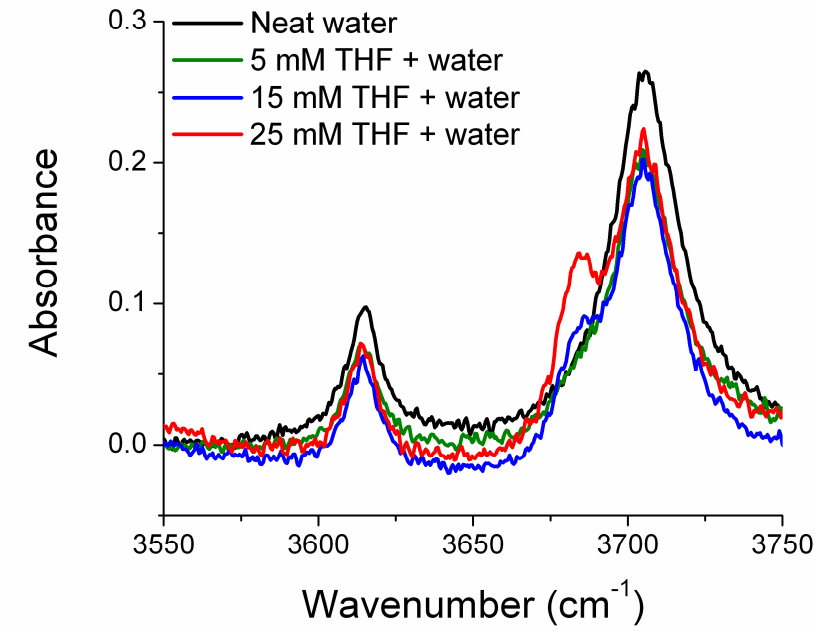


**Figure 6.6** Magnification of the water region in Figure 6.5. Note the presence of the d-OH peak at higher THF concentrations.

A parallel study using salt to pre-form water cluster in $CCl_4$ before introduction of clathrate guest is also performed. Salts are relevant in this context because of their significant concentration in the deep ocean where clathrates naturally exist. Among the halide salts, sodium iodide is chosen due to its ability to induce formation of aqueous nanodrops in $CCl_4$.[58] Figure 6.7 shows the spectrum of 15 mM THF and water at -5 $^{o}$C in the presence and absence of 1M NaI. The most noticeable difference upon the addition of salt is a peak at 3643 $cm^{-1}$, assigned to dangling OH of a water molecule H-bonded to another water molecule. As noted previously, the prominent H-bonded peak at 3468 $cm^{-1}$ may suggest a strained water structure. Since NaI by itself does not produce a visible *d*-OH peak for water, the spectrum may indicate an initial step in forming a partial water cage. This result indicates that NaI induces a more structured THF-water complex, which may explain the role of salts in clathrate formation in the ocean.

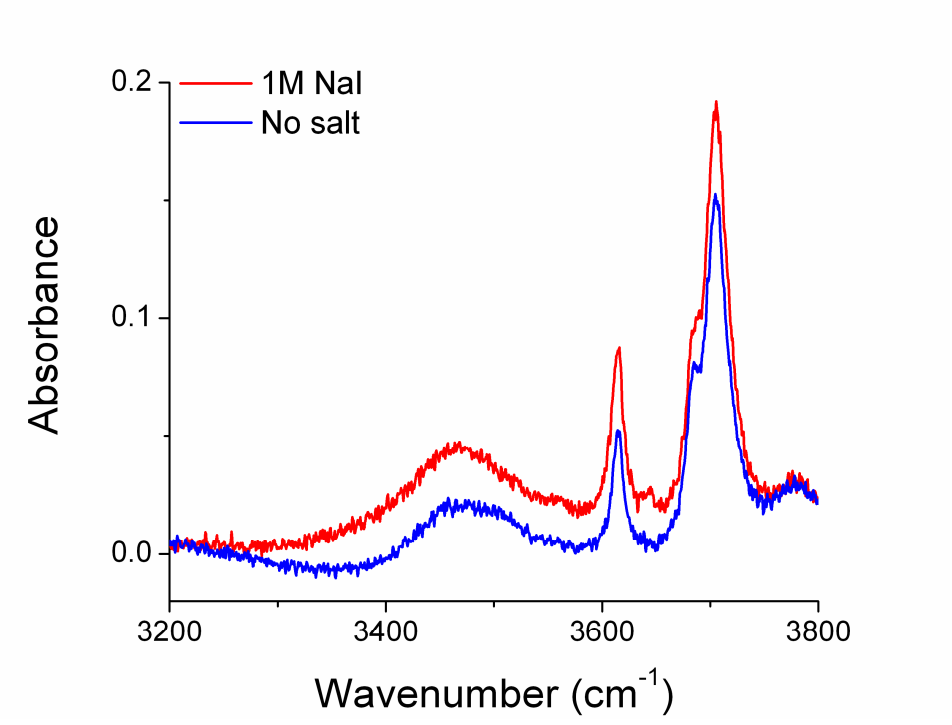


**Figure 6.7 S**pectra of 15 mM THF and water in $CCl_4$ at -5 $^{o}$C with (red) and without (blue) the presence of 1M NaI.

# Chapter 7 Cyclopentane Clathrate

* Materials presented in this chapter have not yet been published as of May 1st, 2013.

Formation of a complete clathrate hydrate lattice hinges on the making of five- and six-membered rings and the arrangement of these rings into a cage structure. The analysis of THF hydrate in Chapter 6 shows that the water structure is considerably more rigid in the presence of a clathrate former compared to that of pure water. Since THF is itself a rigid 5-membered ring, it is conjectured that water molecules in the vicinity of this solute could also form a pentacyclic structure with the guest that could serve as a template for hydrate nucleation. In that context, the clathrate guest can be thought of as a "structure maker" for water. In the case of THF, it should be noted that the total miscibility with water is an important contributing factor in forming the clathrate, since the guest is already present at high concentrations in the aqueous phase.[17] Most natural hydrate guests, in contrast, are insoluble in water and thus the mechanism of THF hydrate formation could be very different from that of hydrophobic guests. As a result, hydrate of cyclopentane, the hydrophobic analog of THF, is examined in this chapter to assess the notion of a five-membered ring structure as the nucleation seed.

## *7.1 Cyclopentane Hydrate Thin Film*

A macroscopic sample of cyclopentane hydrate is prepared as described in Section 6.1a, namely by exposing a 19 wt% aqueous solution through a temperature cycle. Figure 7.1 compares the resulting cyclopentane clathrate at 3 $^{o}$C with an *n*-pentane/water mixture that has gone through the same procedure. The latter is included to highlight the role of the cyclic nature of the guest in promoting hydrate formation. It is worth pointing out that *n*-pentane is five times

more soluble in water than cyclopentane (the solubility of cyclopentane is 0.143 mM at 20 $^{o}$C).[17] Yet the cyclopentane/water solution forms solid, snow-like particles while the *n*-pentane/water mixture results in phase separation.


**Figure 7.1** Macroscopic sample of cyclopentane hydrate (left) formed by temperature cycling a 19 wt% solution and a phase-separated mixture of *n*-pentane and water at 3 $^{o}$C. Note that pentane is 5 times more soluble in water than cyclopentane.

The respective thin film spectra (Figure 7.2) affirm the macroscopic observation. Due to the insolubility of both *n*-pentane and cyclopentane in water, the presence of cyclopentane vibrational bands at 2800 - 3000 cm$^{-1}$ (panel a) suggests its incorporation into the hydrate lattice. The absence of such resonances and the constancy of the water spectrum with temperature in the pentane-water mixture (panel b) confirm that pentane does not form a hydrate by itself. These observations clearly indicate a specific interaction between water and cyclopentane and a lack

thereof between pentane and water. The next section discusses results from the matrix-isolation experiments that will provide further insights into the nature of the water-cyclopentane interaction.

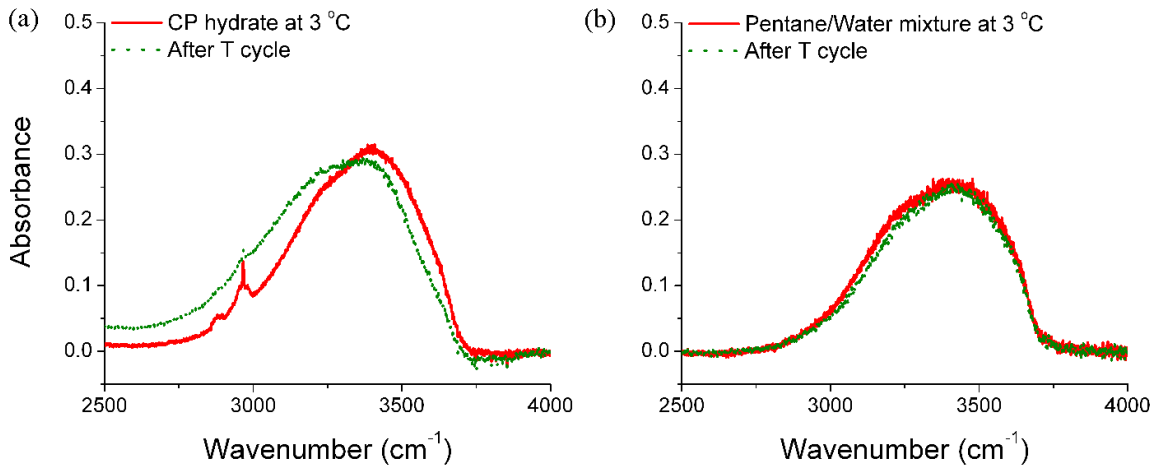


**Figure 7.2** Infrared spectra of 85 μm films of (a) CP clathrate hydrate and (b) *n*-pentane/water mixture at 3 °C before (red solid) and after (green dot) T cycling to -27 °C. Presence of C-H resonances in (a) confirms incorporation of CP into the hydrate lattice.

*7.2 Matrix-Isolation Experiments*

a) Sample Preparation

Since cyclopentane can form clathrates by itself at atmospheric pressure, the need for the high-pressure cell is eliminated; instead, a 1-in. glass cell equipped with quartz windows (detailed in Section 2.3) is used for all experiments. The cell and the quartz windows are fully silanized before use to prevent hydrogen bonding of water to the internal surfaces. Saturated solutions of water in $CCl_4$ are made by mixing 46 μL of nanopure $H_2O$ with 20 mL of the dried solvent and left to phase-separate at room temperature for at least 24 h. The cell is then cooled to

-5 $^{o}$C overnight before data acquisition. 0.9 mM of cyclopentane or pentane is then added volumetrically, resulting in a molar ratio of 3 water : 1 guest at -5 $^{o}$C. Temperature cycling is achieved using the method described in Section 6.1a, going from -5 $^{o}$C to -20 $^{o}$C and back to -5 $^{o}$C (the freezing point of carbon tetrachloride is -23 $^{o}$C). A solution of HOD in $CCl_4$ is also made by introducing 46 μL of a 1:1 v/v mixture of water and $D_2O$ into dried $CCl_4$ and left to equilibrate overnight. DFT calculation of a cyclopentane + $3H_2O$ complex in the gas phase is performed at the B3LYP 6-31G* level of theory using Spartan '08. Bond length and angle constraints are implemented in order to generate the final configuration. The complex is found to be in a true local energy minimum, confirmed by the absence of imaginary vibrational frequencies after equilibrium optimization.

b) Results

Figure 7.3a plots the spectrum of saturated water in $CCl_4$ at -5 $^{o}$C before (top) and after (bottom) cooling to -20 $^{o}$C. The presence of the symmetric stretch, the asymmetric stretch, and the rotational wings are easily identified, and no change in the water spectrum is observed after the T cycle. These spectral signatures verify that water molecules exist solely as monomers at -5 $^{o}$C and do not cluster with changes in temperature. Upon the addition of cyclopentane (Figure 7.3c), however, two new features emerge: a broad H-bonded resonance centered at 3400 cm$^{-1}$ and a shoulder at 3636 cm$^{-1}$ near the symmetric stretch (magnified in the inset). An analogous experiment on the *n*-pentane/water system (Figure 7.3b) yields spectra resembling those of pure water and reveals no evidence for additional features. Since water neither clusters by itself nor with the addition of pentane, the distinct 3400 cm$^{-1}$ feature with cyclopentane must be due to H-bonded water cluster caused by the presence of the cyclic guest. Furthermore, the magnitude of the O-H frequency shift upon hydrogen bonding is a well-established indicator of the strength the

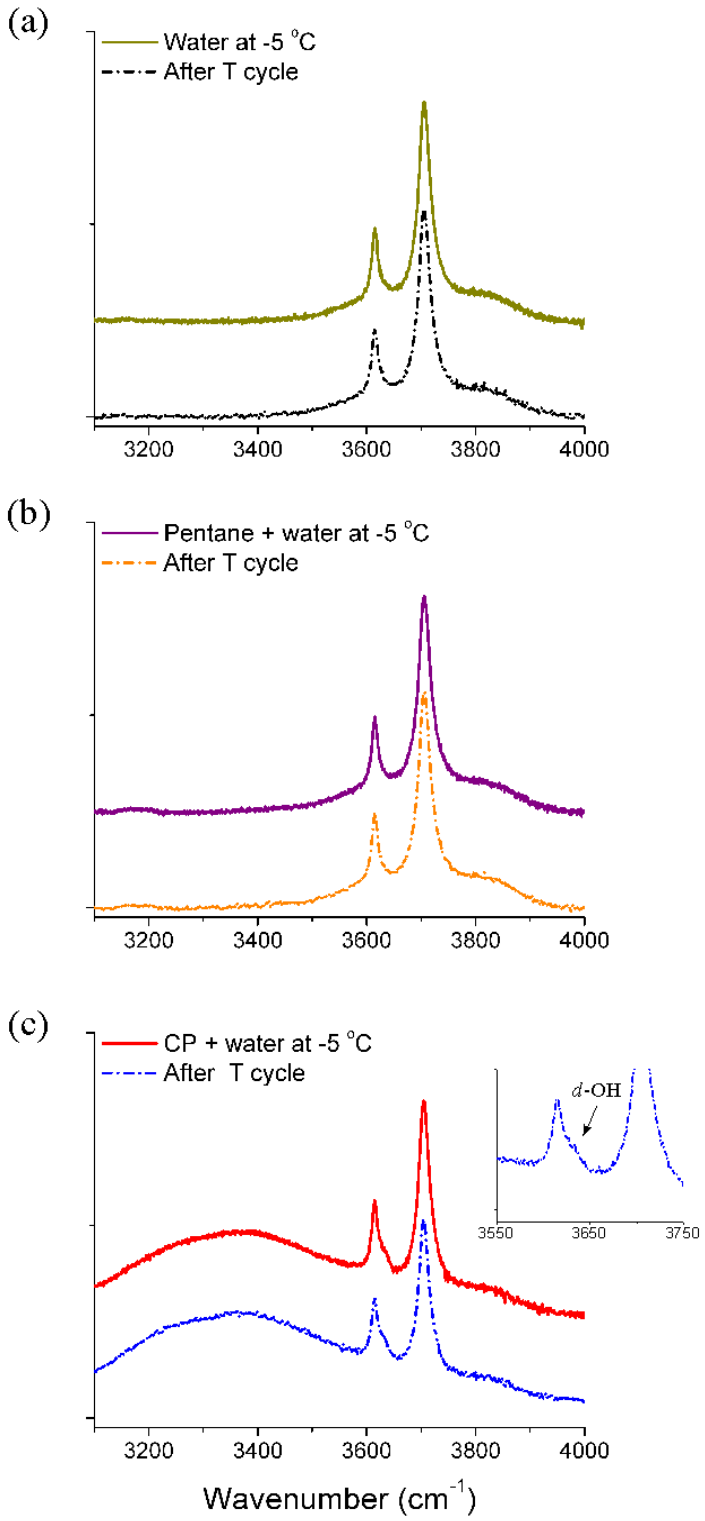


**Figure 7.3** Absorption spectra of (a) saturated water, (b) 0.9 mM pentane + water, (c) 0.9 mM cyclopentane + water in $CCl_4$ at -5 $^{o}$C before and after T cycle. Note the H-bonded resonance at 3100-3500 $cm^{-1}$ and the *d*-OH feature at 3636 $cm^{-1}$ (inset) in (c).

hydrogen bonds.[79,80] The moderate red shift (~ 200 $cm^{-1}$) from the frequency of gaseous water observed in the cyclopentane-induced cluster indicates that the water H-bonds are somewhat strained. It is hence concluded that the cyclopentane-water interaction is responsible for incorportation of water into a relatively inflexible H-bonded structure.

In addition to the induced H-bonded feature, the OH region of the water/cyclopentane system reveals an additional shoulder at 3636 $cm^{-1}$ (Figure 7.3c, inset). Since this peak occurs in between the two fundamental vibrations, it is attributed to the dangling OH group (*d*-OH) of single-donor water molecules. However, its frequency is slightly lower than that observed for the propane-induced water cluster (Figure 4.4). Thus, a room-temperature spectrum of a 1:1 v/v mixture of water and $D_2O$ in $CCl_4$ (Figure 7.4) is obtained to aid the analysis of this *d*-OH feature. The product of the 1:1 scrambling reaction between $H_2O$ and $D_2O$ is a 1:2:1 solution

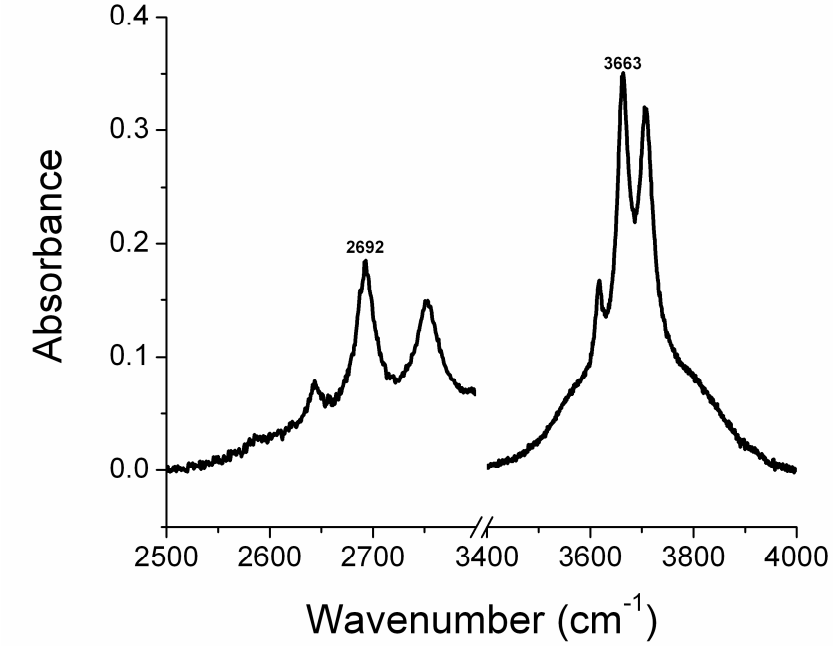


**Figure 7.4** Infrared spectrum of a 1:1 v/v mixture of $H_2O$ and $D_2O$ in $CCl_4$ at room temperature. The free O-H stretch is observed at 3663 $cm^{-1}$ while the free O-D stretch is seen at 2692 $cm^{-1}$.

consisting of $H_2O$, HOD and $D_2O$. As a result, the spectrum is comprised of a free OH peak on top of the normal water features and an overlapping free OD peak at 2692 $cm^{-1}$ with the $D_2O$ features. The frequency of the free OH peak (3663 $cm^{-1}$) is precisely at the average of the symmetric and the asymmetric stretch frequencies as expected. The frequency of the *d*-OH peak in the cyclopentane-induced cluster, however, is red shifted from that of the free OH in HOD.

To gain insights into the nature of the companion *d*-OH bonds in different hydrogen-bonding environments, a B3LYP density functional computation of a water trimer bonded to two adjacent methylene groups of cyclopentane was performed using the 6-31G* basis set (Figure 7.5). As usual, the computational approach yields an overestimate for the absolute vibrational frequencies (hence the 0.967 correction), but the relative peak positions are nonetheless applicable to assignment of the experimental bands. Due to attractive interactions between the oxygen atoms of water and the methylene groups, there exist 3 different types of water in the cylopentane/water trimer complex: a single H-donor with direct dispersive interaction with the cyclopentane ring (Type 1), a single H-acceptor with direct dispersive interaction to the cyclopentane ring (Type 3), and a single donor – single acceptor bridging water (Type 2). Examination of the free OH region of the simulated spectrum reveals that the type-2 *d*-OH water molecule is red shifted from type 1 *d*-OH by 14 $cm^{-1}$. This reflects the decreased coupling between the OH bonds of the bridging water when it participates in the H-bonded network. The effect can be rationalized by the abstraction of electron density from the oxygen atom, which weakens and lengthens the free OH bond. As a result, the *d*-OH of the bridging water molecule is observed in the IR spectrum as a peak at lower frequency than that of the free OH in HOD. The observed small shoulder at 3636 $cm^{-1}$ in the water/cyclopentane mixture is hence assigned to the *d*-OH of a bridging water molecule.

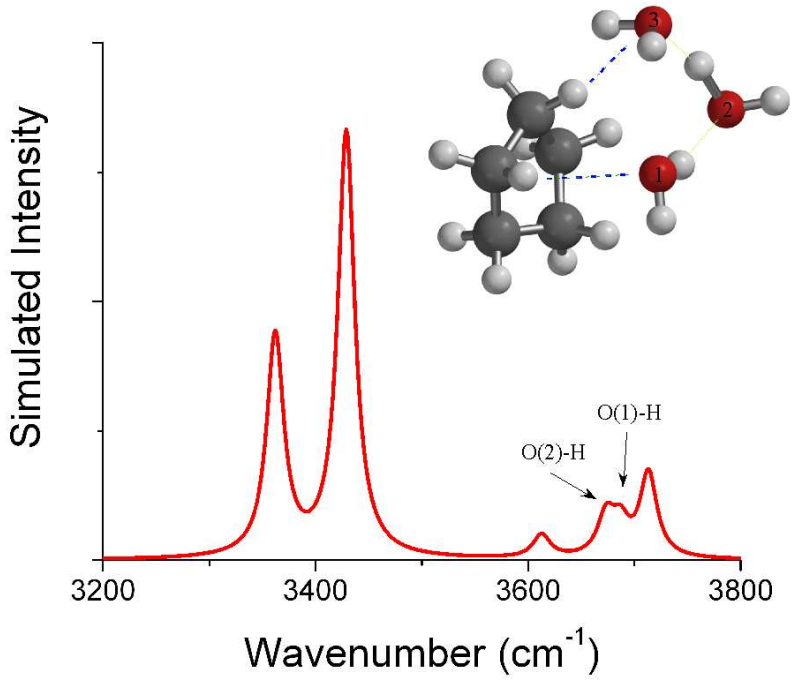


**Figure 7.5** Calculated infrared spectrum of a cyclopentane-water trimet complex (frequency is corrected by a factor of 0.967). The blue dashes represent van der Waals intercations between the oxygen atoms of water and the methylene hydrogen atoms of cyclopentane

The stark contrast between the ability of cyclopentane and the inability of *n*-pentane to form clathrates exemplifies the role of a pentacyclic motif ($3H_2O$ + C-C) in clathrate nucleation. It has been suggested that the pentagonal dodecahedron is the first nucleation seed, and that it should be the longest lived structure in the reverse process, namely isochoric melting.[18] There are also a number of instances where pentagon-based ice structures are found to exist in other environments.[81-83] In our case, it is plausible that the flexible methyl end groups of *n*-pentane could potentially block the approach of new water from forming H-bonded clusters, thereby preventing the ordered structuring of water around the guest species and raising the entropic cost of forming clathrate cages. Cyclopentane, on the other hand, offers the rigidity that is critical for stabilization of relatively strong H-bonded water clusters with minimal strain.

# Chapter 8 Summary and Future Work

The present project is part of an ongoing effort to understand the nucleation mechanism of clathrate hydrates. The focus has been on the fundamental molecular interactions between small clusters of water and various clathrate guests under typical formation conditions. A picture of the interaction could help guide efforts to either stabilize clathrate structures for energy and gas storage purposes or prevent hydrate formation in natural gas pipelines.

Hydrogen bonding interactions are at the core of hydrate formation, and infrared spectroscopy is among the most effective methods for probing them. However, the infrared opacity of water has made it challenging to study interactions in bulk aqueous media. This work takes advantage of the existing picture of water in carbon tetrachloride at ambient temperature. The matrix-isolation studies have shown that in the presence of the hydrophobic guests, water molecules form H-bonded clusters with restricted motion, the first step towards nucleation of a crystal. The interaction that induces the clustering of water molecules is identified to be an attractive van der Waals interaction between the oxygen lone pairs of water and the methylene groups of the hydrocarbons. Methanol interferes with this process by proton donation to water and, to some extent, suppress formation of propane-water nucleating clusters. The combined evidence from experimental results and theoretical calculations of the cyclopentane/water system reveals the presence of a bridging water molecule in the guest-induced cluster. This supports the notion of a locally ordered, five-membered ring motif in which water molecules are forced to reorganize around the guest species in a cyclic manner. This configuration restricts the motion of the water molecules to some degree and thus bears some characteristic of the hydrate cavity, such as the distance among and the orientation of water molecules. From an entropic point of

view, this picture seems to support the local structuring hypothesis of hydrate nucleation, as it is unlikely that an ordered phase will first nucleate in a different phase with symmetry distinct from the final crystal.[18] The molecular-level depiction of water-guest interactions presented hitherto has contributed to a better understanding of clathrate nucleation/inhibition dynamics and may have implications for the control and manipulation of clathrate hydrates at the macroscale.

Future work might involve observation of the hydrate nucleation event at the ice-gas interface by means of sum frequency generation (SFG). In such experiments, the surface of single crystal ice can either be directly exposed to elevated pressure of the guest gas or submerged under carbon tetrachloride doped with THF or cyclopentane. The objective there would be to determine which surface modes of ice are most sensitive to hydrate guest incorporation.

# Chapter 9 Spectral Signature of Hydroxide Ion in $CCl_4$

* Materials presented in this chapter are published in Vu, T. H.; Shultz, M. J. *Chem. Phys. Lett.* **2013,** accepted article in press, doi: http://dx.doi.org/10.1016/j.cplett.2013.04.038

This chapter presents a neat application of the room-temperature matrix-isolation system to address a fundamental question regarding the vibrational signature of the hydroxide ion at the water-vapor interface. The segregation of $OH^-$ (or lack thereof) towards the surface of water is a contentious issue in the literature[84] and one that holds significant implications for the chemistry of many environmental systems where most of the action occurs at the interface. Together with hydronium ions, hydroxides are ubiquitous in aqueous environments and are known to possess high mobility in bulk liquid water by rearranging hydrogen bonds during transport.[85] The presence of $OH^-$ at the water-vapor interface is typically inferred from macroscopic measurements such as zeta-potential[86,87] or drop drift in an electric field. On the contrary, theoretical work[88,89] have found that hydronium ions prefer to adsorb at surface sites, a notion also supported by several SFG experiments.[90-92] However, neither $H_3O^+$ nor $OH^-$ has been specifically identified by the surface studies due to the low number densities and a lack of certainty on the location of these resonances. Knowledge of their spectral signature is thus an essential ingredient for the potential detection of these ions and an important step towards resolving the controversy.

Vibrational spectroscopy is among the most effective probes of water and its constituent ions due to the sensitivity of the O-H stretch to the local chemical environment. As such, infrared and Raman techniques have been extensively used to detect the vibrational mode of hydroxides in various condensed phases.[93-97] The lifetime of $OH^-$ in solution is on the order of ~1.5 ps[98] and

hence the dynamics and the probe have comparable time scales. However, due to the strong interaction of $OH^-$ with the surrounding bulk and the overlapping signal from the much more intense hydrogen-bonded peak of water, almost all studies of hydroxides in solution have relied on band profile deconvolution to extract the $OH^-$ peak. This has led to a relatively broad distribution for the $OH^-$ frequency (3400 $cm^{-1}$ to 3700 $cm^{-1}$) and linewidth (40 to 80 $cm^{-1}$) that largely depends on the bulk concentration and to some extent, the identity of the counterion.[94,96] In addition, there is a well-established solvent-induced blue shift for hydrated hydroxide relative to $OH^-$ in the gas phase.[84] Since the water/vapor interface is generally considered hydrophobic,[99] observation of $OH^-$ in a hydrophobic solvent with limited amounts of water may better reflect its frequency at the surface. In this study, carbon tetrachloride is used to provide isolation of the hydroxide ion from solutions of CsOH and tetramethylammonium hydroxide. Due to the low solubility of water in $CCl_4$, the $OH^-$ vibrational mode is sufficiently decoupled from those of water, resulting in a pure hydroxide resonance. The confined $OH^-$ ion exhibits a sharp resonance at 3634 $cm^{-1}$ and is readily distinguishable from that of the dangling OH bonds by a red shift of 29 $cm^{-1}$. Isotopic substitution reveals an $OD^-$ stretch at 2682 $cm^{-1}$, consistent with the expected mass difference between deuterium and hydrogen. These features are further elaborated below.

*9.1 Sample Preparation*

1M solutions of cesium hydroxide (CsOH) and tetramethylammonium hydroxide (TMAH) are prepared volumetrically from stock solutions of 50 wt% CsOH and 10 wt% TMAH, respectively. Carbon tetrachloride is dried with silica gel for 1 week prior to use. The hydroxide solutions are vigorously mixed with $CCl_4$ and allowed to equilibrate for 3 days at room temperature to ensure complete phase separation. Only the $CCl_4$ layer is used for spectral acquisition. The optical cell (1-in. path length, 20 mL internal volume) is assembled with quartz

windows and is silanized prior to sample introduction. FTIR spectra are obtained at 64 scans and 1 $cm^{-1}$ resolution after the sample compartment has been thoroughly purged with nitrogen gas.

*9.2 Results*

The spectrum of 1M solution of tetramethylammonium hydroxide in $CCl_4$ is shown in Figure 9.1 (red curve). It displays a profile resembling that of neat water, with the addition of a sharp resonance at 3634 $cm^{-1}$ (FWHM = 25 $cm^{-1}$) which is clearly resolved in the difference spectrum (green curve). For neat water (blue plot), the rotational bands are an excellent diagnostic for free water monomers since any H-bonding interaction will restrict the rotational motion by increasing the effective moment of inertia, leading to a collapse of the rotational wings into the central peak. The intensity of the R branch at 3850 $cm^{-1}$ can hence be used as a scaling factor to enable subtraction of the water monomers from the experimental spectra of the hydroxide solutions. Here a scaling factor of 1.1 indicates that the presence of the base brings in 10% more water beyond saturation into the $CCl_4$ layer. These additional water molecules are likely associated with the $(CH_3)_4N^+$ cation due to the preference of water to interact through the oxygen lone pairs.[58] The spectra for CsOH at 1M and 6M (not shown) exhibit a similar profile with a slightly different scaling factor of 0.69 for the higher concentration. Since the frequency of the observed 3634 $cm^{-1}$ peak does not change with concentration or the identity of the counterion, the resonance is assigned to the hydroxide stretch. Note that this feature only develops for bases that are highly soluble in water (a control experiment with 1M NaOH results in dehydration of the $CCl_4$ layer). This observation demonstrates that combination of a small anion and a large cation (i.e. weak ion-ion attraction) is essential to enable a solvent-separated ion pair in $CCl_4$. Here the hydroxide ion appears to interact mainly with the $CCl_4$ solvent shell, as

there is no distinct evidence for interaction with water due to the lack of any hydrogen-bonded features or changes in the rotational structure.

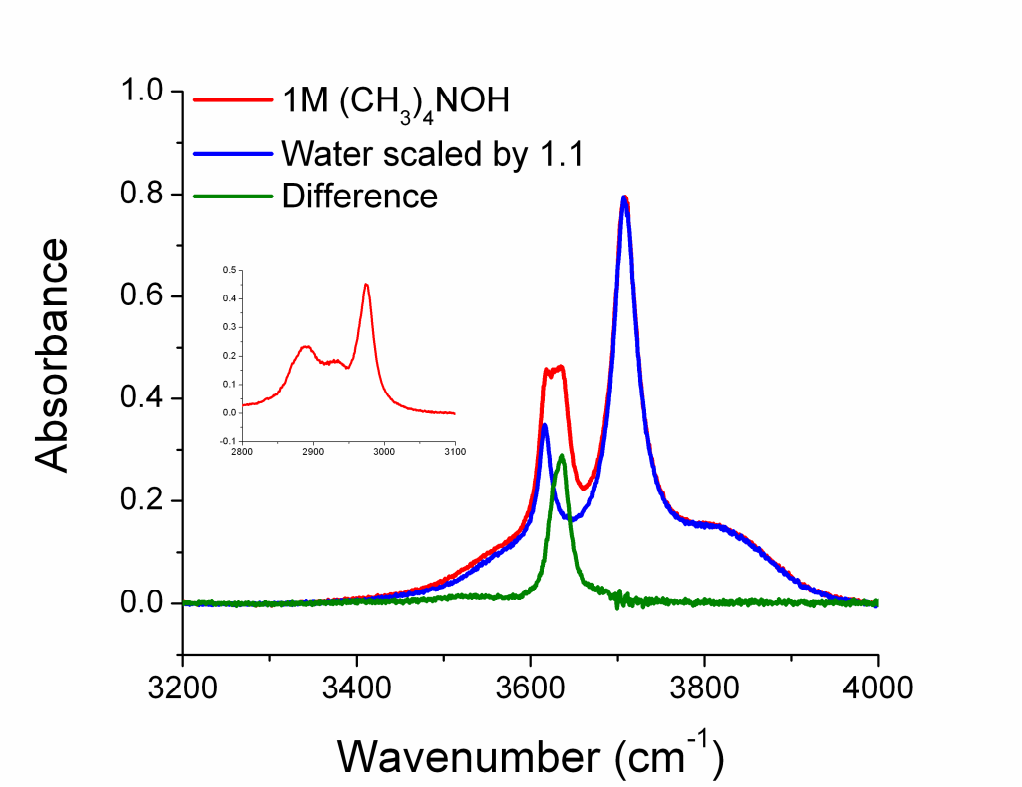


**Figure 9.1** Infrared spectrum of tetramethylammonium hydroxide in $CCl_4$ at room temperature (red) compared to that of neat water (blue). The presence of C-H resonances at 2800-3100 $cm^{-1}$ (inset) indicates the presence of the $(CH_3)_4N^+$ cation in solution. The difference spectrum (red minus blue) reveals a sharp peak, assigned to $OH^-$, at 3634 $cm^{-1}$. Reprinted with permission from Vu, Shultz, *Chem. Phys. Lett.* **2013,** doi: 10.1016/j.cplett.2013.04.038

Spectra with partially deuterated water are subsequently obtained to confirm the hydroxide assignment. The black curve in Figure 9.2 represents the spectrum of a 1:1 v/v mixture of tetramethylammonium hydroxide and $D_2O$ in $CCl_4$ at room temperature. The product of this scrambling reaction is a solution consisting of $H_2O$, $D_2O$, HOD, $OH^-$ and $OD^-$. As a consequence, the spectrum is separated into OH (3200-4000 $cm^{-1}$) and OD (2500-2800 $cm^{-1}$) regions, each comprised of three peaks. From this, the spectrum of a HOD (from a 1:1 v/v

mixing of water and $D_2O$) can simply be subtracted to reveal the $OH^-$ and the $OD^-$ stretch (purple curve). The frequency of the $OD^-$ stretch is found to be 2682 $cm^{-1}$, consistent with a shift due to the mass difference between deuterium and hydrogen. This result confirms that the sharp resonance at 3634 $cm^{-1}$ is indeed due to $OH^-$. More importantly, both of the hydroxide frequencies are discernible from those of the free OD and free OH bonds in HOD by 10 and 29 $cm^{-1}$, respectively. These are the first clear experimental observations of $OH^-$ and $OD^-$ in a hydrophobic environment that is free from interaction with bulk water. This information is of fundamental interest and may help guide the search for the potential presence of hydroxides at aqueous surfaces.

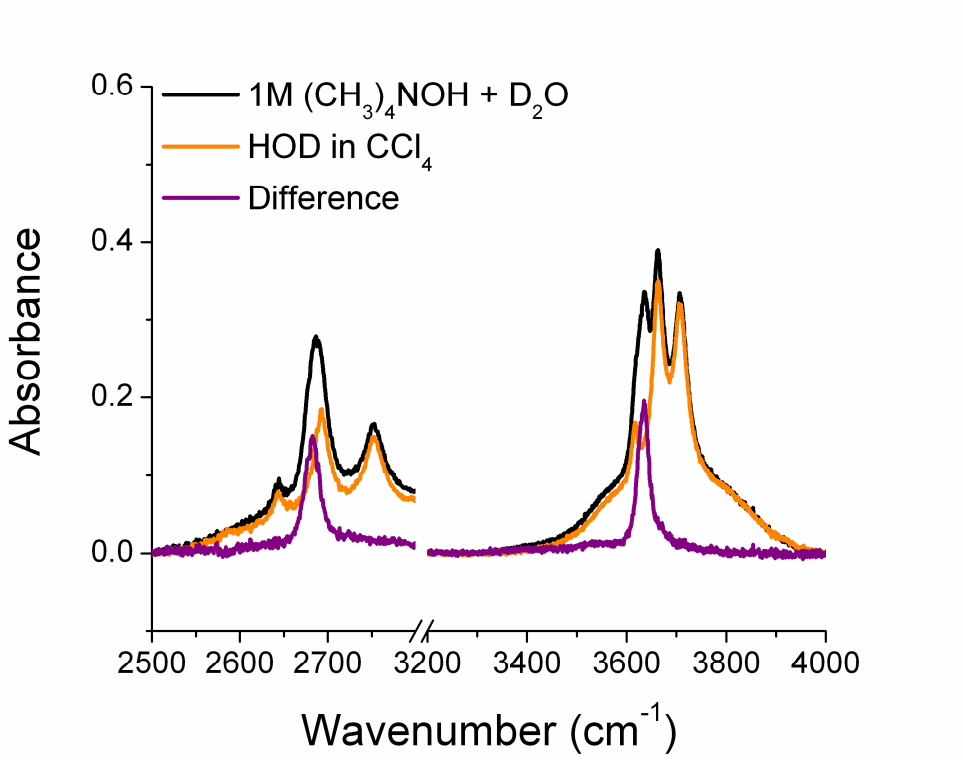


**Figure 9.2** Infrared spectrum of 1:1 v/v mixture of $(CH_3)_4NOH$ and $D_2O$ in $CCl_4$ at room temperature showing the $OD^-$ stretch at 2682 $cm^{-1}$ (purple curve). Both the $OH^-$ and $OD^-$ resonances are distinguishable from the free OH and the free OD bonds in HOD. Reprinted with permission from Vu, Shultz, *Chem. Phys. Lett.* **2013,** doi: 10.1016/j.cplett.2013.04.038

# Chapter 10 Appendix

This section describes a number of miscellaneous experiments that are not presented in the body of the thesis but might be in need for future references.

*10.1 Supercritical Argon*

A supercritical fluid is any substance at pressure and temperature conditions beyond its critical point where distinct gas and liquid phases no longer exist. Supercritical fluids are known to be universal solvents, which made them good candidates as media in which interactions between clathrate components can be probed. In addition, the use of supercritical fluid mimics the pressure conditions under which clathrates naturally form. In the following experiments, argon is chosen as the medium due to its infrared transparency and attainable critical pressure (48.34 atm at room temperature).[100] Approximately 55-60 atm of argon is used for all samples.

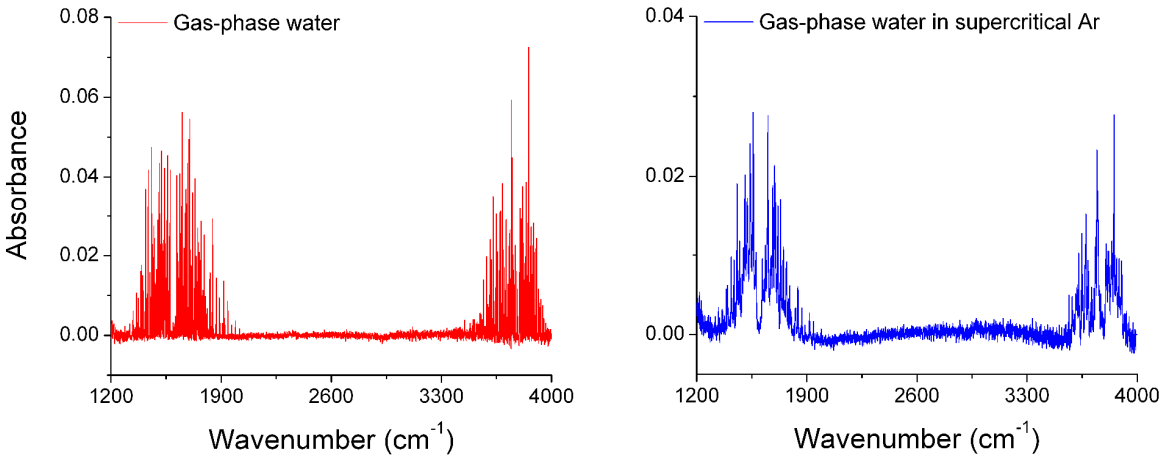


**Figure 10.1** Infrared spectrum of 13.3 torr of water in the gas phase (red) and in supercritical argon (blue, $P_{Ar}$ = 54.26 atm) at room temperature. Note the broadened rotational lines and the vertical scale in the blue spectrum.

Figure 10.1 displays the spectrum of water vapor in vacuum (red) and supercritical argon (blue) at room temperature. In the gas phase, water is an asymmetric rotor giving rise to a complex spectrum featuring rotational lines that extend for hundreds of wavenumbers.[101,102] Correspondingly, the sharp pikes in the spectrum on the left panel correspond to the rotational lines associated with the bending (~1600 $cm^{-1}$) and stretching (3500-4000 $cm^{-1}$) modes of water. In supercritical argon, however, these rotational lines are visibly broadened due to the effect of increased pressure. Some of the water intensity also seems to be lost, presumably due to argon's displacement of water vapor from the beam path. Figure 10.2 shows the effect of cooling water in supercritical argon to 0 °C. The spectrum indicates that some gas-phase water molecules have been gathered into clusters, evidenced by a broad H-bonded feature centered at 3300 $cm^{-1}$ and a decrease in the free water concentration.

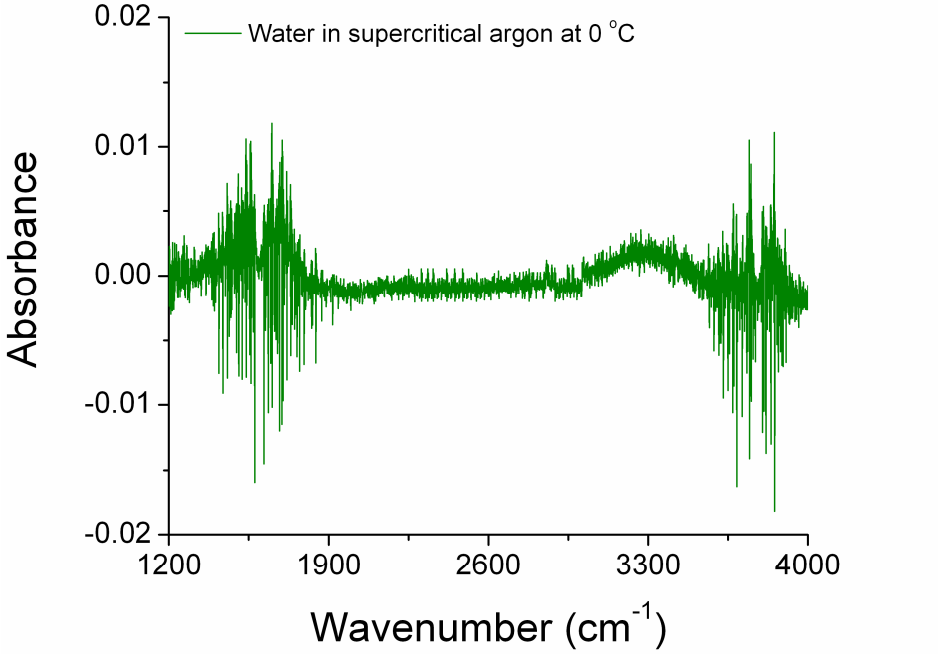


**Figure 10.2** Infrared spectrum of 13.3 torr of water in supercritical argon at 0 °C ($P_{Ar}$ = 54.26 atm). Note the presence of the H-bonded peak centered at 3300 $cm^{-1}$.

In the next sample, 60.03 atm of argon is deposited into the high-pressure cell containing a 17:1 mixture of water vapor to propane gas. The room temperature spectrum (Figure 10.3, left) clearly shows the propane stretching resonances at 2800-3000 $cm^{-1}$ together with the broadened rotational lines of water (the small peak at 2349 $cm^{-1}$ is an artifact of residual $CO_2$ in the cell). As it can be observed, no water cluster formation occurs at room temperature in the presence of propane. Hence, there is not a significant interaction between propane and water under these experimental conditions.

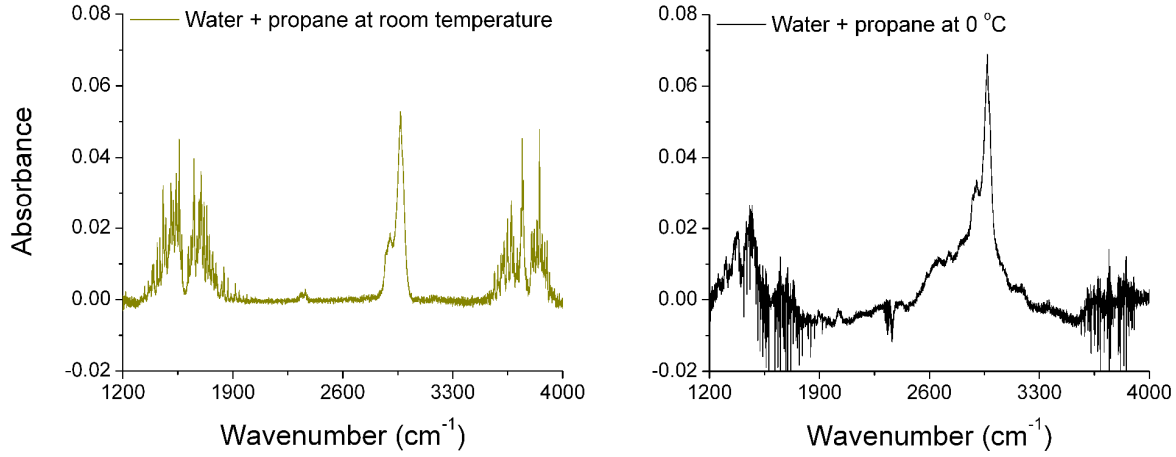


**Figure 10.3** Infrared spectrum of water and propane in 60.03 atm of argon at room temperature (left) and 0 $^{o}$C (right).

When the sample is allowed to cool down to 0$^{o}$C in a freezer over a 24 h period, its spectrum exhibits a strongly hydrogen-bonded feature around 3200 $cm^{-1}$ and also some weaker hydrogen bonding near 3400 $cm^{-1}$ (Figure 10.3, right). The development of these resonances is consistent with a decrease in the free water intensities, especially at 3700-3800 $cm^{-1}$. In addition, the base of the propane peak appears to be broadened. A possible explanation for this effect could be the occlusion of propane molecules in some sort of hydrate cavities. Recent modeling of

the electron density map of propane clathrate suggests that the guest molecule typically resides along the side of the cage rather than in the center.[103] Hence, frequent collisions of propane molecule into the cage walls can potentially lead to broadening of its vibrational signatures. There are also a few subtle features around 2000 – 2250 $cm^{-1}$. As noted previously in the thin film spectrum of water (Figure 6.1a), the broad resonance in this region is ascribed to the $\upsilon_2 + \upsilon_L$ combination band. Librations usually arise when rotations of water molecules are restricted, such as in a cyclic structure. The dependence of this band on hydrogen bonding would make it sensitive to changes in liquid structuring, and could potentially serve as a spectral signature for clathrate formation. The presented results are somewhat preliminary and do not allow for any definitive conclusions to be made, but the data overall do appear to be promising.

*10.2 Surfactants*

Due to the weak van der Waals nature of propane-water interaction, only a small number of water molecules are gathered by propane in carbon tetrachloride (Chapter 4). In an attempt to facilitate assembly of larger water clusters, SDS surfactant (sodium dodecyl sulphate) is added to $CCl_4$. Experiments however seem to indicate that water tends to partition to the surface rather than forming a water pocket in the $CCl_4$ solution because of the low solubility of the surfactant in the organic solvent. Consequently, addition of propane and argon pressure produces no effect in the H-bonded region of water. Another surfactant in the form of dipropylamine (DPA) is subsequently used. The motivation is that the propyl side chains will attract propane molecules by enhanced hydrophobic interaction.

Figure 10.4 shows the spectrum of a DPA/water cluster in $CCl_4$. Note that addition of the amine, a proton acceptor, into water causes broad H-bonded resonances at 3200 – 3400 $cm^{-1}$ and

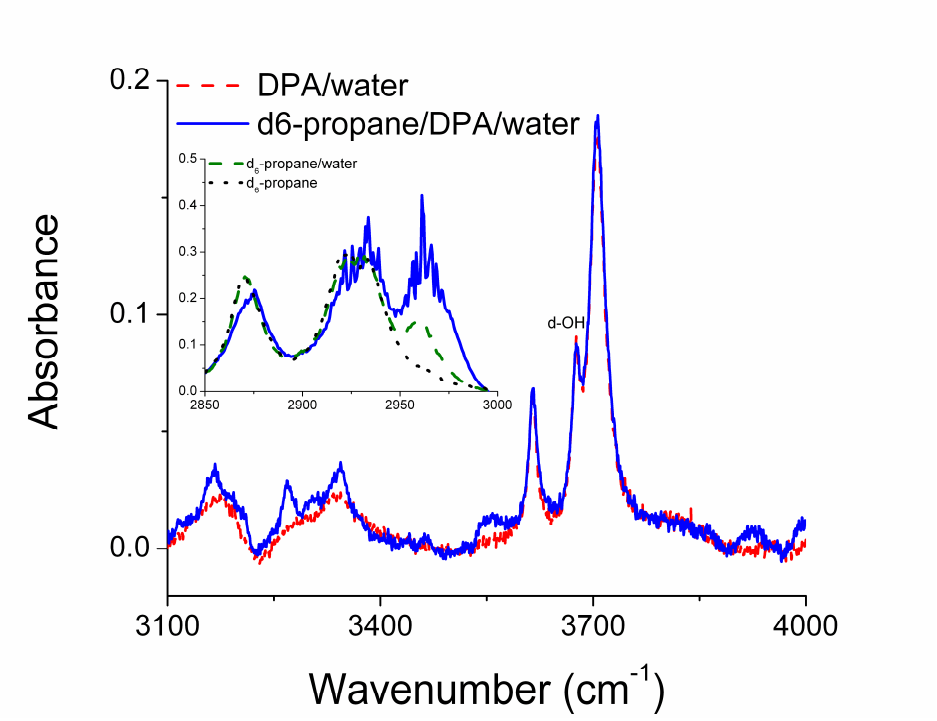


**Figure 10.4** Water clusters created by dipropylamine and $d_6$-propane in $CCl_4$ at -5 $^oC$ and 1 atm. Inset shows the C-H region of $d_6$-propane in the presence of water and amine, contrasted with neat $d_6$-propane and $d_6$-propane-water.

a dangling OH peak to appear (red dash). Here the frequency of the *d*-OH (3676 $cm^{-1}$) is considerably higher than that observed in a water cluster (3643 $cm^{-1}$), consistent with a weaker H-bond between amine and water. The H-bonded resonances at 3200 – 3400 $cm^{-1}$ hence contain contributions from both water-water and water-amine H-bonds. Upon addition of propane (blue solid), these broad H-bonded resonances become sharper and narrower, in addition to a slight red shift indicating a stronger and more compact H-bonded network between water molecules. The C-H stretch region of $d_6$-propane in the presence of amine and water (inset, blue solid) suggests that the propane molecule is gas-like, where sharp/distinct lines suggest longer vibrational lifetime. Recall that when propane interacts with a few water molecules (inset, green dash), the

blue-shifting C-H···O peak is much more broadened. A plausible conclusion is that the propane molecule is enclosed in some kind of H-bonded cavity, which protects it from homogeneous broadening by collision with the $CCl_4$ solvent. Compared to SDS surfactant, the use of dipropylamine improves the stability of the water pool to some extent, but the amine does not bring significantly more water into $CCl_4$ beyond 7.5 mM.

Dioctyl sodium sulfosuccinate (AOT) is an anionic surfactant with high solubility in $CCl_4$ and is more often used to construct stable reverse micellar systems. AOT offers an exceptional capability to increase the water concentration in $CCl_4$ well past the saturation limit. The size of the water nanopool is easily controlled by adjusting the W=[water]/[surfactant] ratio.[104] For $1 \leq W \leq 20$, the size of the reverse micelle can be determined by the following relation[105]

$$\frac{r^3}{(r-L)^3} = 1 + \frac{V_2}{W.V_1}$$

where r is the radius of the droplet in Å, L is the linear length of the surfactant molecule (15 Å for AOT), $V_1$ is the volume of a water molecule (30 $Å^3$) and $V_2$ is the volume of the surfactant molecule (825 $Å^3$ for AOT). Note that this equation is only an approximation of the micellar size, as it does not take into account the effect of different solvents. Figure 10.5 shows the spectrum of the AOT/water/$CCl_4$ reverse micelle at W=20, which corresponds to a pool size of ~12 nm. A number of pump-probe dynamics studies[106,107] have indicated that W=20 is also the point at which the confined water droplet begins behaving like bulk liquid water at room temperature. The water concentration Figure 10.5 is 20 mM, almost triple its saturation limit in $CCl_4$. The reverse micelle spectrum at room temperature (red curve) consists of contributions from both water in the pool and isolated water monomers in $CCl_4$. The intensity at 3850 $cm^{-1}$, attributed to pure water rotation, indicates that the free monomer concentration is about 5 mM

while the rest of the water (15 mM) is in the pool. Upon cooling to -5 $^{o}$C (blue curve) only 1 mM water remains free in $CCl_4$, thus the concentration of the pool has increased to 19 mM. As expected, the H-bond strength in the pool is enhanced as temperature decreases, demonstrated by sharpening of the broad H-bonded resonance and a moderate red shift (~20 $cm^{-1}$). There is also a visible enhancement of the shoulder at around 3250 $cm^{-1}$, which indicates stronger H-bonding at lower temperature.

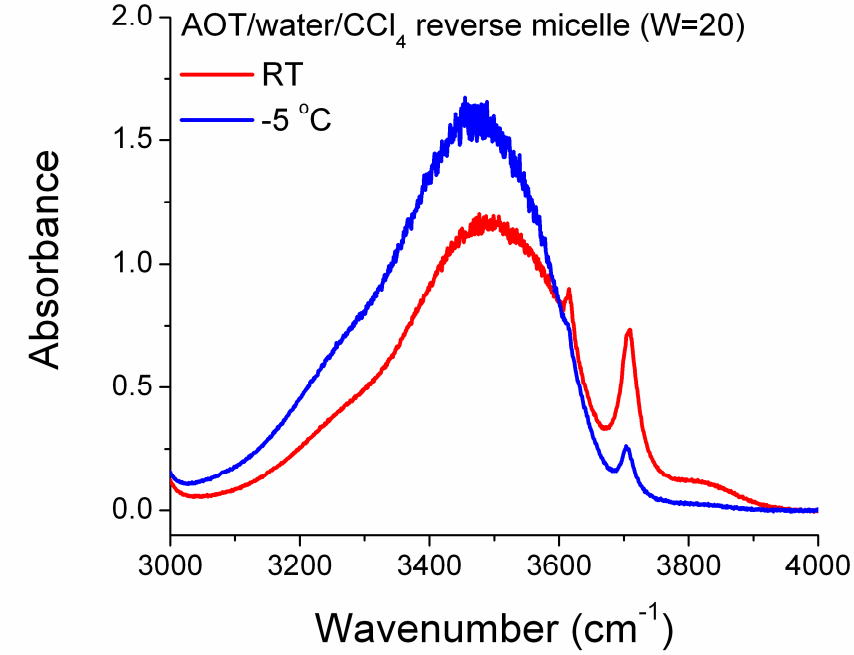


**Figure 10.5** AOT reverse micelle (~12 nm) in $CCl_4$ as a function of temperature. The concentration of AOT is 1 mM and that of water is 20 mM.

In Figure 10.6, the AOT reverse micelle is pressurized with 19.5 mM of propane and 20 atm of argon pressure at -5 $^{o}$C. Emergence of strong H-bonded peaks at 3150-3350 $cm^{-1}$ and scaling of the primary H-bonded intensity at 3472 $cm^{-1}$ point out that about 25% of the water pool has been converted to strongly H-bonded structures in the presence of propane. The

difference spectrum also reveals a very small, but observable, *d*-OH feature at ~3650 $cm^{-1}$. The features at 3700-3900 $cm^{-1}$ are tentatively assigned to propane-water combination bands in a clathrate cage, since these bands are not present in the smaller clusters where propane is associated with 2-3 water molecules.

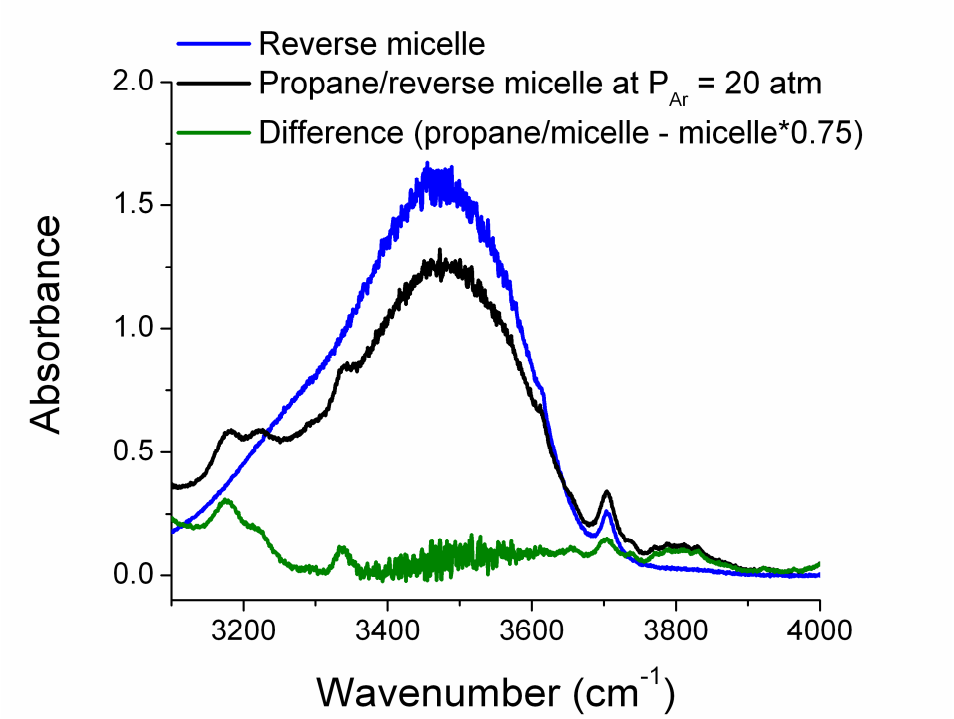


**Figure 10.6** AOT reverse micelle (W = 20) in $CCl_4$ at -5 $^oC$ in the presence (black) and absence (blue) of propane. The difference spectrum (where the blue spectrum is scaled down by 25%) shows emergence of H-bonded resonances at 3100-3400 $cm^{-1}$

Pressurization of propane and argon, however, decreases the micellar size progressively over time as hydrate crystals nucleate and float out of solution (hydrates are less dense than the $CCl_4$ solvent). This process is found to be completely reversible: when hydrates dissociate either by increasing the temperature or releasing the pressure, water is spontaneously incorporated back into the reverse micelle and its original size is restored. The precipitation phenomenon at high pressure, however, does not allow for direct observation of the enclathrating process.

*10.3 Silica Gel*

An alternative approach of using silica gel to absorb water into silica pores is also explored. The idea is to form clathrate within the pores of the gel, which are on the order of ~30 nm. A few beads of silica gel are ground into fine grains using mortar and pestle. To avoid spectral saturation of the H-bonded region, only a small amount of the powder (about the tip of a spatula) is introduced into the cell and dried under vacuum overnight before injection of wet $CCl_4$. The system is magnetically stirred to allow water to be absorbed into the silica grains (water absorption is indicated by a color change of the silica grains from clear to faint yellow). The solution is then cooled down to -5 $^{o}$C and its spectrum obtained (Figure 10.7, red).

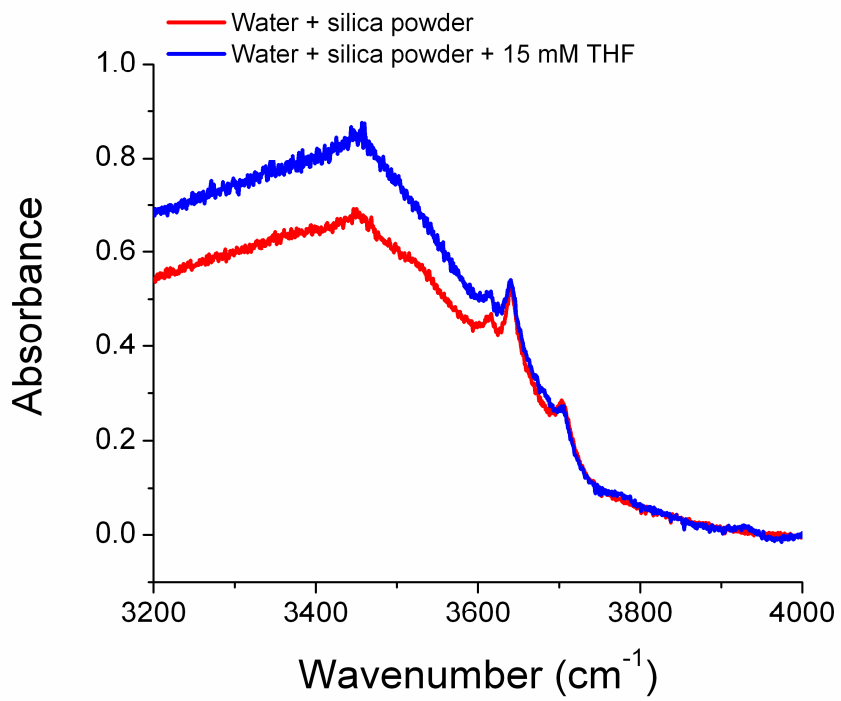


**Figure 10.7** Infrared spectrum of water/silica powder in $CCl_4$ at -5 $^{o}$C with (blue) and without (red) 15 mM THF.

THF is subsequently introduced at a concentration of 15 mM and the solution is stirred at room temperature for 18 h before cooling to -5 $^{o}$C. The resulting spectrum (Figure 10.7, blue) shows a broad, intense H-bonded region and a strong *d*-OH, similar to a thin film of water. As a result, not much information about the water structure can be reasonably deduced.

*10.4 Interaction between Benzene/Hexafluorobenzene and Water*

Due to the equal number of donor and acceptor sites in water, the tendency is to view it as a symmetrically interacting molecule. However, water has consistently shown a propensity to interact through the oxygen lone pair.[58] In an attempt to assess its willingness to donate a proton to a hydrophobic solute, benzene is added to the $CCl_4$-isolated water monomers as a model molecule. In particular, the slightly higher electronegativity of carbon relative to hydrogen and the overall $D_{6h}$ symmetry of benzene leads to a permanent negative quadrupole moment, which can act as a weak H-bond acceptor for water.[108] This type of O-H$^{\cdots}\pi$ interaction belongs to a rather unusual class of hydrogen bonding that has only been recently explored due to its potential role at biological surfaces containing aromatic amino acids.[109] Figure 10.8 shows the spectrum of a 1:1 mixture of water and benzene in $CCl_4$ at room temperature, where a dangling OH feature at 3644 cm$^{-1}$ is clearly visible. Due to its relatively low frequency, this *d*-OH peak is assigned to a water molecule that is H-bonded to another water molecule rather than to the aromatic ring of benzene. In this context, benzene behaves more or less similarly to large anions of halide salts in $CCl_4$.[58] The little bump at 3450 cm$^{-1}$ is thus inferred to be due to small H-bonded water clusters. There is also a small feature at 3588 cm$^{-1}$ (better seen through magnification) which could be due to the O-H$^{\cdots}\pi$ interaction. This interpretation is in reasonable agreement with a value of ~3610 cm$^{-1}$ obtained from Raman scattering measurements of a dilute (~22 mM) solution of benzene in water.[109] A DFT calculation of an isolated benzene-water dimer in Spartan (Figure 10.8, inset)

shows that water is positioned above the aromatic ring with both hydrogen atoms pointing inward to the π-electron cloud and a binding constant of -12.5 kJ/mol.

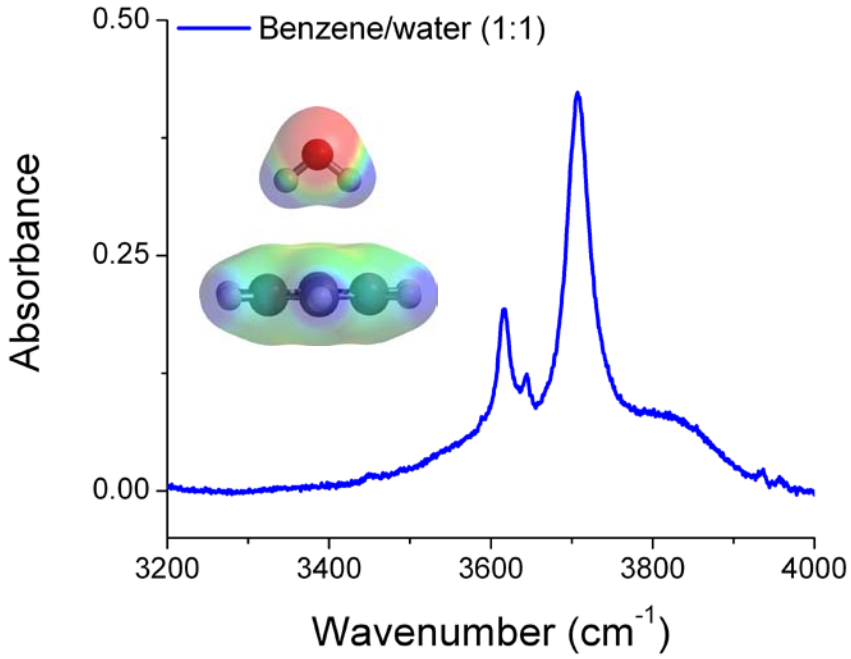


**Figure 10.8** Infrared spectrum of a 1:1 mixture of water and benzene in $CCl_4$ at room temperature and 1 atm. The concentration of each species is 7.5 mM. Note the presence of the *d*-OH resonance between the symmetric and asymmetric stretches of water.

Figure 10.9 presents the spectrum of a mixture of hexafluorobenzene and water in $CCl_4$. $C_6F_6$ shares similar structural properties with benzene, but has a very different π-electron system (i.e. a positive quadrupole moment).[108] A number of theoretical investigations have found a preferred water orientation that is roughly opposite to that of the benzene-water dimer.[108,110] Spartan calculation of a $C_6F_6$-water dimer (Figure 10.9, inset) also converges at a geometry in which water is situated directly above the aromatic ring with both hydrogen atoms pointing out and a binding energy of -10.4 kJ/mol. The magnitude of this interaction is quite comparable to that between water and benzene (-12.5 kJ/mol). Hence, there appears to be no significant

enthalpic penalty for pairing the oxygen lone pair with the π system. The experimental spectrum reflects the theoretical picture, as no *d*-OH resonance is observed for the $C_6F_6$/water system. Moreover, interaction at the oxygen lone pair would result in enhancement of the symmetric stretch transition dipole of water.[111-113] For neat water in $CCl_4$, the ratio of the asymmetric to symmetric stretch is 2.3 while this number decreases to 2.1 in the $C_6F_6$/water system. This slight enhancement of the symmetric stretch intensity thus supports the presence of an attractive interaction between the aromatic ring of $C_6F_6$ and water via the oxygen atom. The experimental results on both systems seem to indicate that the π-hydrogen and π-lone pair interactions dominate in benzene and hexafluorobenzene, respectively, leading to different orientations of water near the two species.

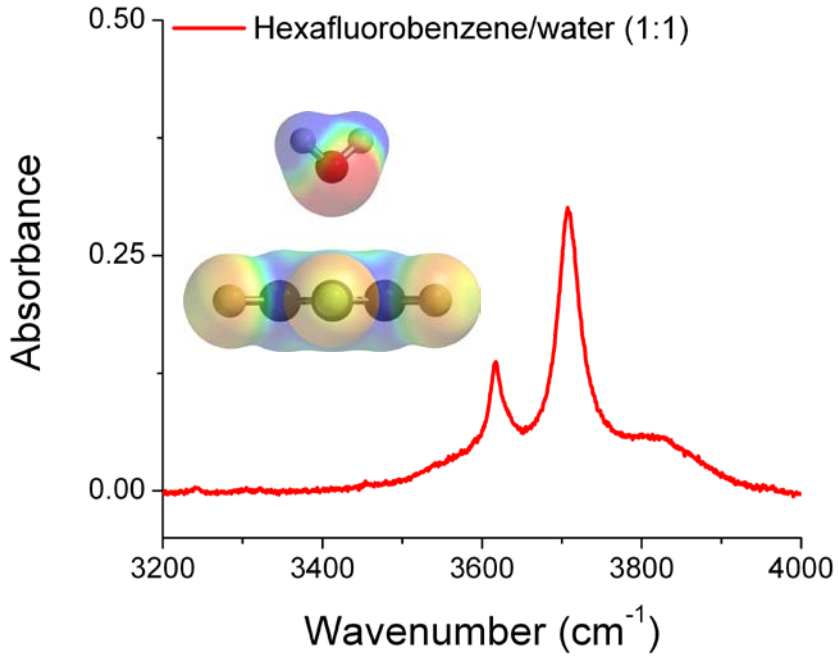


**Figure 10.9** Infrared spectrum of a 1:1 mixture of water and hexafluorobenzene at room temperature and 1 atm. The concentration of each species is 7.5 mM.

*10.5 Free Rotation of $CO_2$ in Freon Clathrate at Ambient Conditions*

The free rotation of guest molecules inside clathrate cavities is a notion that has been suggested by a number of theoretical studies.[103,114] However, experimental observations of such phenomenon are scarce: only one account of rotational motions of molecular hydrogen in $C_{60}$ at 6 K has been reported.[115] In addition to the extreme temperature, $H_2$ is a small guest and the $C_{60}$ cage is a larger and much more spherical host than for normally encountered clathrate systems. This section documents an unexpected observation of the rotational fine structure of $CO_2$ confined in trichlorofluoromethane at ambient conditions. In Figure 10.10, the red curve represents the IR spectrum of a standard batch of $CCl_3F$ (Freon™ 11, Sigma Aldrich ≥ 99.5% purity) containing some adventitious $CO_2$ at room temperature and 1 atm. Well-resolved

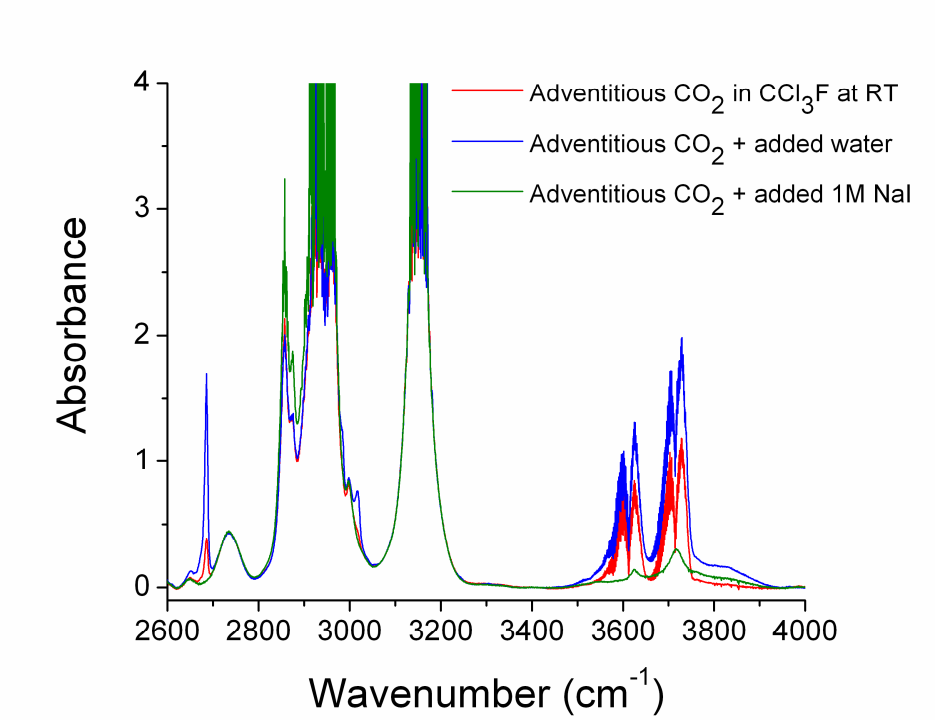


**Figure 10.10** Infrared spectrum of adventitious $CO_2$ in trichlorofluoromethane at room temperature showing the rotational lines of $CO_2$ at 3500-3800 $cm^{-1}$ (red). Addition of water (blue) enhances the rotational line intensity while the presence of 1M NaI quenches it (green).

rotational lines in each of the P and R branches associated with the $\nu_3 + 2\nu_2$ (3613 $cm^{-1}$) and $\nu_3 + \nu_1$ (3714 $cm^{-1}$) combination bands of $CO_2$ are clearly exhibited. A close-up of these structures is shown in Figure 10.11, where a gas-phase spectrum of $CO_2$ obtained from sublimating dry ice is also included for comparison (black curve). The spacing between the sharp lines in both spectra is found to be 1.8 $cm^{-1}$, confirming that the observed structures are indeed due to $CO_2$. The fact that oxygen is a boson requires the wavefunction to be symmetric with respect to interchange of the two oxygen atoms. As rotational symmetry follows the rotational quantum number J – even J's are symmetric and odd J's are antisymmetric – only even J's are observed. The line spacing is thus 4B, which leads to a rotational constant of B = 0.45 $cm^{-1}$.

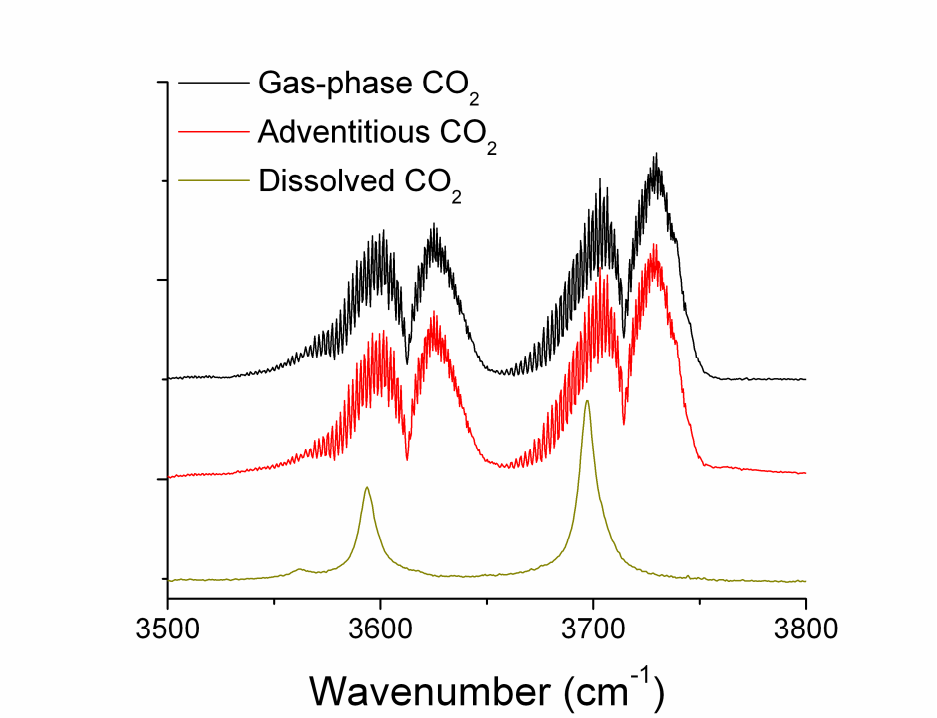


**Figure 10.11** Infrared spectrum of 680 torr $CO_2$ (g) dissolved in another batch of $CCl_3F$ (yellow) compared to one that contains adventitious $CO_2$ in Figure 10.10 (red). The spectrum of gaseous $CO_2$ (black) is included for comparison. All spectra are obtained at room temperature.

The spectra in Figure 10.10 also show a peculiar feature at 2686 $cm^{-1}$ that seems to directly associate with the existence of $CO_2$ rotational lines in Freon. When water is added to $CCl_3F$ containing adventitious $CO_2$, the intensity of this peak as well as that of the rotational lines are greatly enhanced (blue curve). The presence of 1M NaI, on the other hand, completely suppresses this resonance and collapses the $CO_2$ lines (green spectrum). As a consequence, this sharp 2686 $cm^{-1}$ feature is interpreted to be due to some impurity in the freon. As impurities vary from batch to batch, the rotational lines are also not reproducible (samples from another bottle of $CCl_3F$ purchased from Sigma Aldrich a few months later exhibit neither 2686 $cm^{-1}$ peak nor adventitious $CO_2$). When external $CO_2$ gas is dissolved in such a batch, the spectrum only shows two sharp features without any rotational fine structure (Figure 10.11, yellow). Attempts to identify the impurity responsible for the free rotation of $CO_2$ in freon have yet to be

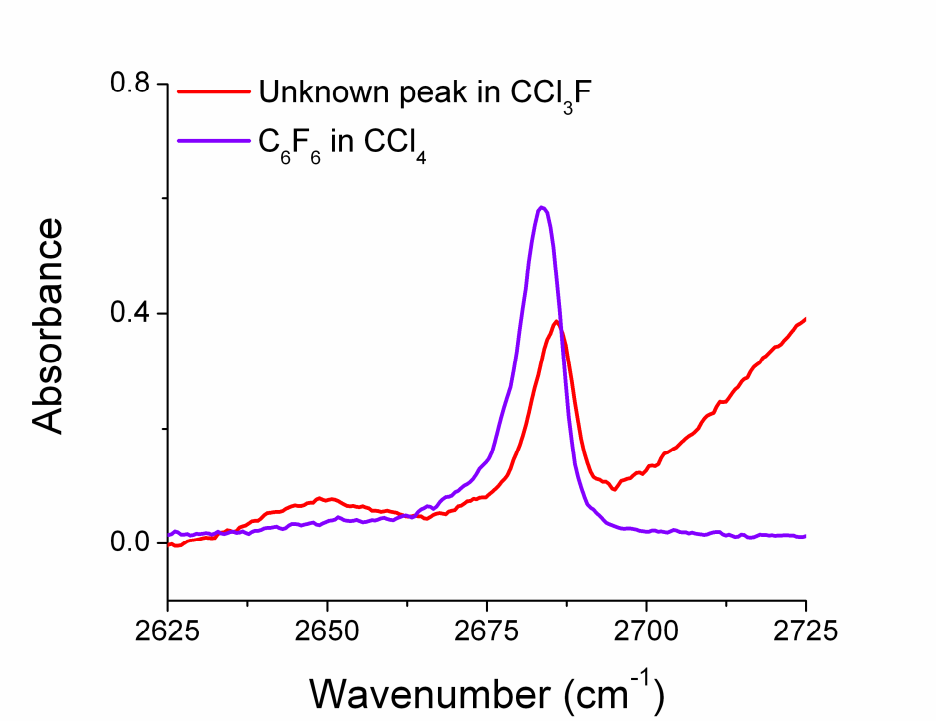


**Figure 10.12** Unknown peak associated with free rotation of $CO_2$ in $CCl_3F$ compared to the spectrum of $C_6F_6$ in $CCl_4$ in the 2625-2725 $cm^{-1}$ region.

successful. $C_6F_6$ is among a few fluoro-containing compounds that have a sharp absorption resonance in this region. Figure 10.12 shows that the $C_6F_6$ peak in $CCl_4$ comes reasonably close in frequency with the unknown peak at 2686 $cm^{-1}$ in $CCl_3F$. The wavenumber shift owing to the difference in dielectric constant between the two solvents should be taken into account when comparing these two spectra.

In short, the fortuitous experiments described in this section provide new spectroscopic evidence for the existence of a $CO_2$ clathrate in Freon-11 at room temperature and ambient pressure. The IR spectrum exhibits unusually detailed condensed-phase dynamics indicating a gas-like environment characteristic of an enclathrated guest. $CO_2$ is believed to be rotating freely in the solvent cage with a rotational constant similar to that in the gas phase. The origin and formation process of this type of $CO_2$ clathrate, however, remain unknown as impurities in $CCl_3F$ appear to play a defining role.

# Bibliography

** Publications of Tuan H. Vu*


(1) Davy, H. On Some of the Combinations of Oxymuriatic Gas and Oxygene, and on the Chemical Relations of these Principles to Inflammable Bodies. *Phil. Trans. Roy. Soc. Lond.* **1811**, *101*, 1-35.

(2) Faraday, M.; Davy, H. On Fluid Chlorine. *Phil. Trans. Roy. Soc. Lond.* **1823**, *113*, 160-165.

(3) Murthy, S. S. N. Detailed Study of Ice Clathrate Relaxation: Evidence for the Existence of Clathrate Structures in Some Water-Alcohol Mixtures. *J. Phys. Chem. A* **1999**, *103*, 7927-7937.

(4) Bagherzadeh, S. A.; Englezos, P.; Alavi, S.; Ripmeester, J. A. Influence of Hydrated Silica Surfaces on Interfacial Water in the Presence of Clathrate Hydrate Forming Gases. *J. Phys. Chem. C* **2012**, *116*, 24907–24915.

(5) Dartois, E.; Deboffle, D. Methane Clathrate Hydrate FTIR Spectrum - Implications for Its Cometary and Planetary Detection. *Astron. Astrophys.* **2008**, *490*, L19-L22.

(6) Haq, B. U. Methane in the Deep Blue Sea. *Science* **1999**, *285*, 543-544.

(7) Max, M. D.: *Natural Gas Hydrate: In Oceanic and Permafrost Environments*; Kluwer Academic Publishers: Boston, 2000.

(8) Kvenvolden, K. A.; Ginsburg, G. D.; Soloviev, V. A. Worldwide Distribution of Subaquatic Gas Hydrates. *Geo-Mar. Lett.* **1993**, *13*, 32-40.

(9) MacDonald, G. J. Role of Methane Clathrates in Past and Future Climates. *Climactic Change* **1990**, *16*, 247-281.

(10) Uchida, T.; Ohmura, R.; Ikeda, I. Y.; Nagao, J.; Takeya, S.; Hori, A. Phase Equilibrium Measurements and Crystallographic Analyses on Structure-H Type Gas Hydrate Formed from the $CH_4$−$CO_2$−Neohexane−Water System. *J. Phys. Chem. B* **2006**, *110*, 4583-4588.

(11) Henning, R. W.; Schultz, A. J.; Thieu, V.; Halpern, Y. Neutron Diffraction Studies of $CO_2$ Clathrate Hydrate: Formation from Deuterated Ice. *J. Phys. Chem. A* **2000**, *104*, 5066-5071.

(12) He, Y.; Rudolph, E. S. J.; Zitha, P. L. J.; Golombok, M. Kinetics of $CO_2$ and Methane Hydrate Formation: An Experimental Analysis in the Bulk Phase. *Fuel* **2011**, *90*, 272-279.

(13) Glavatskiy, K. S.; Vlugt, T. J. H.; Kjelstrup, S. Toward a Possibility To Exchange $CO_2$ and $CH_4$ in sI Clathrate Hydrates. *J. Phys. Chem. B* **2012**, *116*, 3745-3753.

(14) Kennedy, M.; Mrofka, D.; von der Borch, C. Snowball Earth Termination by Destabilization of Equatorial Permafrost Methane Clathrate. *Nature* **2008**, *453*, 642-645.

(15) Long, J.; Sloan, E. D., Jr. Quantized Water Clusters Around Apolar Molecules. *Mol. Simul.* **1993**, *11*, 145-161.

(16) Ohno, H.; Kida, M.; Sakurai, T.; Iizuka, Y.; Hondoh, T.; Narita, H.; Nagao, J. Symmetric Stretching Vibration of $CH_4$ in Clathrate Hydrate Structures. *ChemPhysChem* **2010**, *11*, 3070-3073.

(17) Dirdal, E. G.; Arulanantham, C.; Sefidroodi, H.; Kelland, M. A. Can Cyclopentane Hydrate Formation be Used to Rank the Performance of Kinetic Hydrate Inhibitors? *Chem. Eng. Sci.* **2012**, *82*, 177-184.

(18) Førrisdahl, O. K.; Kvamme, B.; Haymet, A. D. J. Methane Clathrate Hydrates: Melting, Supercooling and Phase Separation from Molecular Dynamics Computer Simulations. *Mol. Phys.* **1996**, *89*, 819-834.

(19) Raghavendra, B.; Arunan, E. Hydrogen Bonding with a Hydrogen Bond: The Methane-Water Complex and the Penta-Coordinate Carbon. *Chem. Phys. Lett.* **2008**, *467*, 37-40.

(20) Jiang, H.; Jordan, K. D.; Taylor, C. E. Molecular Dynamics Simulations of Methane Hydrate Using Polarizable Force Fields. *J. Phys. Chem. B* **2007**, *111*, 6486-6492.

(21) McCarthy, V. N.; Jordan, K. D. Structure and Stability of the $(H_2O)_{21}$ and $(H_2O)_{20}.(H_2S)$ Clusters: Relevance of Cluster Systems to Gas Hydrate Formation. *Chem. Phys. Lett.* **2006**, *429*, 166-168.

(22) Yasuda, K.; Takeya, S.; Sakashita, M.; Yamawaki, H.; Ohmura, R. Binary Ethanol-Methane Clathrate Hydrate Formation in the System $CH_4$-$C_2H_5OH$-$H_2O$: Confirmation of Structure II Hydrate Formation. *J. Phys. Chem. C* **2009**, *113*, 12598-12601.

(23) Buchanan, P.; Aldiwan, N.; Soper, A. K.; Creek, J. L.; Koh, C. A. Decreased Structure on Dissolving Methane in Water. *Chem. Phys. Lett.* **2005**, *415*, 89-93.

(24) Cady, G. H. Composition of Clathrate Gas Hydrates of $H_2S$, Xe, $SO_2$, $Cl_2$, $CH_3Cl$, $CH_3Br$, $CHClF_2$, $CCl_2F_2$, and $C_3H_8$. *J. Phys. Chem.* **1983**, *87*, 4437-4441.

(25) Allison, S. A.; Barrer, R. M. Clathration by Phenol and Quinol 1. Equilibria. *Trans. Farad. Soc.* **1968**, *64*, 549-556.

(26) Allison, S. A.; Barrer, R. M. Clathration by Phenol and Quinol 2. Kinetics. *Trans. Farad. Soc.* **1968**, *64*, 557-563.

(27) Barrer, R. M.; Edge, A. V. J. Gas Hydrates Containing Argon, Krypton, and Xenon - Kinetics and Energetics of Formation and Equilibria. *Proc. Roy. Soc. Ser. A: Math. Phys. Sci.* **1967**, *300*, 1-9.

(28) Whitman, C. A.; Mysyk, R.; White, M. A. Investigation of Factors Affecting Crystallization of Cyclopentane Clathrate Hydrate. *J. Chem. Phys.* **2008**, *129*, 174502.

(29) Lee, J. D.; Song, M.; Susilo, R.; Englezos, P. Dynamics of Methane-Propane Clathrate Hydrate Crystal Growth from Liquid Water with or without the Presence of *n*-Heptane. *Cryst. Growth Des.* **2006**, *6*, 1428-1439.

(30) Peng, B. Z.; Dandekar, A.; Sun, C. Y.; Luo, H.; Ma, Q. L.; Pang, W. X.; Chen, G. J. Hydrate Film Growth on the Surface of a Gas Bubble Suspended in Water. *J. Phys. Chem. B* **2007**, *111*, 12485-12493.

(31) Murshed, M. M.; Kuhs, W. F. Kinetic Studies of Methane-Ethane Mixed Gas Hydrates by Neutron Diffraction and Raman Spectroscopy. *J. Phys. Chem. B* **2009**, *113*, 5172-5180.

(32) Wang, W.; Bray, C. L.; Adams, D. J.; Cooper, A. I. Methane Storage in Dry Water Gas Hydrates. *J. Am. Chem. Soc.* **2008**, *130*, 11608-11609.

(33) Smelik, E. A.; King, H. E., Jr. Crystal-Growth Studies of Natural Gas Clathrate Hydrates Using a Pressurized Optical Cell. *Am. Mineral.* **1997**, *82*, 88-98.

(34) Thompson, H.; Soper, A. K.; Buchanan, P.; Aldiwan, N.; Creek, J. L.; Koh, C. A. Methane Hydrate Formation and Decomposition: Structural Studies via Neutron Diffraction and Empirical Potential Structure Refinement. *J. Chem. Phys.* **2006**, *124*, 164508.

(35) Kini, R. A.; Dec, S. F.; Sloan, E. D. Methane + Propane Structure II Hydrate Formation Kinetics. *J. Phys. Chem. A* **2004**, *108*, 9550-9556.

(36) Lehmkühler, F.; Paulus, M.; Sternemann, C.; Lietz, D.; Venturini, F.; Gutt, C.; Tolan, M. The Carbon Dioxide-Water Interface at Conditions of Gas Hydrate Formation. *J. Am. Chem. Soc.* **2009**, *131*, 585-589.

(37) Boewer, L.; Nase, J.; Paulus, M.; Lehmkühler, F.; Tiemeyer, S.; Holz, S.; Pontoni, D.; Tolan, M. On the Spontaneous Formation of Clathrate Hydrates at Water−Guest Interfaces. *J. Phys. Chem. C* **2012**, *116*, 8548-8553.

(38) Hirai, S.; Okazaki, K.; Tabe, Y.; Kawamura, K. $CO_2$ Clathrate-Hydrate Formation and Its Mechanism by Molecular Dynamics Simulation. *Energ. Conv. Manage.* **1997**, *38*, S301-S306.

(39) Shepherd, T. D.; Koc, M. A.; Molinero, V. The Quasi-Liquid Layer of Ice under Conditions of Methane Clathrate Formation. *J. Phys. Chem. C* **2012**, *116*, 12172-12180.

(40) Christiansen, R. L.; Sloan, E. D., Jr. Mechanisms and Kinetics of Hydrate Formation. *Ann. N. Y. Acad. Sci.* **1993**, *715*, 283-305.

(41) Rodger, P. M. Stability of Gas Hydrates. *J. Phys. Chem.* **1990**, *94*, 6080-6089.

(42) Radhakrishnan, R.; Trout, B. L. A New Approach for Studying Nucleation Phenomena Using Molecular Simulations: Application to $CO_2$ Hydrate Clathrates. *J. Chem. Phys.* **2002**, *117*, 1786-1796.

(43) Moon, C.; Taylor, P. C.; Rodger, P. M. Molecular Dynamics Study of Gas Hydrate Formation. *J. Am. Chem. Soc.* **2003**, *125*, 4706–4707.

(44) Muro, M.; Harada, M.; Hasegawa, T.; Okada, T. Formation and Growth of Tetrahydrofuran Hydrate at the Ice/Hexane Interface. *J. Phys. Chem. C* **2012**, *116*, 13296-13301.

(45) Zhang, J.; Hawtin, R. W.; Yang, Y.; Nakagava, E.; Rivero, M.; Choi, S. K.; Rodger, P. M. Molecular Dynamics Study of Methane Hydrate Formation at a Water/Methane Interface. *J. Phys. Chem. B* **2008**, *112*, 10608–10618.

(46) Nada, H. Anisotropy in Growth Kinetics of Tetrahydrofuran Clathrate Hydrate: A Molecular Dynamics Study. *J. Phys. Chem. B* **2009**, *113*, 4790–4798.

(47) Spartan '08. Spartan '08 v. 1.1.1 ed.; Wavefunction, Inc.: Irvine, CA.

(48) Prado, M. R.; Pham, A.; Ferazzi, R. E.; Edwards, K.; Janda, K. C. Gas Clathrate Hydrates Experiment for High School Projects and Undergraduate Laboratories. *J. Chem. Educ.* **2007**, *84*, 1790-1791.

(49) Sloan, E. D., Jr.; Koh, C. A.: *Clathrate Hydrates of Natural Gases*; 3rd ed.; CRC Press: Boca Raton, FL, 2008.

(50) Prado, M. R.; Cazares, Y.; Janda, K. C. Toward the Efficient Production of Methane/Propane Double Hydrate. *Ind. Eng. Chem. Res.* **2009**, *48*, 5160-5164.

(51) Abbondondola, J. A.; Fleischer, E. B.; Janda, K. C. Propane Clathrate Hydrate Formation Accelerated by Xenon. *J. Phys. Chem. C* **2009**, *113*, 4717–4720.

(52) Kuo, M. H.; David, A.; Kamelamela, N.; White, N.; Shultz, M. J. Nitric Acid−Water Interaction Probed via Isolation in Carbon Tetrachloride. *J. Phys. Chem. C* **2007**, *111*, 8827-8831.

(53) Kuo, M. H.; Kamelamela, N.; Shultz, M. J. Rotational Structure of Water in a Hydrophobic Environment: Carbon Tetrachloride. *J. Phys. Chem. A* **2008**, *112*, 1214-1218.

(54)* Vu, T. H.; Kälin, S. D.; Shultz, M. J. Spectroscopic Identification of Water-Propane Interaction: Implications for Clathrate Nucleation. *J. Phys. Chem. A* **2010**, *114*, 6356-6360.

(55) Gu, Y.; Kar, T.; Scheiner, S. Fundamental Properties of the CH···O Interaction: Is It a True Hydrogen Bond? *J. Am. Chem. Soc.* **1999**, *121*, 9411-9422.

(56) Hobza, P.; Havlas, Z. Blue-Shifting Hydrogen Bonds. *Chem. Rev.* **2000**, *121*, 4253-4264.

(57) Masunov, A.; Dannenberg, J. J.; Contreras, R. H. C−H Bond-Shortening upon Hydrogen Bond Formation: Influence of an Electric Field. *J. Phys. Chem. A* **2001**, *105*, 4737-4740.

(58)* Shultz, M. J.; Vu, T. H.; Meyer, B.; Bisson, P. Water: A Responsive Small Molecule. *Acc. Chem. Res.* **2012**, *45*, 15-22. 4th most read article in the first quarter.

(59) Devlin, J. P. Preferential Deuterium Bonding at the Ice Surface: A Probe of Surface Water Molecule Mobility. *J. Chem. Phys.* **2000**, *112*, 5527-5529.

(60) Engdahl, A.; Nelander, B. On the Relative Stabilities of H- and D-Bonded Water Dimers. *J. Chem. Phys.* **1987**, *86*, 1819-1823.

(61) Fennell, C. J.; Kehoe, C.; Dill, K. A. Oil/Water Transfer is Partly Driven by Molecular Shape, Not Just Size. *J. Am. Chem. Soc.* **2010**, *132*, 234-240.

(62)* Vu, T. H.; Shultz, M. J. Competitive Binding of Methanol and Propane for Water Via Matrix-Isolation Spectroscopy: Implications for Inhibition of Clathrate Nucleation. *J. Phys. Chem. A* **2011**, *115*, 998-1002.

(63) Koh, C. A.; Westacott, R. E.; Zhang, W.; Hirachand, K.; Creek, J. L.; Soper, A. K. Mechanism of Gas Hydrate Formation and Inhibition. *Fluid Phase Equilib.* **2002**, *194-197*, 143-151.

(64) Anderson, B. J.; Tester, J., W.; Gorghi, G. P.; Trout, B. L. Properties of Inhibitors of Methane Hydrate Formation via Molecular Dynamics Simulations. *J. Am. Chem. Soc.* **2005**, *127*, 17852-17862.

(65) Bobev, S.; Tait, K. T. Methanol - Inhibitor or Promotor of the Formation of Gas Hydrates from Deuterated Ice? *Am. Mineral.* **2004**, *112*, 6804-6816.

(66) Williams, K. D.; Devlin, J. P. Formation and Spectra of Clathrate Hydrates of Methanol and Methanol-Ether Mixtures. *J. Mol. Struct.* **1997**, *416*, 277-286.

(67) Devlin, J. P.; Monreal, I. A. Clathrate-Hydrate Ultrafast Nucleation and Crystallization from Supercooled Aqueous Droplets. *Chem. Phys. Lett.* **2010**, *492*, 1-8.

(68) Koga, K.; Tanaka, H.; Nakanishi, K. Stability of Polar Guest-Encaging Clathrate Hydrates. *J. Chem. Phys.* **1994**, *101*, 3127-2134.

(69) Levinger, N. E.; Davis, P. H.; Fayer, M. D. Vibrational Relaxation of the Free Terminal Hydroxyl Stretch in Methanol Oligomers: Indirect Pathway to Hydrogen Bond Breaking. *J. Chem. Phys.* **2001**, *115*, 9352-9360.

(70) Kristiansson, O. Investigation of the OH Stretching Vibration of $CD_3OH$ in $CCl_4$. *J. Mol. Struct.* **1999**, *477*, 105-111.

(71) Bonner, O. D. A Comparison of Hydrogen- and Deuterium-Bonding in Carbon Tetrachloride Solutions of Methanol. *J. Chem. Thermodyn.* **1970**, *2*, 577-581.

(72) England-Kretzer, L.; Fritzsche, M.; Luck, W. A. P. The Intensity Change of IR OH Bands by H-bonds. *J. Mol. Struct.* **1988**, *175*, 277-282.

(73) Symons, M. C. R.; Thomas, V. K. Structure of Methanol + Inert Solvent Systems. *J. Chem. Soc., Faraday Trans. 1* **1981**, *77*, 1883-1890.

(74) Bahr, S.; Toubin, C.; Kempter, V. Interaction of Methanol with Amorphous Solid Water. *J. Chem. Phys.* **2008**, *128*, 134712.

(75) Mao, W. L.; Koh, C. A.; Sloan, E. D., Jr. Clathrate Hydrates Under Pressure. *Phys. Today* **2007**, *60*, 42-47.

(76) Zhang, Y.; Debenedetti, P. G.; Prud'homme, R. K.; Pethica, B. A. Differential Scanning Calorimetry Studies of Clathrate Hydrate Formation. *J. Phys. Chem. B* **2004**, *108*, 16717-16722.

(77) Venyaminov, S. Y.; Prendergast, F. G. Water ($H_2O$ and $D_2O$) Molar Absorptivity in the 1000–4000 $cm^{-1}$ Range and Quantitative Infrared Spectroscopy of Aqueous Solutions. *Anal. Biochem.* **1997**, *248*, 234-245.

(78) Libnau, F. O.; Christy, A. A.; Kvalheim, O. M. Determination of the Equilibrium Constant and Resolution of the HOD Spectrum by Alternating Least-Squares and Infrared Analysis. *Appl. Spectrosc.* **1995**, *49*, 1431-1437.

(79) Corcelli, S. A.; Skinner, J. L. Infrared and Raman Line Shapes of Dilute HOD in Liquid $H_2O$ and $D_2O$ from 10 to 90 $^oC$. *J. Phys. Chem. A* **2005**, *109*, 6154-6165.

(80) Eaves, J.; Tokmakoff, A.; Geissler, P. Electric Field Fluctuations Drive Vibrational Dephasing in Water. *J. Phys. Chem. A* **2005**, *109*, 9424-9436.

(81) Ma, B.-Q.; Sun, H.-L.; Gao, S. Cyclic Water Pentamer in a Tape-Like Structure. *Chem. Commun.* **2004**, 2220-2221.

(82) Naskar, J. P.; Drew, M. G. B.; Hulme, A.; Tocherc, D. A.; Datta, D. Occurrence of Ribbons of Cyclic Water Pentamers in a Metallo-Organic Framework Formed by Spontaneous Fixation of $CO_2$. *Cryst. Eng. Comm.* **2005**, *7*, 67-70.

(83) Carrasco, J.; Michaelides, A.; Forster, M.; Haq, S.; Raval, R.; Hodgson, A. A One-Dimensional Ice Structure Built from Pentagons. *Nat. Mater.* **2009**, *8*, 427-431.

(84) Hermansson, K.; Bopp, P. A.; Spångberg, D.; Pejov, L.; Bakó, I.; Mitev, P. D. The Vibrating Hydroxide Ion in Water. *Chem. Phys. Lett.* **2011**, *514*, 1-15.

(85) Shin, K.; Cha, J.-H.; Seo, Y.; Lee, H. Physicochemical Properties of Ionic Clathrate Hydrates. *Chem. Asian J.* **2010**, *5*, 22-34.

(86) Graciaa, A.; Morel, G.; Saulner, P.; Lachaise, J.; Schechter, R. S. The ζ-Potential of Gas Bubbles. *J. Coll. Interface Sci.* **1995**, *172*, 131-136.

(87) Creux, P.; Lachaise, J.; Graciaa, A.; Beattie, J. K. Specific Cation Effects at the Hydroxide-Charged Air/Water Interface. *J. Phys. Chem. C* **2007**, *111*, 3753-3755.

(88) Petersen, M. K.; Iyengar, S. S.; Day, T. J. F.; Voth, G. A. The Hydrated Proton at the Water Liquid/Vapor Interface. *J. Phys. Chem. B* **2004**, *108*, 14804–14806.

(89) Buch, V.; Milet, A.; Vácha, R.; Jungwirth, P.; Devlin, J. P. Water Surface is Acidic. *Proc. Nat. Acad. Sci.* **2007**, *104*, 7342-7347.

(90) Tian, C.; Ji, N.; Waychunas, G. A.; Shen, Y. R. Interfacial Structures of Acidic and Basic Aqueous Solutions. *J. Am. Chem. Soc.* **2008**, *130*, 13033–13039.

(91) Levering, L. M.; Sierra-Hernández, M. R.; Allen, H. C. Observation of Hydronium Ions at the Air−Aqueous Acid Interface: Vibrational Spectroscopic Studies of Aqueous HCl, HBr, and HI. *J. Phys. Chem. C* **2007**, *111*, 8814–8826.

(92) Tarbuck, T. L.; Ota, S. T.; Richmond, G. L. Spectroscopic Studies of Solvated Hydrogen and Hydroxide Ions at Aqueous Surfaces. *J. Am. Chem. Soc.* **2006**, *128*, 14519–14527.

(93) Busing, W. R. Infrared Spectra and Structure of NaOH and NaOD. *J. Chem. Phys.* **1955**, *23*, 933-936.

(94) Busing, W. R.; Hornig, D. F. The Effect of Dissolved KBr, KOH or HCl on the Raman Spectrum of Water. *J. Phys. Chem.* **1961**, *65*, 284-292.

(95) Librovich, N. B.; Sakun, V. P.; Sokolov, N. D. $H^+$ and $OH^-$ Ions in Aqueous Solutions. Vibrational Spectra of Hydrates. *Chem. Phys.* **1979**, *39*, 351-366.

(96) Corridoni, T.; Sodo, A.; Bruni, F.; Ricci, M. A.; Nardone, M. Probing Water Dynamics with $OH^-$. *Chem. Phys.* **2007**, *336*, 183-187.

(97) Roberts, S. T.; Petersen, P. B.; Ramasesha, K.; Tokmakoff, A.; Ufimtsev, I. S.; Martinez, T. J. Observation of a Zundel-Like Transition State during Proton Transfer in Aqueous Hydroxide Solutions. *Proc. Nat. Acad. Sci.* **2009**, *106*, 15154-15159.

(98) Roberts, S. T.; Petersen, P. B.; Ramasesha, K.; Tokmakoff, A.: The Dynamics of Aqueous Hydroxide Ion Transport Probed via Ultrafast Vibrational Echo Experiments. In *Springer Series in Chemical Physics*; Corkum, P., Ed.; Springer-Verlag, 2009; Vol. 92; pp 481-483.

(99) Tian, C. S.; Shen, Y. R. Structure and Charging of Hydrophobic Material/Water Interfaces Studied by Phase-Sensitive Sum-Frequency Vibrational Spectroscopy. *Proc. Nat. Acad. Sci.* **2009**, *106*, 15148-15153.

(100) Weast, R. C.: *CRC Handbook of Chemistry and Physics*; 84th ed.; The Chemical Rubber Company: Cleveland, OH, 2003.

(101) Hall, R. T.; Dowling, J. M. Pure Rotational Spectrum of Water Vapor. *J. Chem. Phys.* **1967**, *47*, 2454-2461.

(102) Judge, R. H.; Clouthier, D. J. AsyrotWin: A 32-bit Windows Version of Asyrot, A Program for the Analysis of High Resolution Singlet-Singlet Band Spectra of Asymmetric Tops. *Comput. Phys. Commun.* **2000**, *135*, 293-311.

(103) Kirchner, M. T.; Boese, R.; Billups, W. E.; Norman, L. R. Gas Hydrate Single-Crystal Structure Analyses. *J. Am. Chem. Soc.* **2004**, *126*, 9407.

(104) Hirose, C.; Akamatsu, N.; Domen, K. Formulas for the Analysis of Surface Sum Frequency Generation Spectrum by CH Stretching Modes of Methyl and Methylene Groups. *J. Chem. Phys.* **1992**, *96*, 997-1004.

(105) Chandrasekharan, N.; Kamat, P. V. Tuning the Properties of CdSe Nanoparticles in Reverse Micelles. *Res. Chem. Intermed.* **2002**, *28*, 847-856.

(106) Fayer, M. D. Dynamics of Water Interacting with Interfaces, Molecules, and Ions. *Acc. Chem. Res.* **2012**, *45*, 3-14.

(107) Costard, R.; Levinger, N. E.; Nibbering, E. T. J.; Elsaesser, T. Ultrafast Vibrational Dynamics of Water Confined in Phospholipid Reverse Micelles. *J. Phys. Chem. B* **2012**, *116*, 5752-5759.

(108) Allesch, M.; Schwegler, E.; Galli, G. Structure of Hydrophobic Hydration of Benzene and Hexafluorobenzene from First Principles. *J. Phys. Chem. B* **2007**, *111*, 1081-1089.

(109) Gierszal, K. P.; Hands, J. G. D. M. D.; Wilcox, D. S.; Slipchenko, L. V.; Ben-Amotz, D. π-Hydrogen Bonding in Liquid Water. *J. Phys. Chem. Lett.* **2011**, *2*, 2930-2933.

(110) Danten, Y.; Tassaing, T.; Besnard, M. On the Nature of the Water-Hexafluorobenzene Interaction. *J. Phys. Chem. A* **1999**, *103*, 3530-3534.

(111) Vaden, T. D.; Forinash, B.; Lisy, J. M. Rotational Structure in the Asymmetric OH Stretch of $Cs^+(H_2O)Ar$. *J. Chem. Phys.* **2002**, *117*, 4628-4631.

(112) Vaden, T. D.; Weinheimer, C. J.; Lisy, J. M. Evaporatively Cooled $M^+(H_2O)Ar$ Cluster Ions: Infrared Spectroscopy and Internal Energy Simulations. *J. Chem. Phys.* **2004**, *121*, 3102-3107.

(113) Vaden, T. D.; Lisy, J. M.; Carnegie, P. D.; Pillai, E. D.; Duncan, M. A. Infrared Spectroscopy of the $Li^+(H_2O)Ar$ Complex: The Role of Internal Energy and Its Dependence on Ion Preparation. *Phys. Chem. Chem. Phys.* **2006**, *8*, 3078-3082.

(114) Davidson, D. W. The Motion of Guest Molecules in Clathrate Hydrates. *Can. J. Chem.* **1971**, *49*, 1224-1242.

(115) Mamone, S.; Ge, M.; Hüvonen, D.; Nagel, U.; Danquigny, A.; Cuda, F.; Grossel, M. C.; Murata, Y.; Komatsu, K.; Levitt, M. H.; Rõõm, T.; Carravetta, M. Rotor in a Cage: Infrared Spectroscopy of an Endohedral Hydrogen-Fullerene Complex. *J. Chem. Phys.* **2009**, *130*, 081103.